ΠΑΝΕΠΙΣΤΗΜΙΟ ΚΡΗΤΗΣ

ΤΜΗΜΑ ΧΗΜΕΙΑΣ

ΜΕΤΑΠΤΥΧΙΑΚΟ ΔΙΠΛΩΜΑ ΕΙΔΙΚΕΥΣΗΣ
Γενικό Μεταπτυχιακό Χημείας

«Κατασκευή τρισδιάστατων ικριωμάτων μέσω πολυφωτονικού πολυμερισμού για εφαρμογές στην αναγεννητική ιατρική και μηχανική ιστών»

Κωνσταντίνος Παρκατζίδης

Υπεύθυνος Καθηγητής/τρια: Εμμανουήλ Στρατάκης και Μαρία Βαμβακάκη

ΗΡΑΚΛΕΙΟ 2018

Περίληψη

Η πολυφωτονική λιθογραφία, βασισμένη στον πολυφωτονικό πολυμερισμό, είναι μία πανήσχυρη τεχνική κατασκευής τρισδιάστατων ικριωμάτων, για εφαρμογές στην αναγεννητική ιατρική, μηχανική ιστών καθώς και σε άλλες βιοεφαρμογές. Ο πολυφωτονικός πολυμερισμός είναι βασισμένος σε εστιασμένο πολυμερισμό/διασταύρωση του φωτοευαίσθητου υλικού, με τη χρήση υπερταχείων παλμών λέιζερ, ενώ χρήση φωτοεκκινητή για την έναρξη της διαδικασίας του πολυμερισμού είναι αναγκαία. Στη παρούσα μεταπρυχιακή διατριβή, σχεδιάστηκαν υλικά και μέθοδοι κατάλληλοι για πολυφωτονικό πολυμερισμό, για να κατασκευαστούν πορώδη τρισδιάστατες δομές για αναγεννητική ιατρική και μηχανική ιστών.

Στο δεύτερο κεφάλαιο παρουσιάζεται η χημική τροποποίηση της ζελατίνης, το οποίο είναι ένα πρωτεϊνικός φύσεως ευρέως γνωστό βιουλικό, μέσω του μεθακριλυκού ανυδρίτη, ώστε να προσδεθούν στην κύρια ανθρακική αλυσίδα φωτοπολυμεριζώμενες ομάδες μεθακρυλαμιδίου. Επιπρόσθετα στην εργασία αυτή έγινε κατασκευή τρισδιάστατων δομών της χημικά τροποποιημένης ζελατίνης χωρίς τη χρήση του φωτοεκκινητή. Μια τέτοια προσέγγιση είναι υψίστης σημασίας για βιολογικές εφαρμογές, καθώς αποφεύγεται η χρήση τοξικών μορίων του φωτοεκκινητή, καθώς και των προϊόντων διάσπασης του που είναι ευκίνητες ρίζες. Η βιοσυμβατότητα του υλικού αυτού ελέγχτηκε, τόσο σε δισδιάστατες συμβατές καλλιέργειες όσο και στις τρισδιάστατες δομές. Για το λόγω αυτό χρησιμοποιήθηκαν κύτταρα ινοβλαστών, NIH 3T3, καθώς και τεχνικές ανοσοιστοχημείας και ταυτόχρονης χρώσης ζωντανών νεκρών κυττάρων.

Στο κεφάλαιο 3, συνθέσαμε χημικά τροποποιημένη ζελατίνης καθώς και υδατοδιαλυτό και φωτοπολυμεριζόμενο παράγωγο χιτοζάνης. Το υβριδικό αυτό υλικό των δύο βιοπολυμερών χρησημοποιήθηκε για κατασκευή τρισδιάστατων ικριωμάτων για κυτταροκαλλιέργιες. Λέιζερ το οποίο εκπέμπει στο εγγύς υπέρυθρο, στα 800 nm, χρησιμοποιήθηκε για τον πολυμερισμό, χρησιμοποιώντας την εοσίνη ως υδατοδιαλυτό και βισυμβατό φώτοεκκινητή, εγκεκριμένο από το FDA, χωρίς να χρησιμοποιηθούν συνμονομερή η συνεκκινητές, γεγονός το οποίο αναφέρεται στη βιβλιογραφία. Ως μηχανισμό πολυμερισμού, προτείνουμε ότι η τροποποιημένη ζελατίνη καθώς και η χιτοζάνη λειτουργούν σαν συνεκκινητές του συστήματος υποστιρίζοντας έτσι τον πολυφωτονικό πολυμερισμό. Η κυτταρική συμπεριφορά τόσο σε υμένια όσο και σε τρισδιάστατες δομές του υβριδικού αυτού υλικού, ελέγχτηκε χρησιμοποιώντας πρωτόγεννη ανθρώπινα μεσυγχηματικά κύτταρα απομονωμένα από τον πολφό του δοντιού, τα οποία έδειξαν εξαιρετική κυτταρική προσκόλληση και πολλαπλασιασμό, υπογραμμίζοντας την εξαιρετική βιοσυμβατότητα του υβριδικού αυτού υλικού.

Στο τελευταίο κεφάλαιο αναπτύχθηκαν πολύ-λειτουργικά 3D ικριώματα, για μηχανική ιστών και αναγεννητική ιατρική. Χρησιμοποιήσαμε ένα υβριδικό οργανικό-ανόργανο υλικό, το οποίο είχε εμπλουτιστεί με λειτουργικές ομάδες τροποποιημένης θυμόλης ως ένα βιοσυμβατό και αντιμικροβιακό υλικό για τις εφαρμογές μηχανικής ιστών. Η θυμόλη, ως φυσικό προϊόν, προερχόμενο από αιθέρια έλαια των φυτών, έχει οσχυρή αντιμικροβιακή δράση. Τα 3D ικριώματα του υβριδικού υλικού έδειξαν εξαιρετική βιοσυμβατότητα και ταυτόχρονα ισχυρή αντιμικροβιακή δράση. Οι βιολογικές μελέτες με χρήση μεσυγχηματικών κυττάρων οδοντικού πολφού έδειξαν αυξημένη κυτταρική προσκόλληση και πολλαπλασιασμό στα 3D ικριώματα, ενώ η αντιμικροβιακή τους συμπεριφορά επιβεβαιώθηκε από καλλιέργεια βακτηρίων e-coli σε παρατεταμένες μικροβιακές καλλιέργιες.

Abstract

Multiphoton lithography, based on photopolymerization, is a powerful technique for the fabrication of 3D structures used in tissue engineering, regenerative medicine, and other biomedical applications. Multiphoton polymerization is based on the localized polymerization / cross-linking of photosensitive materials induced by femtosecond laser pulses. The use of a suitable photoinitiator is required to initiate the polymerization / cross-linking process and attain the 3D structures. In the current Master Thesis, we have developed materials and processes suitable for multiphoton polymerization to fabricate 3D porous scaffolds for tissue engineering and regenerative medicine applications.

In Chapter 2, the modification of gelatin, which is a well known biopolymer, with a methacrylic anhydride in order to introduce photopolymerizable moieties of the methacrylamide group is presented. In addition, we have investigated the suitability of this gelatin methacrylamide biopolymer in the fabrication 3D scaffolds in the absence of any photoinitiator. Such an approach is highly desirable in biological application, due to the elimination of the toxic photoinitiator molecules, as well as the highly diffusive free radicals which are produced by these molecules. The biocompatibility of the synthesized material, both in the form of 2D films as well as in 3D porous scaffolds, was examined via biocompatibility assays of live/dead cells as well as via immunocytochemistry for actin assay using NIH 3T3 fibroblast cells.

In Chapter 3, we have synthesized gelatin methacrylamide and a photopolymerizable water soluble chitosan derivative. Hybrid materials of these two biopolymers were used to fabricate 3D scaffolds for cell culture application.. Near IR laser irradiation, operated at 800nm, was employed to fabricate 3D scaffolds, in the presence of eosin-Y, as a water soluble, FDA-approved and biocompatible photoinitiator, in the absence of any other co-initiators or co-monomers reported in the literature. We saggasted that the free amine groups of GelMA and the chitosan derivative act as co-initiator

moieties ans support the photopolymerization process. Cell behavior on the hybrid materials on 2d films as well as 3D scaffolds was examined, using primary dental pulm stem cells, which showed excellent cell adhesion, growth and proliferation verifying the biocompatibility of this hybrid material.

In the last Chapter, dual functional 3D scaffolds, for tissue engineering and regenerative medicine were developed. We employed a hybrid organic-inorganic material, functionalized with thymol methacrylate moieties as a biocompatible and antimicrobial material for tissue engineering applocations. Thymol, as a natural product derived from essential oils of the plants, has great antimicrobial activity. 3D scaffolds of material developed showed excellent biocompatibility and simultaneously strong antimicrobial action. Biological studies using primary dental pulm stem cells showed an increased cell adhesion and proliferation on the 3D scaffolds whereas their antifouling behavior was confirmed by e-coli bacteria culture in prolonged of microbial assays.

Ευχαριστίες

Τελειώνοντας τη παρούσα μεταπτυχιακή διατριβή, θα ήθελα να ευχαριστήσω όλους όσους συνέβαλαν, άλλοι περισσότερα και άλλοι λιγότερα, στη παρούσα μεταπτυχιακή εργασία.

Πρωτίστως, ένα μεγάλο ευχαριστώ οφείλω στην υπεύθυνη μου καθηγήτρια, τη Μαρία Βαμβακάκη, για όλη τη στήριξη, εμπιστοσύνη, ενθάρρυνση και γνώση που μου προσέφερε σε όλη τη διάρκεια των μεταπτυχιακών αλλά και τον προπτυχιακών σπουδών.

Επιπλέον θα ήθελα να ευχαριστήσω την συνεπιβλέπουσα, σε αυτή την εργασία, τη Δρ. Μαρία Φαρσάρη, για τη στήριξη της και την εμπιστοσύνη που έδειξε στο πρόσωπό μου.

Μεγάλο ευχαριστώ οφείλω και στον καθηγητή Εμμανουήλ Στρατάκη, ο οποίο; δέχτηκε να είναι ο υπεύθυνος καθηγητής μου, καθώς και μέλος της τριμελούς επιτροπής.

Επίσης θα πρέπει να ευχαριστήσω το τμήμα χημείας και το ινστιτούτο ηλεκτρονικής δομής και λέιζερ για υλικοτεχνική καθώς και εκπαιδευτική υποστήριξη του.

Τέλος, θα ήθελα να ευχαριστήσω όλους τους συνεργάτες, χωρίς τους οποίους η διατριβή αυτή δεν θα μπορούσε να πραγματοποιηθεί.

Chapter 1

Intoduction

1 Indroducrion

1.1 Principle of tissue engineering and regenerative medicine

In 1993, Langer and Vacanti defined TE as "an interdisciplinary field that applies the principles of engineering and life sciences toward the development of biological substitutes that restore, maintain, or improve tissue function or a whole organ".[1]
There are tissues within the human body with a limited capability of repair/regeneration, posing a challenge that is often difficult for clinicians to overcome, therefore the contribution of tissue engineering (TE) and regenerative medicine (RM), in modern medicine is of paramount importance. TE evolved from the field of biomaterials development and refers to the practice of combining scaffolds, cells, and biologically active molecules into functional tissues. The goal of TE is to assemble functional constructs that restore, maintain or improve damaged tissues or whole organs. Artificial skin and cartilage are examples of engineered tissues that have been approved by the food and drug administration (FDA).
On the other hand, RM has been defined as "*the process of replacing or regenerating human cells, tissues or organs to restore or establish normal function*".[2] RM is a broad field that includes TE, but also incorporates research on self-healing in which the body uses its own systems, sometimes with the help of foreign biological materials, to recreate cells and rebuild tissues and organs. The terms "tissue engineering" and "regenerative medicine" have become largely interchangeable, as the field hopes to focus on cures instead of treatments for complex, often chronic, diseases.
The most promising strategies in TERM involve the integration of a triad comprising a biomaterial, living cells, and biologically active molecules to engineer synthetic environments that closely mimic the healing milieu present in human tissues, and that stimulate tissue repair and regeneration.[3] To be clinically effective, these environments must replicate as closely as possible the main characteristics of the native extracellular matrix (ECM) on a cellular and subcellular scale.[4] Even though 2D cell culture techniques have been extensively used by cell biologists to derive valuable information regarding cellular processes and cell behavior, over the past decades, cell culture research has lately witnessed a paradigm shift into the third dimension. 3D cultured cells behave differently to their monolayer (2D) counterparts and their responses resemble better the native tissues.[5] The eventual goal of TERM is the creation of 3D artificial cell culture scaffolds that mimic the natural extracellular environment features sufficiently, so that cells function, in the artificial medium, as they would do *in vivo***.** The strategy of using bioresorbable porous synthetic scaffolds as artificial ECM was introduced by Langer and Vacanti and according to Agarwal and Ray, is essential for scaffolds for use in TERM.[6]

Therefore, artificial scaffolds should combine the following characteristics:

- Biocompatiblity
- Bioresorbability and hence capability of being remodeled
- Degrade in tune with the tissue repair or regeneration process
- Highly porosity and permeability to allow cell infiltration as we as proper nutrient and gas diffusion
- Appropriate pore sizes for the cell type used
- Possess appropriate mechanical properties to provide the correct micro-stress environment for the cells
- Promote cell attachment
- Encourage the deposition of ECM by promoting cellular functions
- Carry and present biomolecular signals for favorable cellular interactions

One of the key elements in most TERM approaches is the use of a cell population that will induce new tissue formation through the interaction the resident cells of the tissue to be regenerated.[7] The initial rationale for the use of cells in TERM approaches was based on the premise that they would replace the cells lost during the injury/degenerative process and at the same time contribute to the formation of new tissue. In this sense, stem cells of either pluripotent or multipotent origin have been proposed for the regeneration of tissues. Among the different stem cell populations, one stands out in particular the mesenchymal stem cells (MSCs)[8] which can *in vitro* differentiate into osteoblasts, adipocytes, and chondroblasts to name just a few.[9] The great potential of MSCs has been associated with their widespread availability throughout the human body, along with the fact that, when isolated, they display great proliferative potential with minimal senescence through multiple passages.[10]
Another consideration related to TERM constructs is the presence of chemical and mechanical stimuli, such as soluble growth and differentiation factors, anti-microbial agents as well as mechanical forces. Among the chemical factors that have frequently been applied are bone morphogenetic proteins (BMPs), basic fibroblast growth factor (bFGF or FGF-2), vascular endothelial growth factor (VEGF), and transforming growth factor-β (TGF-β). Although these are soluble factors, they can be incorporated into the ECM during scaffold fabrication.[11] In fact, one of the key nonstructural functions of the natural ECM *in vivo* is to bind, retain, and present growth factors to cells attached to the ECM. Controlled delivery schemes can also be used to increase the longevity of the original soluble factor load. Applied techniques include their encapsulation in small biodegradable particles, the use of transfected cells to express and release the factors and their chemical conjugation to the scaffold material itself.[12] TERM experiments *in vitro* start with the isolation of cells from the patients. Nowadays, mesenchymal stem cells are preferable as they are powerful cells which can be differentiated into any kind of cell types. After the isolation, cells are cultured in 2D cell cultures in order to obtain a huge number of cells that are required for *in vitro* studies. The next step of TERM is the selection of the appropriate biomaterial, which will mimic physicochemically as well as biologically the target tissues. These

biomaterials should be structurable in order to form 3D porous scaffolds of appropriate shape, which will support cell growth, proliferation, differentiation and communication. Following the scaffold fabrication and sterilization, cell culture is performed on the 3D constructs. One can use biomolecules, such as growth factors or other molecules which induce different cell's reactions. After 3D cell culture *in vitro* the created tissue can be implanted in the body. There are two main scaffolds categories, the biodegradable ones which degrade during the formation of tissue *in vivo* and the non-degradable analogues which are used as a mechanical support, such as the majority of the implants used for bone and/or dental restoration (**figure 1.1**).

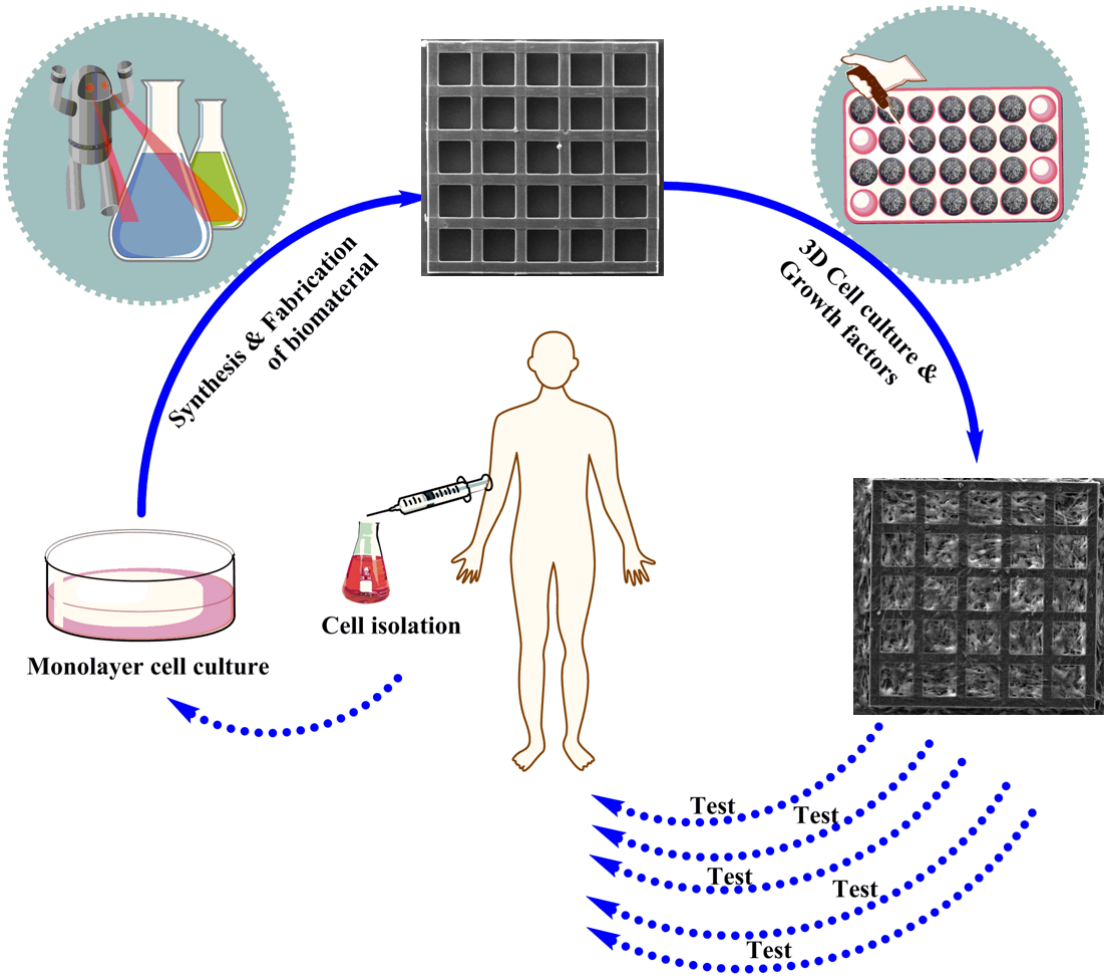

Figure 1. 1: Schematically illustration of the basic principle of TERM

1.2 Biocompatibility

Researchers have coined the words `biomaterial' and `biocompatibility' to indicate the biological performance of materials.
Biomaterials is Any substance (other than a drug) or combination of substances, synthetic or natural in origin, which can be used for any period of time, as a whole or as a part of a system which treats, augments, or replaces any tissue, organ, or function of the body.[13] The Williams Dictionary of Biomaterials[14] defined biocompatibility as the ‘‘*ability of a material to perform, with an appropriate host response, in a specific situation*’’.
In other words, materials which are biocompatible are called biomaterials, and biocompatibility is a descriptive term which indicates the ability of a material to perform with an appropriate host response, in a specific application. In simple terms it implies compatibility or harmony of the biomaterial with the living systems. Biocompatibility is the ability to exist in contact with tissues of the human body without causing an unacceptable degree of harm to the body. Therefore, it is not only associated to toxicity, but to all other potential adverse effects of a material in a biological system. It must not adversely affect the local and systemic host environment of interaction (bone, soft tissues, ionic composition of plasma, as well as intra and extracellular fluids). It refers to a set of properties that a material must have to be used safely in a biological organism. It should be non-carcinogenic, non-pyrogenic, non-toxic, non-allergenic, blood compatible, non-inflammatory. The operational definition of biocompatibility is "*The patient is alive so it must be biocompatible*"**.** [15]

1.3 Biomaterials

The physicochemical properties of biomaterials are very important in TERM applications. From the mechanical point of view, ideally, the scaffold should have mechanical properties consistent with the anatomical site into which it is to be implanted and, from a practical perspective, it must be strong enough to allow surgical handling during implantation. Given the above, there are different categories of materials that are extensively used in specific TERM applications[16] (**figure 1. 2)**

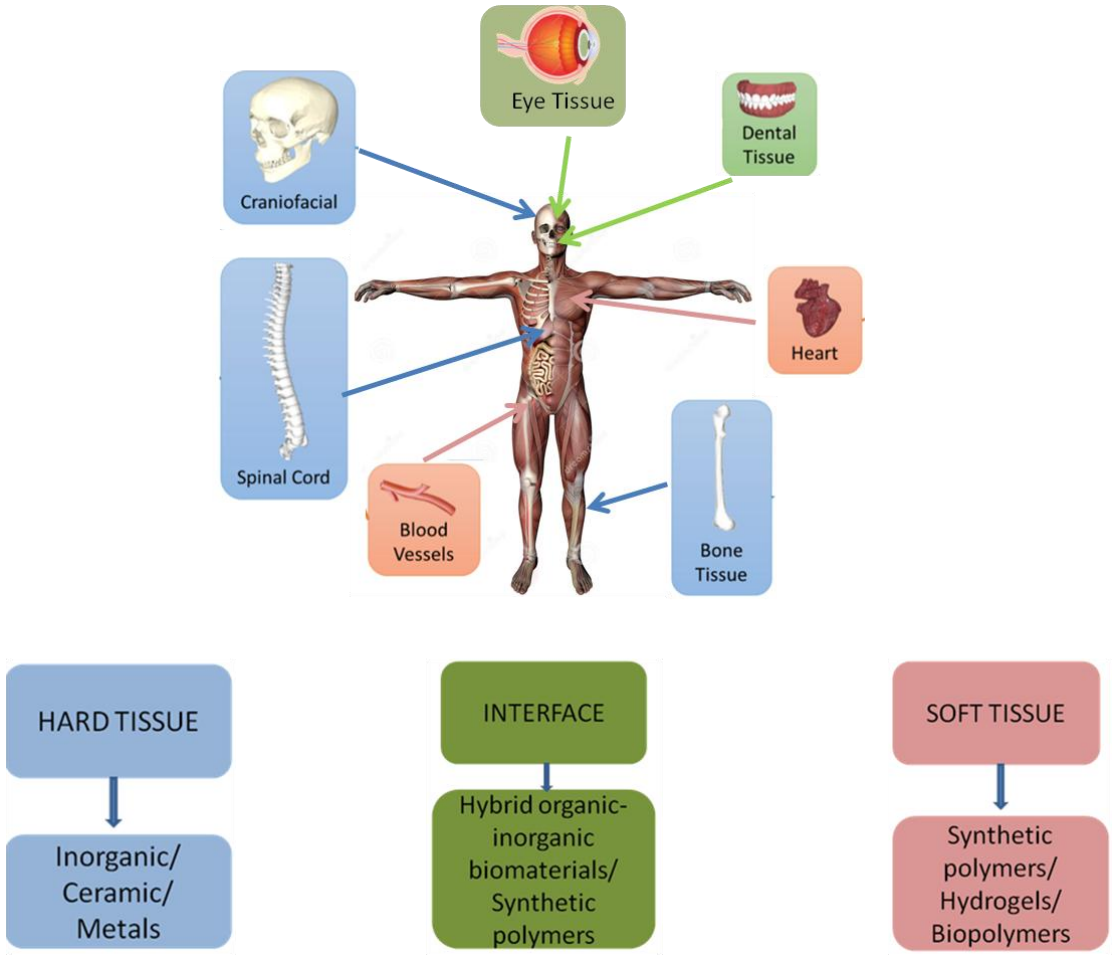

Figure 1. 2: Biomaterials required for different TERM applications.

Common degradable and non-degradable implant materials can be divided into synthetically produced materials and natural materials. Both of these categories have further subcategories. Synthetic materials could be of organic or inorganic origin. Given that, synthetic biomaterials used today both in clinical and research, are polymers, such as polyethylene glycol (PEG)[17], polycaprolactone (PCL)[18], polylactic acid (PLA)[19], polyurethanes[20], ceramics, such as hydroxyapatite (HA)[21], calcium triphosphate,[22] etc, and metals/metal alloys, such as zirconium[23] and titanium-based alloys[24]. On the other hand natural and modified natural materials have attracted great attention during the last decade, for use in TERM, due to their higher biocompatibility and similarity with the materials comprising the ECM. These kind of materials are normally used in the form of hydrogels for soft tissue regeneration. Naturally, derived materials can be split into two main categories based on their origin, proteins and polysaccharides. Protein based materials are collagen[25], gelatin[26], fibrin skill[27] etc while polysaccharides include chitosan[28], hyaluronan[29], alginate,[30] etc.

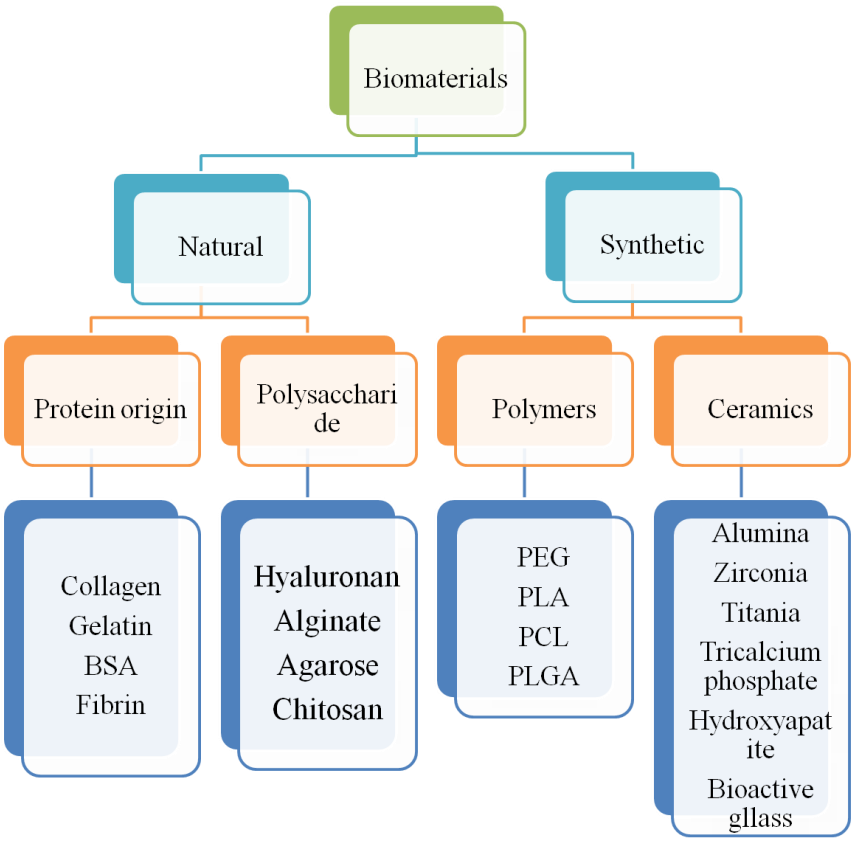

Figure 1. 3: Categories of biomaterials

Polymers

Synthetic polymeric materials have been widely used in medical disposable supply, prosthetic materials, dental materials, implants, dressings, extracorporeal devices, encapsulants, polymeric drug delivery systems, tissue engineered products, and orthodoses as that of metal and ceramics substituents.[31] The main advantages of the polymeric biomaterials compared to metal or ceramic materials are their ease of manufacturability to produce various shapes (latex, film, sheet, fibers, etc.), ease of secondary processability, reasonable cost and availability with desired mechanical and physical properties. Homopolymers are composed of a single type of monomer and there are many homopolymer biomaterials. Copolymers consist of different monomers used to obtain a polymer which combines the properties of the individual components. The required properties of polymeric biomaterials are similar to those of other biomaterials, that is, biocompatibility, sterilizability, adequate mechanical and physical properties and manufacturability.[32]

Ceramics

Ceramics are defined as materials with regularly-aligned mineral crystal molecules. Both surgeons and researchers have shown great interest for these biomaterials.

Ceramics include a variety of biomaterials, such as calcium phosphates and alumina. Hydroxyapatite (HAp) has a olayed a dominant role, being used for both oral and maxillofacial surgery as bone substitute and as coating for metal and carbon implants. It is found in different parts of the body as a constituent of various types of calcified tissues.[33] The main characteristics of ceramic materials are hardness and brittleness, great strength and stiffness, resistance to corrosion and wear and low density. They work mainly on compression forces whereas on tension forces, their behavior is quite poor. Ceramics are typically electrical and thermal insulators and are used in several different fields such as dentistry, orthopedics and as medical sensors.[34]

Metals and Alloys

Biomaterials for skeletal systems mainly comprise metals. Metals have been used almost exclusively for loadbearing implants, such as hip and knee prostheses and fracture fixation wires, pins, screws, and plates. Although pure metals are sometimes used, alloys frequently provide improvement in material properties, such as strength and corrosion resistance.[35] Three material groups dominate biomedical metals: stainless steel, cobalt-chromium-molybdenum alloy, titanium and titanium alloys. The main considerations in selecting metals and alloys for biomedical applications are their excellent electrical and thermal conductivity, biocompatibility, appropriate mechanical properties, corrosion resistance and reasonable cost. The physical and chemical properties of the different metallic materials used in any surgery as well as their interactions with the host tissue of the human body are of paramount importance in such applications.[36]

Naturally derived biomaterials show several advantages compared to synthetic biomaterials. The former are biocompatibility, biodegradability and bioactivity. These advantages render them the most popular biomaterials nowadays. They are usually applied to replace or restore structure and function of damaged tissues/organs. Due to their bioactivity, they can promote cell functions, such as cell adhesion, migration, proliferation and differentiation. When these kinds of materials are implanted into a damaged tissue area, they can enhance the attachment and migration of cells from the surrounding environment, therefore, induce extracellular matrix formation and promote tissue repair. The main disadvantage, of naturally derived biomaterials, is their weak mechanical properties. Therefore, there are many studies on the modification of natural polymers in order to enhance their mechanical properties and their stability without altering their biocompatibility and bioactivity.

Collagen

Collagen is the main component of the ECM characterized by exceptional biocompatibility, low antigenicity, increased adhesion capacity and high degree of biodegradability. Collagen enhance the attachment, growth and migration of cells due to the presence of bioactive sequences, such as the arginine-glycine-aspartic acid (RGD) tripeptide. These characteristic properties render it an ideal scaffold for tissue engineering.[37]

Gelatin

Gelatin is defined as a product obtained by the partial hydrolysis of collagen which is derived from the skin, the white connective tissue and the bones of animals. Two types of gelatin are obtained, depending on the pre-treatment procedure, known commercially as type-A and type-B gelatin. Type A gelatin is obtained by the acid treatment of collagen at pH 1–2 and has an isoelectric point (IEP) around pH 7–9, while type B gelatin is produced by alkali treatment at pH 12–13 and has an IEP around pH 5–6. Gelatin can produce thermoresponsive hydrogels. Below 30-35°C it is in a gel form while above 35°C in becomes a liquid. Due to its origin, it also contains the RGD tripeptide which enhances its bioactivity.[38-39]

Chitosan

Chitosan is a polysaccharide, derivative of the alkaline deacetylation of chitin. Chitosan is a random copolymer of two repeat units, D-glucosamine which is the deacetylated unit and N-acetyl-D-glucosamine which is the acetylated form. It contains several reactive side groups, such as amine, primary and secondary hydroxyl groups, therefore, chitosan turns out to be a highly reactive polysaccharide. Many of the physicochemical properties of this polysaccharide are based on the above mentioned side groups. There are many strategies to modify chitosan in order to produce chitosan-based biomaterials with good solubility in water and/or biological fluids, mechanical properties, biocompatibility and bioactivity.[40]

Alginate

Alginate, also known as alginic acid, is an anionic polysaccharide found in the cell walls of algae and is produced by two bacterial genera, *Pseudomonas* and *Azotobacter*. Structurally, alginates are linear co-polymers comprising covalently linked blocks of β-D-mannuronic acid and α-L-guluronic acid residues. Due to it's anionic origin, alginate is often used in the form of gels, produced by cations such as Ca^{2+}, or by chemical modification of its hydroxyl and/or carboxylic acid side groups. Alginate is a biocompatible, biodegradable, cell friendly biomaterial which is used in TERM applications for wood healing, cell delivery and as a drug delivery/release system.[41]

Hyaluronan or hyaluronic acid

Hyaluronic acid is a natural polysaccharide and a major component of mammalian ECM. It consists of a linear polysaccharide comprising alternating units of D-glucuronic acid and N-acetyl-D-glucosamine. Hyaluronic acid is usually extracted from the synovial fluid, umbilical cord, vitreous humor, rooster combs, or bacterial cultures in the laboratory. It is used in TERM applications as a non-allergenic, non-toxic, and biocompatible hydrogel.[42]

1.4 Multiphoton lithography

As mentioned above, the fabrication of highly accurate 3D scaffolds are of paramount importance for biomedical applications. There are several techniques, which provide

the possibility to create 3D scaffolds. On the one hand, these techniques can reproduce 3D scaffolds via chemical modification of the material, whereas on the other hand, the 3D scaffolds are formed via physical changes of the material properties. The former type is normally based on a photo-induced chemical reaction such as photopolymerization, photocrosslinking or photodegradation. Techniques based on photochemical reactions have great advantages in controlling the shape of the structures. One powerful technique, in 3D structuring, is multiphoton lithography (MPL) which is based on multiphoton polymerization (MPP) and has the ability to fabricate 3D scaffolds with a resolution below 100nms.[43]

1.5 Multi-photon absorption

Multi-photon absorption (MPA) is a process proposed initially by Göppert-Mayer (1931) and experimentally developed by Kaiser and Garett with the development of the Laser.[44] In order to explain the MPA process, first, one photon absorption (OPA) should be understood. Photochemistry states that each absorbed photon activates one molecule to carry out a photochemical reaction. According to the OPA, a molecule can be excited from its ground state, E_g, to an energetically higher state, E_e if it absorbs a photon with energy equal or larger than the energetic gap between the two states $E = E_e - E_g = h\omega a$. An exception to this rule is nonlinear absorption, in which more than one photon is consumed for each reaction. Two photon absorption (TPA) describes a similar process, where ΔE is realized by the almost coincidental absorption of two photons with $\Delta E = h\omega k + h\omega l$. If a photon of energy $h\omega k < \Delta E$ interacts with the molecule, no real transition from E_g to E_e is allowed. However, for a short period of time $\Delta t = \frac{h}{2h\omega k}$, given by the energy time uncertainty principle, the molecule can be elevated to a virtual state E_v. During this time, a second photon has only to overcome the energy gap $h\omega l = \Delta E - h\omega k$ and a real transition can occur. This transition is only possible, if the combined energy of the two incident photons is sufficient to bridge the gap between the ground and the excited state of the molecule:

$h\omega k + h\omega l - h\omega i - h\omega e = 0$

$h\omega k + h\omega l = h\omega a$

Of practical importance is the degenerate case $h\omega k = h\omega l = 1/2 h\omega a$, where two photons of the same energy are absorbed. In terms of technical implementation this means that only a single laser source is required to initiate TPA processes. From this simple picture the activation rate can be approximated.[45]

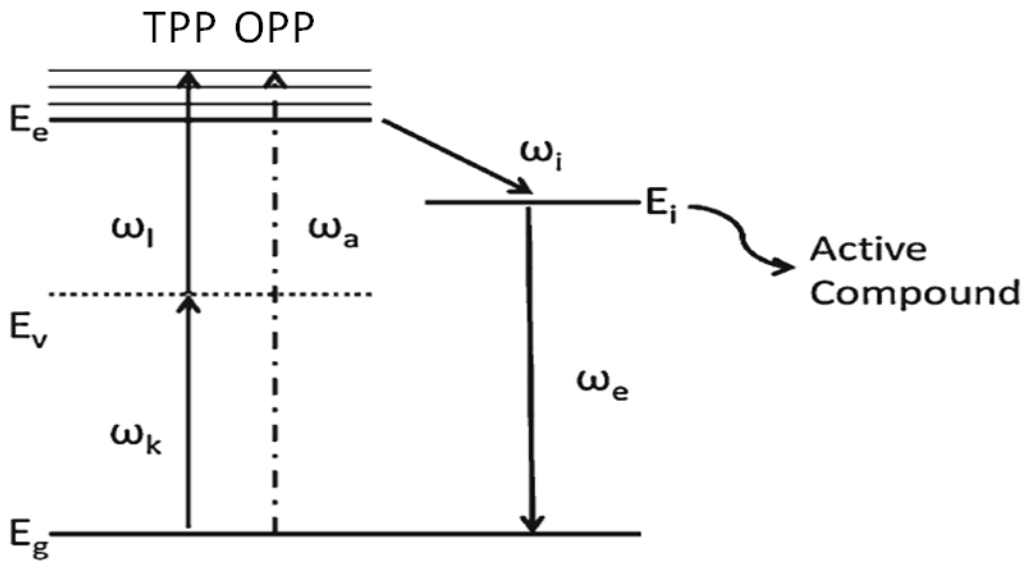

Figure 1. 4: Energy level diagram for the single and two photon absorption process. Both processes can lead to the generation of an active compound for photochemical processes.[46]

Right after the excitation several things may happen: 1) Radiationless deactivation. The molecule goes back to the ground state by vibration (thermal) deactivation (no light emission). The energy goes to the solvent/environment of the molecule. 2) Intersystem crossing leads to a triplet state by spin inversion, where the initiator has as high energy as required in order to undergo bond cleavage, producing radicals for photopolymerization. 3) Emission of light and return to the ground state (luminescence, fluorescence, phosphorescence). During the excitation of molecules, quenching of the excited state, as well as d radicals, are present, by molecules called, monomer and radical quencher. The TPA differs from the OPA in the resonance time of the molecule. In an OPA, the electric field of the photon is in resonance with the molecule for a longer period; it oscillates in phase with the polarisation resulting in a finite transition probability. In TPA, however, the molecule is only in resonance for a short time rendering no probability for an OPA. This depends on the photons interacting with a molecule nearly simultaneously (within a time frame of 10-15 s).[47]

1.6. Multi photon polymerization

The difference between OPP and TPP lies in how the energy is provided. In OPP, there is a linear response of the material to the light intensity. However, if the material response is proportional to the square of the photon density, the integrated material response is greatly enhanced at the focal point, as illustrated in **figure 1. 5**

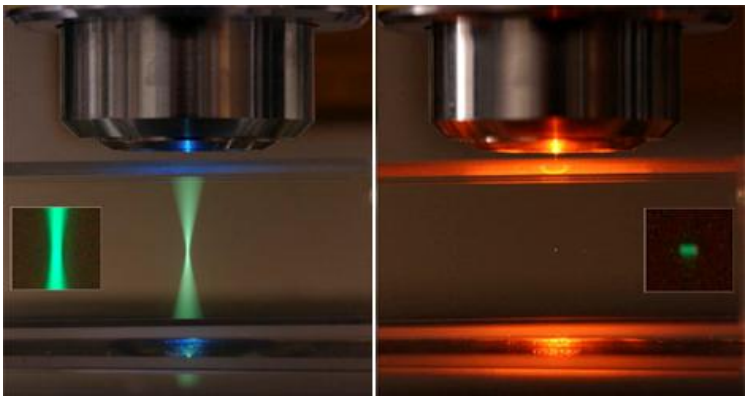

Figure 1. 5: Comparison between OPP (left) and TPP(right). Image by Steve Ruzin and Holly Aaron, UC Berkeley.

Multi-photon polymerization (MPP) is a kind of photopolymerization. In most cases the mechanism of polymerization is that of free-radical polymerization. However, there are some examples in the literature, in which MPP is based on ionic polymerization.

The first step in photopolymerization is *initiation*, in which a light-sensitive compound (a photoinitiator) is required to produce active species (radicals or cations) upon irradiation with UV, Vis or IR light. The photoinitiator can dissociate to form primary radicals or can react with a second species, via hydrogen abstraction, forming secondary radicals. Regarding the mechanism involved in photolysis, the photoinitiation includes radical polymerization (through photocleavage and hydrogen abstraction) and cationic polymerization.[48] A comparison of the photopolymerization mechanisms is shown in **figure 1.6** Photocleavage-based radical polymerization involves the formation of active species under light irradiation by cleavage of chemical bonds (e.g. C-C, C=O, C-S, C-Cl). The photoinitiators used can be classified in Norrish type I and II. Type I photoinitiators can be photo-fragmented into radicals upon absorption of light, whereas type II photoinitiators require the presence of a co-initiator such as amines or alcohols. In the case of Norrish type II systems, the radicals are generated at the co-initiator after the transfer of a hydrogen atom to the photoinitiator. Radical photopolymerization by hydrogen abstraction involves aromatic ketones which, under light exposure, undergo hydrogen abstraction from a proton donor molecule to form a ketyl radical and a donor radical. Conventionally, the H-donor radical initiates the polymerization, while the ketyl radical undergoes radical coupling to the growing macromolecular chain.[49] Cationic polymerization requires

the use of a cationic initiator transferring a charge to a monomer unit, which becomes reactive and interacts similarly with other units leading to polymer chain growth. The most commonly used cationic initiators are the Bronsted acids arenediazonium, diarylodonium and various sulfonium salts. In TERM, however, cationic initiators are avoided because they generate protonic acids that, due to their strong acidic character, affect cell cultures negatively.

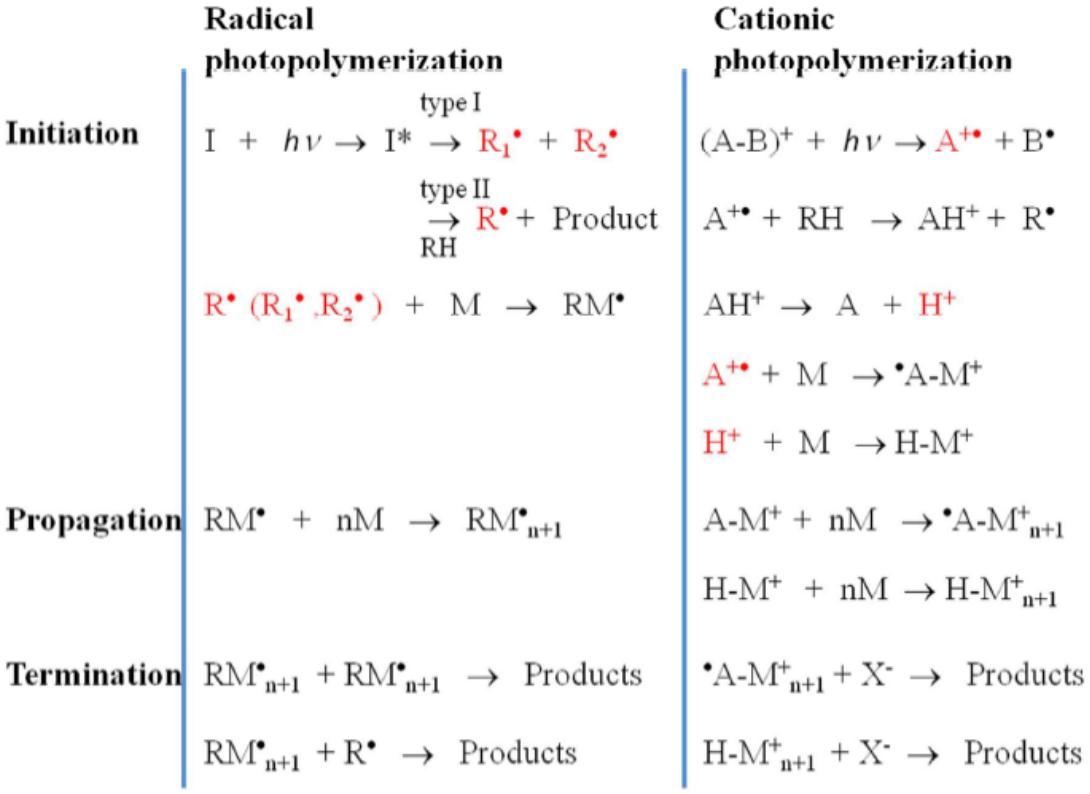

Figure 1. 6: Mechanisms of radical and cationic polymerizations.[50]

1.7 Experimental Setup

The MPL experimental setup resembles that of a scanning laser microscope, where the laser is used for polymerization rather than vision. A typical experimental setup is shown in **figure1. 7** The necessary components are (1) an ultrafast laser, (2) a beam/sample motion system, (3) a microscope objective, (4) a beam intensity controler, (5) an online camera, and (6) a control software. These components are detailed below.

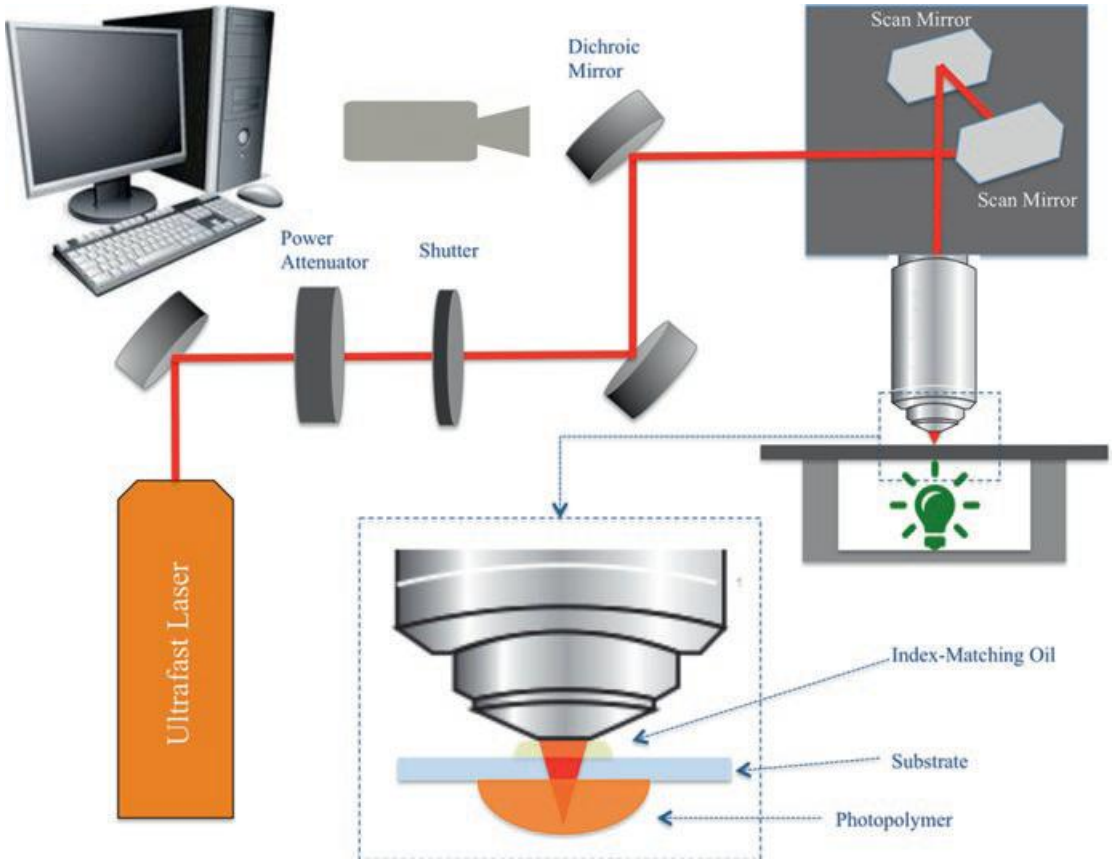

Figure 1. 7: Experimental set-up of MPL[51]

1. Laser: There are typically three kinds of lasers used: (a) Ti:sapphire femtosecond oscillator (occasionally amplifiers also) operating at around 800 nm; (b) second harmonic fiber lasers, typically operating at 780 nm; and (c) amplified ultrafast YAG (yttrium aluminum garnet) laser operating at the second harmonic (green) 520nm. As the laser sources vary so much, the energy required for MPL can also vary and depends on the photopolymer, the photoinitiator, and the focusing but also on the laser wavelength and repetition rate.

2. Motion control: The "writing" of the structures inside the photopolymer is achieved by two different methods: (a) The focused laser beam moves inside the photopolymer, using galvanometric scanners. The structure is built in a layer-by-layer format, and after each layer is complete, the sample moves on the z-axis using a linear translation stage. The advantage of this option is speed, as galvanometric scanners can reach speeds of 5 m/s. (b) The beam remains immobile, and the sample moves by high-resolution xyz stages. In this case the stages move in all three directions. The advantage of this method is accuracy, which, depending on the stages used, can be down to the nm range. In practice, it is very common to have both galvanometric scanners and high-resolution stages in one system and switch between them depending on the requirements of a specific application.

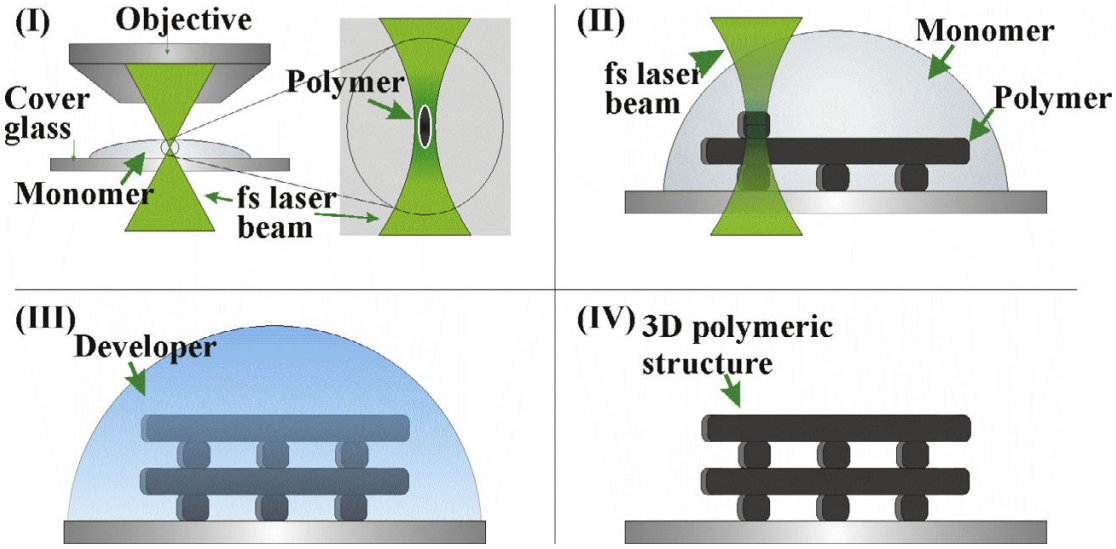

Figure 1. 8: MPL experimental procedure. (I) The laser beam is focused inside the volume of the resin. (II) The beam moves relatively to the sample following a computer-generated design. (III) After laser writing, the sample is immersed into a solvent. (IV) The freestanding structure is revealed.[52]

3. Microscope objective: The diameter of the focused laser beam is given by the equation

$$d \approx \frac{2\lambda}{\pi * NA}$$

where λ is the laser wavelength and NA is the numerical aperture of the microscope objective used to focus the laser beam. In order to have high resolution, high NA objectives need to be employed. If the NA of the objective is higher than 1, then a matching-index oil is required between the objective and the sample.

4. Beam intensity controllers : The output power of the laser used in MPL often cannot be controlled directly. This can be done using manual or motorized attenuators (neutral density filters or a combination of a polarizer and a waveplate).

5. Control software: The optical and mechanical components described above need to be controlled centrally and synchronized using an appropriate software.

The experimental procedure for fabricating a 3D structure by MPL is shown in **figure 1.8.**

In order for a material to be suitable for MPL, it should fulfill the following requirements:
1. It should contain monomers, oligomers or a mixture of those, which will be linked through the MPL process to provide the final polymer backbone making up the polymer structure.

2. It should be completely transparent to the wavelength of the laser used to carry out MPL.
3. There should be at least one solvent that dissolves the monomer but not the final polymer, in order to allow structure development and the removal of the unpolymerized resin.
4. The multi-photon polymerization threshold of the resin should be lower than its ablation threshold.

References

1. R. Langer et. al., *Science*, **1993**, 14, 920.
2. C. Masonet. al., *Regen. Med.*, **2008**, 3, 1.
3. V. Mironov et. al., *trends in biotechnol.*, **2003**, 4, 157.
4. J. Drury et. al., *Biomaterials*, **2003**, 24, 4337.
5. D. Huh et. al., *Trends Cell Biol.*, **2011**, 21, 745.
6. C. Agrawal, *J Biomed Mater Res.*, **2001**, 55, 141-50.
7. A. Caplan et. al., *J. Cell. Physiol.*, **2007**, 213, 341.
8. Y. Chen et. al., *Int. J. Biochem. Cell Biol.*, **2008**, 40, 815.
9. M. Dominici et. al., *Cytotherapy*, **2006**, 8, 315.
10. A. Uccelli et. al., *Best Pract. Res. Clin. Haematol.*, **2011**, 24, 59.
11. P. Van der Kraan et. al., *Osteoarth. Cartil*., **2002**, 10, 631.
12. F. Chen et. al., *Biomaterials*, **2010**, 31, 6279.
13. N. Patel et. al., *Int. J. Emerg. Technol. Adv. Eng.*, **2012**, 2, 91.
14. I. Armentano et. al, *Polym. Degrad. Stab*., **2010**, 95, 2126.
15. A textbook on Biomaterials, ch-1, p, 9-10.
16. A. Enas, *Res. Adv. Res*., **2015**, 6, 105-121.
17. C. Lin et. al., *Pharm. Res.*, **2009**, 26, 631.
18. S. Oh et. al., *Biomaterials*, **2007**, 28, 1664.
19. V. Melissinaki et. al., *Biofabrication*, **2011**, 3, 045005.
20. L. Gabriel et. al., *Nanomedicine*, **2017**, 13, 201.
21. H. Zhou et. al., *Acta biomater.*, **2011**, 7, 2769.
22. S. Samavedi et. al., *Acta biomater.*, **2013**, 9, 8037.
23. M. Chatzinikolaidou et. al., *Mater. Sci. Eng. C*, **2015**, 48, 301.
24. A. Khorasani et. al., *J. Biomater. Tissue Eng*, **2015**, 5, 593.
25. J. Ramshaw et. al., *Biotechnol. Genet. Eng. Rev.*, **1996**, 13, 335.
26. J. Rose et. al., *Materials*, **2014,** 7, 3106.
27. P. Janmey et. al., *J. R. Soc. Interface*., **2008**, 6, 1.
28. S. Madihally et. al., *Biomaterials*, **1999**, 20, 1133.
29. D. Allison et. al., *Tissue. Eng.*, **2006**, 12, 2131.
30. J. Venkatesan et. al., *Int. J. Biol. Macromol*., **2015**, 72, 269.
31. E. Engel et. al., *trends in biotechnol.*, **2008**, 26, 39.
32. A Systems Approach to Engineering Concepts **2017**, ch.9, 205-238.
33. G. Tripathi et. al., *ceramics international*, **2012**, 38, 341.

34. A Systems Approach to Engineering Concepts **2017**, ch.8, 185-204.
35. K. Prasad et. al., *Materials,* **2017**,10, 884.
36. A Systems Approach to Engineering Concepts **2017**, ch.7, 159-185.
37. J. Glowacki et. al., *Biopolymers,* **2008** 89, 338.
38. M. Echave et. al., *Curr. Pharm. Des.*, **2017**, 23, 3567.
39. A. Brown et. al., *acta biomaterialia,* **2014**, 10, 1502.
40. F. Croisier et. al., *Eur. Polym. J.*, **2013**, 49, 780.
41. J. Venkatesan et. al., *Int. J. Biol. Macromol.*, **2015**, 72, 269.
42. Z. Zhu et. al., *Plast. Aesthet. Res.*, **2017**, 4, 219.
43. A. Selimis et. al., *Microelectronic Engineering*, **2015**, 132, 83.
44. W. Kaiser et. al., *Phys. Rev. Lett*., **1961**, 7, 229.
45. J. Xing et. al., *Chem. Soc. Rev*., **2015**, 44, 5031.
46. Laser technology in biomimetics, Direct laser writing, **2013**, 13-65.
47. C. Kowollik et. al., *Angew. Chem. Int. Ed*., **2017**, 56, 15828.
48. C. Decker et. al., *J. Coat. Technol.*, **1987**, 59, 97–106.
49. K. Haraguchi et. al., *Adv. Mater.*, **2002**, 14, 1120–1124.
50. A. Ciuciu et. al., *RSC Adv.***, 2014**,4, 45504.
51. Polymer and photonic Materials Towards Biomedical Breakthroughs, Polymer Processing Through Multiphoton Absorption, 49-69.
52. A. Selimis et al., *Microelectron. Eng*., **2015**, 132, 83.

Chapter 2

Initiator free, multiphoton polymerization of gelatine methacrylamide

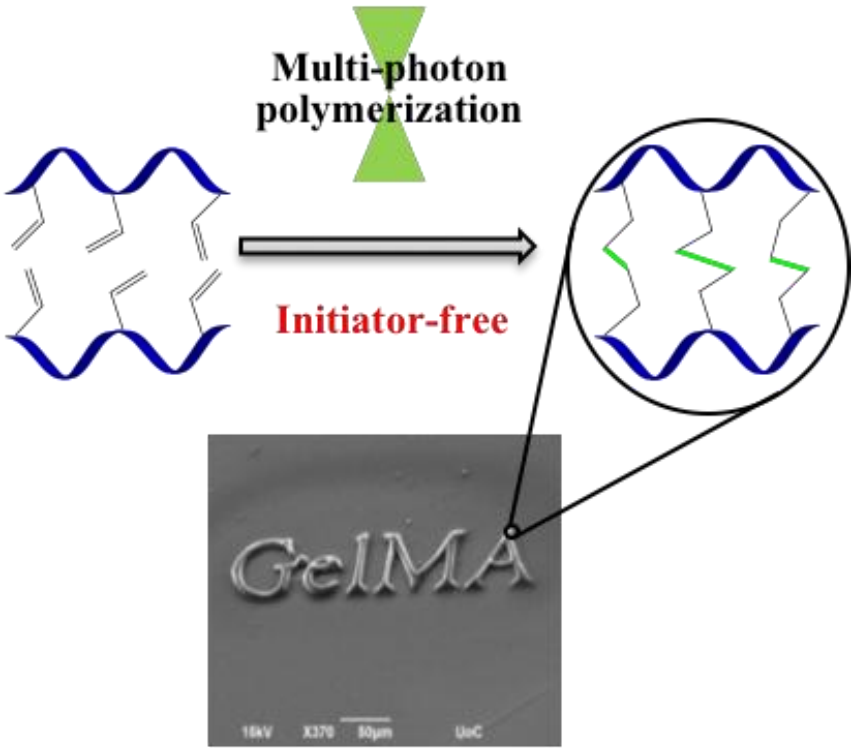

1. Introduction

3D cell cultures have attracted particular attention lately in TERM as they mimic more closely compared to their 2D counterparts, the cell environment and tissue regeneration processes in native tissues[1]. Hydrogels, derived both from synthetic and natural polymers, have attracted immense attention in the last decades for biomedical applications, due to their physicochemical as well as their biological properties[2-4]. Hydrogels are 3D hydrophilic, polymer networks which are insoluble in solvents due to the presence of covalent or physical crosslinks between the chains, but they can absorb a huge amount of water or biological fluid and become swollen. These kinds of networks comprese homopolymers or copolymers, resulting in a plethora of materials with diverse properties[5]. Hydrogels' characteristic features, comprising a cross-linked network of polymer chains with a high fluids content and increased elasticity, mimic very closely the soft tissue and the ECM and constitute a friendly microenvironment for the growth of cells and tissues. Thus, hydrogels are used in the field of medicine[6], cosmetic[7], drug delivery[8], TE[9] and RM[10]. While natural polymers provide the closest imitation to the ECM, they don't have the mechanical properties required to act as 3D scaffolds. To overcome this problem, researchers chose to modify natural polymers. This can be done by linking (meth)acrylate/(meth)acrylamide groups to the natural polymers. By this modification the biocompatibility, biodegradability as well as the mechanical properties, of the polymers are guarantee. The most widely used modified natural polymer, in MPL, is gelatin methacrylamide (GelMA). The modification of gelatin to bear methacrylamide moieties, was first reported by Van Der Bulcke et al. and has been the most commonly employed approach so far. It involves the reaction of the amine groups of gelatin with methacrylic anhydride to produce a gelatin methacrylamide derivative which can be photo-cross-linked to give a 3D hydrogel microenvironment for cell adhesion and proliferation[11]. The multi-photon-cross-linking of GelMA to fabricate three-dimensional scaffolds was first reported by Ovsianikov et al., who studied the biodegradability of the scaffold [12] and the cell behavior on the 3D structures[13]. Several approaches were investigated to improve the mechanical properties of the obtained hydrogel[14], among which was the increase of the intensity of the laser beam. However, that was shown to reduce the cell adhesion on the 3D scaffolds[15]. In most cases, MPP is based on a free radical polymerization/cross-linking mechanism[16], which requires the use of a photoinitiator (PI), apart from the monomer, to initiate the reaction by the production of free radicals following a multi-photon absorption. However, it is well known that the PIs and the derived free radicals are endogenous to the cells as they cause deadly changes to the cell's components[17]. In a pioneering work Ovsianikov and coworkers studied the *in situ* photo-cross-linking of GelMA and showed that the radiation of the laser beam at 800 nm, was harmless to the cells, however, the free radicals produced by the photoinitiators induced cell death[18]. The same group, recently, managed to

synthesize a non toxic disulpho based photoinitiator, which was used for the *in situ* polymerization of GelMA with great cell viability during and after MPP[19].

In this chapter, the fabrication of 3D GelMA scaffolds using MPL in the absence of a photoinitiator is reported. This was achieved by employing a green femtosecond laser at 520 nm, which produces high energy photons for the direct multi-photon absorption and cleavage of the double bonds of the photopolymer. The proposed approach is biologically friendly due to the avoidance of the toxic PIs and the highly mobile free radicals produced by them. Therefore, it is envisaged that the process will be highly advantageous in the *in-situ* fabrication of 3D scaffolds in the presence of cells since the only source of free radicals in the material will be the photo-cross-linkable polymer, GelMA, which produces radicals of low diffusion rates and therefore low cytotoxicity. The 3D GelMA structures were characterized by scanning electron microscopy (SEM). Furthermore, the viability of NIH-3T3 fibroblast cells on the 3D scaffolds was investigated.

2. Experimental

2.1 Materials

Gelatin from bovine skin, gel strength ~225 g Bloom, type B, methacrylic anhydride (MAA) 94%, deuterium oxide (D_2O) 99.9 % atom D, phosphate buffered saline (PBS), 3-(trimethoxysilyl)propyl methacrylate, Triton X-100 and paraformaldehyde (PFA) were purchased from Sigma-Aldrich. 1,2,3-Indantrione monohydrate ninhydrin was obtained from Fluka. Dulbecco's modified Eagle's medium (DMEM) was purchased from GIBCO, Thermo Fisher Scientific, Inc., Waltham, MA, USA. Fetal bovine serum (FBS) and Bovine Serum Albumin (BSA) were obtained from Biosera, France. The LIVE/DEAD® Viability/Cytotoxicity Kit for mammalian cells, the antifade reagent containing DAPI (ProLong™ Gold Antifade Mountant) and the Alexa Fluor 568 Phalloidin and the Trypsin/EDTA (0.25%) solution were purchased from Invitrogen, Thermo Fisher Scientific, Inc., Waltham, MA, USA.

2.2 Photopolymer synthesis

GelMA was synthesized following the procedure reported earlier by Van Den Bulcke et al.[11]. Briefly, a 10 w/v% solution of gelatin in phosphate buffer saline (PBS) was prepared at 50 ℃. Methacrylate anhydride was added to the gelatin solution at a 0.1:1 ratio (mL of MAA to g of gelatin), at 50 ℃ under continuous stirring. The reaction was allowed to proceed for 3h before diluting the solution with excess PBS (**figure 2. 1.a**.) The mixture was dialyzed against nanopure water, using a 3500 kDa dialysis membrane, at 40 ℃ for 7 days in order to remove the unreacted MAA and the methacrylic acid by-product of the reaction. Finally, the pure product was recovered by lyophilization and was stored at 4 ^{o}C until further use.

2.3 Photopolymer characterization

The modification of gelatin was confirmed using proton nuclear magnetic resonance (^{1}H NMR) spectroscopy. The samples were dissolved in deuterium oxide (D_2O) at 50 ℃. High-resolution ^{1}H NMR spectra were acquired on a Bruker Advance 500 MHz spectrometer at 50 ℃. The degree of modification (DM), defined as the change of the ratio of the peak integrals attributed to the methylene protons of lysine and hydroxylysine, to the protons of phenylalanine, that remained constant during the reaction, was determined, **figure 2. 1b**.

The DM was also determined by the ninhydrin assay, percentage decrease of the free primary amine groups of lysine and hydroxylysine of gelatin. Briefly, the reaction of ninhydrin with the free amino groups, at 100 ℃, leads to a purple compound, with a characteristic absorption at 570 nm. Comparison of the absorption intensity at 570 nm for the two samples, unmodified and modified gelatin, at the same polymer concentration allowed to calculate the concentration of free amino groups in the two samples using a calibration curve **figure 2. 2**. The DM was calculated from the absorption intensities at 570 nm using the following formula:

$$\% \text{ DM} = \frac{absorption\ of\ gelatin - absorption\ of\ GelMA}{absorption\ of\ gelatin} * 100 \qquad (1)$$

A Perkin Elmer Lambda 25 UV/Vis spectrometer was employed to record the UV/Vis absorption spectra of the samples.

2.4 Scaffold fabrication using MPL

Lyophilized GelMA was dissolved in nanopure water at a 30 w/v% concentration at 40 ℃. The samples were prepared by drop casting the above solution onto 100 μm thick glass substrates silanized with 3-(trimethoxysilyl)propyl methacrylate.

The experimental setup used for the MPL fabrication of the 3D structures has been described in chapter 1. Briefly, a diode pumped solid state laser emitting at 1040 nm was employed as the light source. A NLO crystal was used to acquire the 2nd harmonic, which corresponds to 520 nm. The repetition rate was 1 MHz and the pulse duration 450 fs. The laser beam was tightly focused into the volume of the photosensitive biopolymer using a 20x microscope objective lens with a NA of 0.8 (Zeiss, Plan Apochromat). Sample movement in the xy plane was achieved using a x-y galvanometric mirror digital scanner (Scanlabs Hurry-Scan II), while for the z axis linear stages (Physik Instrumente) were employed. The MPL procedure was controlled by a computer using the SAMlight software. The structures were fabricated in a layer-by-layer process with the last layer attached to the glass substrate.

Three different scaffold designs were fabricated. The first one comprised a rectangular matrix of square-shaped 3D pores with dimensions 500x500x50 μm^3 **figure 2. 3a**. The structures were fabricated in 25 layers with an interlayer distance of 2 μm. The second scaffold consisted of a rectangular base with 9 rectangular pillars, 3

on each line **figure 2. 3b**. The dimensions of the structure were 250x250x35 μm^3 and comprised 35 layers with an interlayer distance of 1 μm. The third scaffold was a Locky ball shape scaffold. The dimensions of the structure were 1000x1000x100 μm^3 **figure 2. 3c**.

The appropriate energy and velocity for the fabrication of each structure, was selected by scanning these parameters until well-defined structures of appropriate precision were obtained in a few minutes writing time. The appropriate energy-velocity combinations for the three structures described above were found 28/3000, 30/2500 mW-μm/s and 35/2500 mW-μm/s, respectively. Following the completion of the fabrication process, the samples were developed in water at 40 ℃ for 30 min.

The fabricated 3D structures were characterized using SEM, **figure 2. 3 degh** and optical microscopy, **figure 2. 3 f,i.** For SEM characterization, the samples were sputter-coated with a 10 nm thick layer of gold using a sputter coater (Baltec SCD 050) and were observed under a scanning electron microscope (JEOL JSM-6390 LV) at an accelerating voltage of 15 kV.

2.5 Cell culture

Murine fibroblast cell line NIH-3T3, was maintained in DMEM, supplemented with 10% fetal bovine serum at 37 °C in a 5% CO_2 atmosphere. Confluent cells were washed with 1x PBS, passaged after trypsinization (0.25% trypsin in 1 mM EDTA) and cultured on the GelMA-based 3D structures. 2 ml of the cell suspension (6.5×10^5cells/ml) was added in each well, containing the GelMA 3D scaffolds, of a 12 well plate and were cultured for 6 days.

2.6 Cell viability assay

The cell viability on gelatin and GelMA films was investigated using the LIVE/DEAD® Viability/Cytotoxicity Kit, according to the manufacturer's protocol. The samples were prepared by drop casting aqueous solutions of gelatin and GelMA on glass substrates and allowing the samples to dry overnight at RT. Next, 2 ml of the cell suspension (5×10^5cells/ml) were cultured on the polymer films. After 12 hours of cultivation the seeded films were incubated for 30-45 min at room temperature in the presence of 2 μl calcein AM (staining live cells green) and 4 μl ethidium homodimer (EthD-1, staining dead cells red). Cell imaging was performed using an epifluorescence microscope coupled to a high-resolution Carl Zeiss Axiocam colour camera.

2.7 Immunocytochemical assays

Fibroblast cells were stained for F-actin. For this, the cultured cells were fixed with 4% PFA for 15 min and permeabilized with 0.1% Triton X-100 in PBS for 5–7 min. The non-specific binding sites were blocked with 2% BSA in PBS for 30 min. Then, the cells were incubated for 60 min, with Alexa Fluor 568 Phalloidin (1:60 in a 1% PBS–BSA solution) which stains F-actin.
Next, the F-actin stained samples were washed twice with PBS and were mounted on coverslips with antifade reagent containing DAPI for nuclei staining. Cell imaging was performed using an epifluorescence microscope coupled to a high-resolution Carl Zeiss Axiocam colour camera.

3. Results and discussion

3.1 Material synthesis and characterization

The modification of the free amino groups of the lysine and hydroxylysine residues of gelatin was carried out using MAA to produce a photo-cross-linkable gelatin biopolymer bearing methacrylamide moieties. The synthetic procedure followed for the preparation of the photo-cross-linkable biopolymer is shown in **figure 2. 1a**.
The successful synthesis of the functionalized polymer was confirmed by ^{1}H NMR spectroscopy. The ^{1}H NMR spectra of unmodified gelatin and GelMA are presented in **figure 2. 1b**. The appearance of two new peaks in the spectrum of GelMA, H_a and H_b at 5.65 and 5.41 ppm, respectively attributed to the vinylic protons of the methacrylamide moiety, verified the successful functionalization of the biopolymer. Furthermore, the DM was quantified by comparing the peak integrals of the methylene protons of hydoxylysine, H_c at 2.95 ppm, and lysine, H_d at 2.65 ppm, to the aromatic protons of phenylalanine, H_e at 7.3 ppm, in the NMR spectra of gelatin and GelMA. The ratio of the integrals of the peaks of H_c and H_d to the peak H_e was found 3.6 and 3.2, respectively for the unmodified gelatin. These ratios decreased to 1.6 and 0.9 for GelMA suggesting a 55% and 72% modification of the lysine and hydroxylysine residues, respectively and a total of 63% functionalization of the amino groups in the modified biopolymer[20,21].

(a)

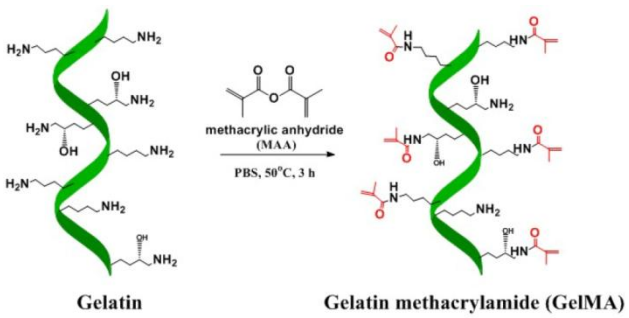

(b)

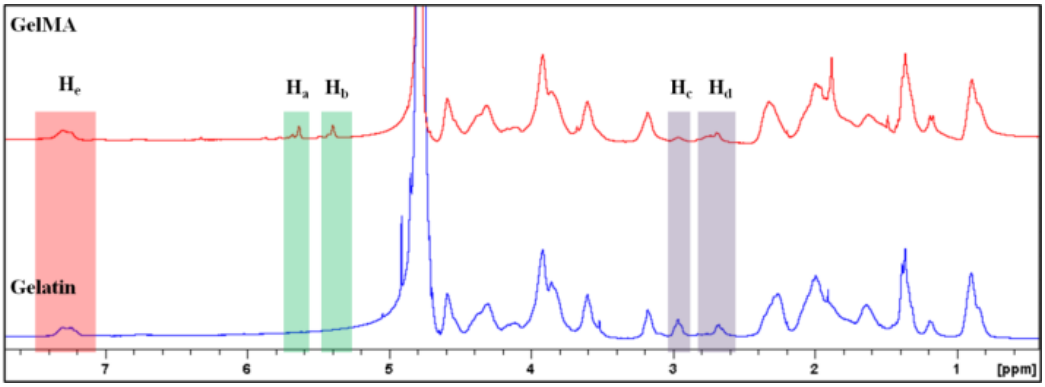

Figure 2. 1: (a) Schematic representation of the reaction employed for the synthesis of GelMA and (b) ^{1}H NMR spectra of gelatin and GelMA in D_2O.

The ninhydrin assay, which quantifies the free amino groups of a sample, was also employed to determine the DM of gelatin, **figure 2. 2**. By comparing the free amino groups on the biopolymer before and after modification with MAA, the DM was calculated from equation (1) at 66% which is in good agreement with the ^{1}H NMR results discussed above.

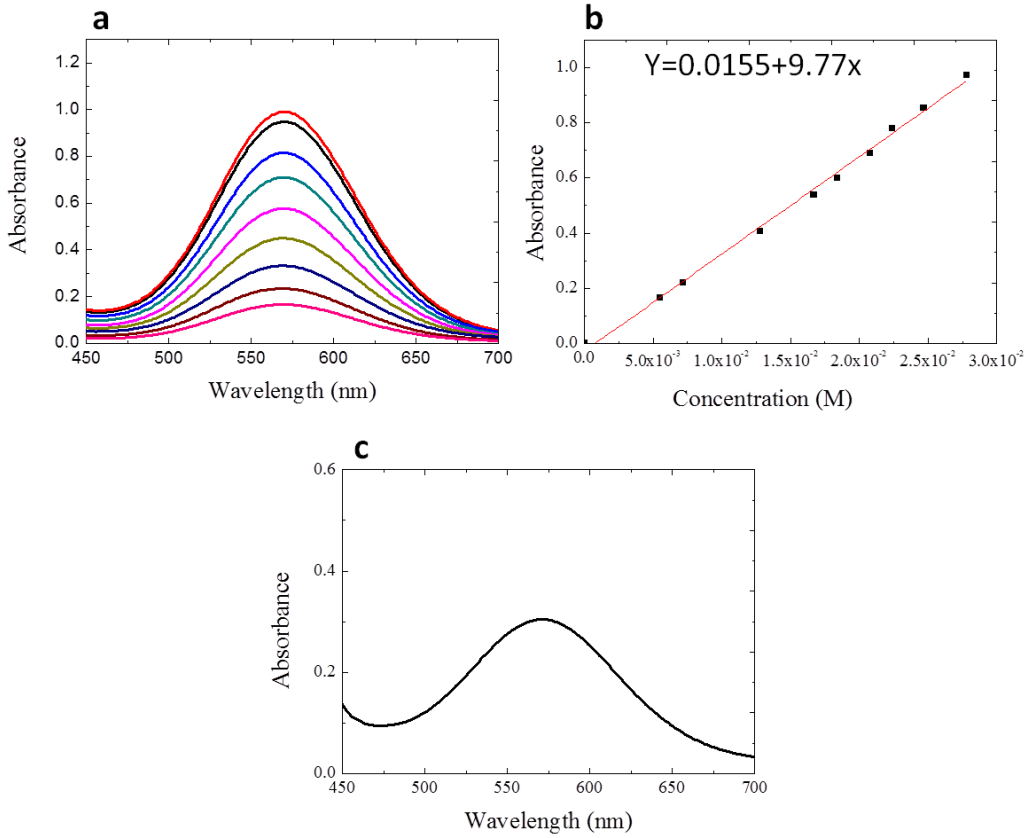

Figure 2. 2: (a) UV/vis spectra of the ninhydrin derivative produced in different gelatin concentration solutions in water, (b) calibration curve for the ninhydrin derivative as a function of the gelatin concentration and (c) UV/vis spectrum of the ninhydrin derivative produced in a 2.6x10-2 M GelMA solution in water.

Next, GelMA was deposited on a glass substrate by drop casting from a 30% solution in water without photoinitiator and 3D structures (**figure 2. 3a-c**) were fabricated by MPL at 520 nm using an appropriate energy- speed combination for each 3D structure design (see discussion above in the Experimental section), followed by development in water at 40 °C for 30 min.

Figures 2. 3 d,e,g,h show SEM images of the fabricated 3D structures. As seen in these images, the structure design has been imprinted accurately, both in details and dimensions, with sufficient precision despite the absence of the photoinitiator. Highly robust and mechanically stable 3D structures were obtained, suggesting a high degree of cross-linking of the photopolymer and therefore, an efficient cross-linking process upon irradiation at 520 nm in the absence of a photoinitiator.

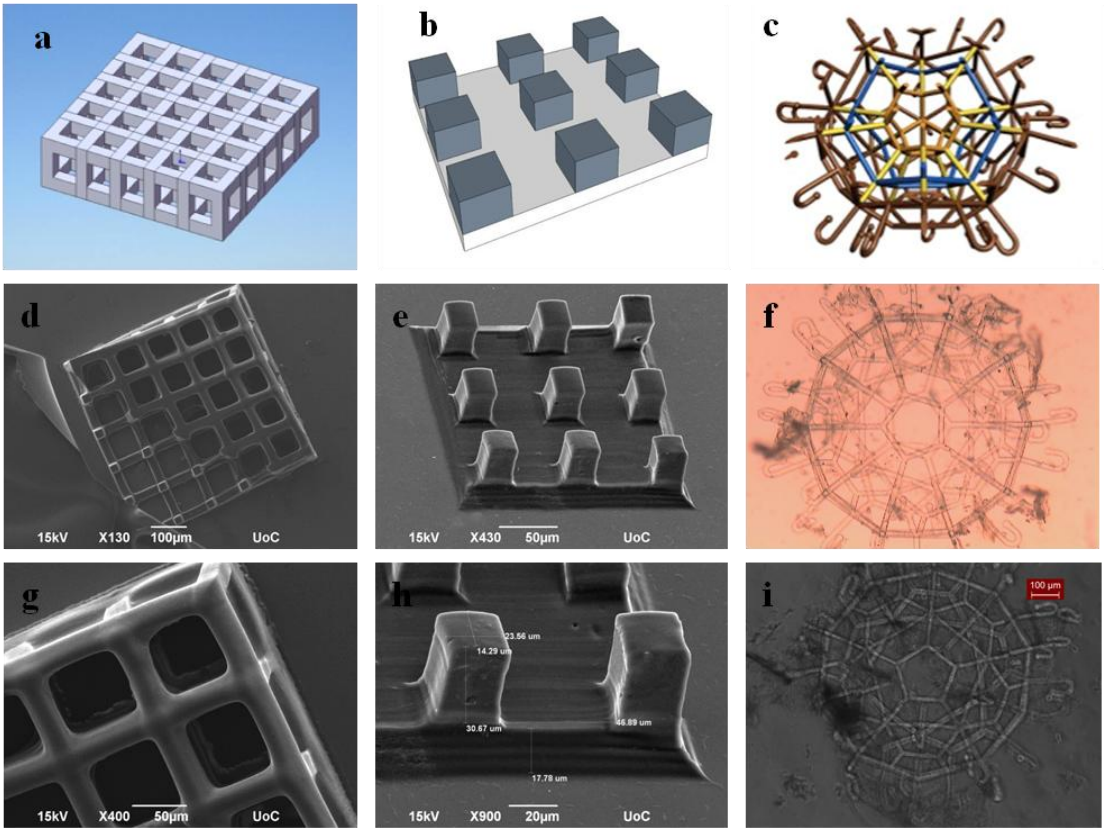

Figure 2. 3: Structure designs of (a) a rectangular matrix of square-shaped 3D pores, (b) a rectangular base with 9 rectangular pillars and (c) Locky ball; the 3D GelMA structures fabricated by MPL, without PI, using a 20× plan achromat lens (N.A. = 0.8) at a (d) 28 mW laser power and writing speed 3000 μm s^{-1}, (e) 30 mW laser power and writing speed 2500 μm s^{-1} and (f) optical microscopy image of locky ball shape scaffold with 35 mW laser power and writing speed 2500 μm s^{-1} (g) and (h) are high magnification images of the 3D scaffolds shown in (d) and (e), respectively, (i) optical microscopy image of locky ball shape scaffold

The SEM characterization of locky balls shape 3D scaffolds was not possible, due to the deformation of the scaffolds, **figure 2. 4**. Scaffolds deformation was attributed, first to the soft organic nature of the photopolymer and second to the processing of the samples under high vacuum for observation by SEM. During this drying step, water is removed from the GelMA hydrogel and the samples become dehydrated causing the deformation of the structures.

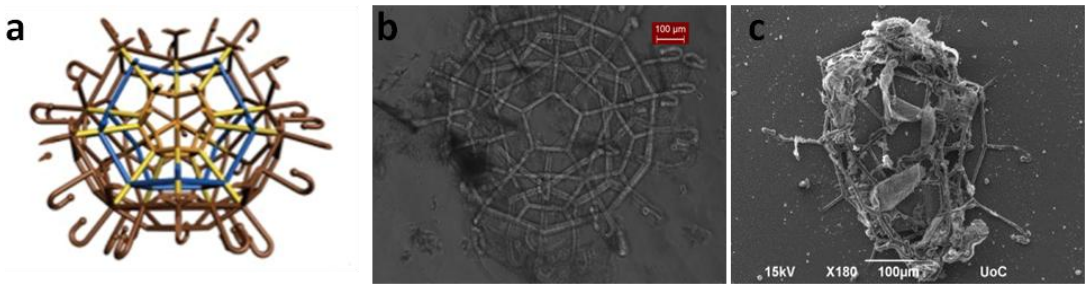

Figure 2. 4: (a) Structure design of a locky ball, (b) optical microscopy image and (c) SEM image of the deformed scaffold.

To the best of our knowledge, this is the first report on the photo-cross-linking of GelMA in the absence of a photosensitizer. To investigate further the photo-cross-linking process, the absorption spectra of GelMA and the unmodified gelatin were obtained **figure 2. 5**. As seen in the inset of **figure 2. 4** the absorption of gelatin drops to almost zero above ~240 nm, whereas after modification of gelatin with MAA, an increase of the absorption intensity between 240 and 260 nm is observed for GelMA. Since the laser operation is at 520 nm, and the material does not absorb in this wavelength see **figure 2. 4**, it is suggested that the functional methacrylamide moieties are activated by multi-photon absorption, resulting in the cleavage of the vinyl double bonds and their direct addition to the double bond of another merthacrylamide moiety leading to the cross-linking process. A similar mechanism has been proposed by Knolle et al. for the direct photopolymerization of acrylates in the absence of a photoinitiator using a 222 nm excimer radiation from a $KrCl^*$ laser[22]. At this wavelength, a triplet state localized on the vinyl bonds of the acrylate monomers was formed by a one photon adsorption process, which led to a biradical following addition of the triple state to the vinyl bond of a second monomer. Such a triplet radical formation is probably the first step in the photo-cross-linking process of GelMA reported in the present study.

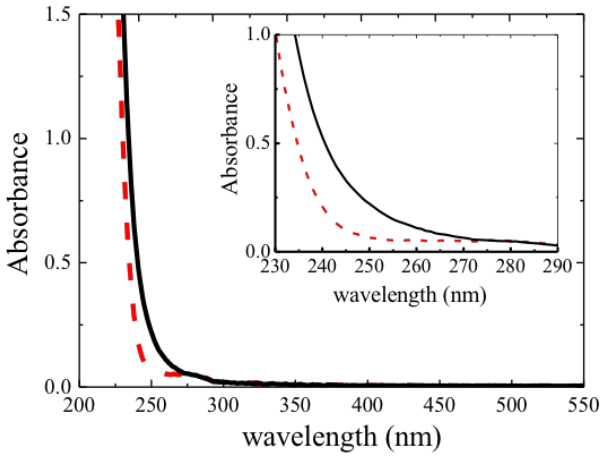

Figure 2. 5: UV/vis spectra of gelatin (red dash line) and GelMA (black solid line) films on a quartz substrate. The inset shows the magnification in the 230 to 290 nm range.

3.2 Biological studies

The biocompatibility of GelMA was assessed in fibroblast cell cultures using the live/dead assay. Two different polymer films were used as cell substrates. The first, comprised unmodified gelatin and was treated as the biocompatible, control substrate for the growth of the fibroblasts. The second, was a GelMA film deposited on a glass substrate. The same cell number (2 ml of a 5×10^5 cells/ml cell suspension) was added on both samples and the cells were cultivated for 12 h before observation by fluorescence microcopy. **Figure 2.6** verifies that the GelMA film supports cell growth equally well to the biocompatible gelatin film and after 12 hours of cultivation all cells are alive (green) and no dead (red) cells were observed neither for the gelatin nor for the GelMA sample.

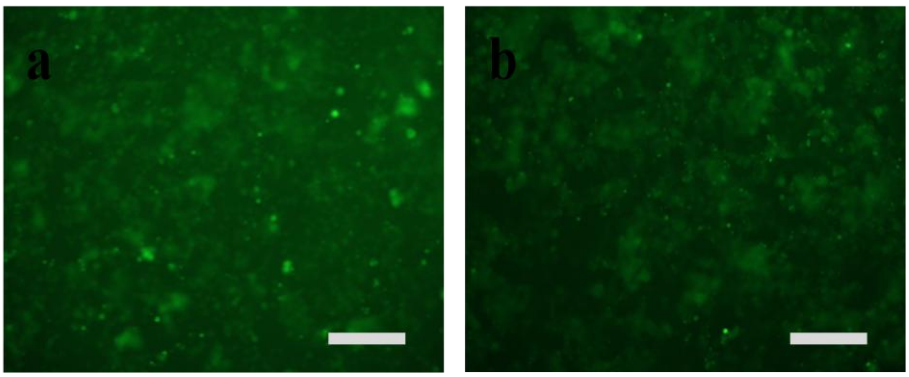

Figure 2. 6: Live/dead assay of fibroblast cells cultured for 12 h on (a) contractual cell culture (unmodified gelatin) and (b) GelMA. Scale bar represents 100 μm, a ×20 objective was used.

Next, the 3D structures fabricated using the above biologically relevant approach, in the absence of toxic photoinitiators, were investigated as biocompatible scaffolds for 3D cell culture. The combination of a non-toxic, proteinaceous biopolymer with the 3D architecture resembles closely the physiological conditions in which the cells grow in living organisms and is very attractive for *in vitro* cell cultures.

The adhesion and growth of NIH-3T3 fibroblast cells on the 3D structures was studied by culturing 2 ml of a 6.5×10^5 cells/ml cell suspension in each well of a 12 well plate containing the scaffolds. The cells were cultured on the scaffolds in the presence of DMEM/10% FBS cell culture medium for 6 days. Immunocytochemistry assays allowed to visualize the cells in the 3D culture and assess their behavior on the 3D scaffolds. For the staining of F -actin, which is a protein of the cell cytoskeleton, fluorescent phalloidin was used, whereas DAPI was employed for nucleus staining. The stained cells were observed by fluorescence microscopy. The microscopy images are shown in **figure 2. 7**. **Figures 2. 7c and 7d** show the DAPI stained cell nuclei which verify that the cells have grown within the 3D scaffolds and have penetrated the porous structure spreading in all three dimensions. **Figures 2. 7e and 7f** show the F-actin stained cells which appear evenly distributed within the scaffolds, indicating that there is no preference in crop-compatible and the cells adhered similarly to the GelMA structures and the surrounding glass. In particular, it is evident from **figure 2. 7f** that the cells have spread well and adhered on the surface of the structures. This pronounced adhesion and spreading of the cell cytoskeleton verifies the compatibility of the material and the preference of the cells to interact with it. Finally, **figures 2. 7g and 7h** show the overlap of the F-actin and DAPI staining.

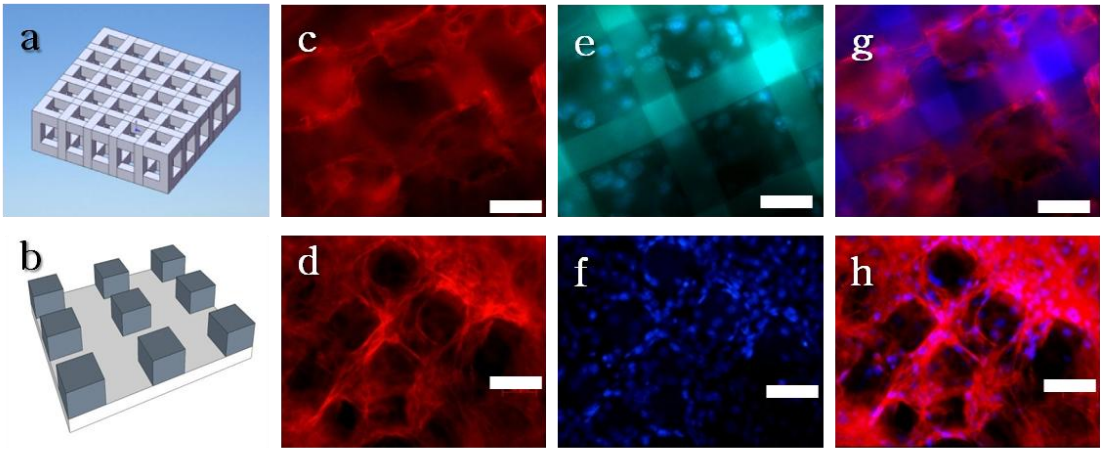

Figure 2. 7: (a) and (b) designs of the 3D structures; fluorescence microscopy images of NIH-3T3 cells cultured on the 3D scaffolds: (c) and (d) nucleus staining, (e) and (f) actin filament staining, (g) and (h) the combination of the two stainings. The cells were stained with phalloidin (red: actin filaments) and DAPI (blue: nucleus). Scale bars are 50μm.

Due to the harsh procedure followed to dry the samples by critical point drying, for the SEM characterization of the cell cultures, observation of the 3D cell cultures by SEM was not possible. **Figure 2. 8** shows the 3D cell culture onto the scaffolds, via optical microscopy.

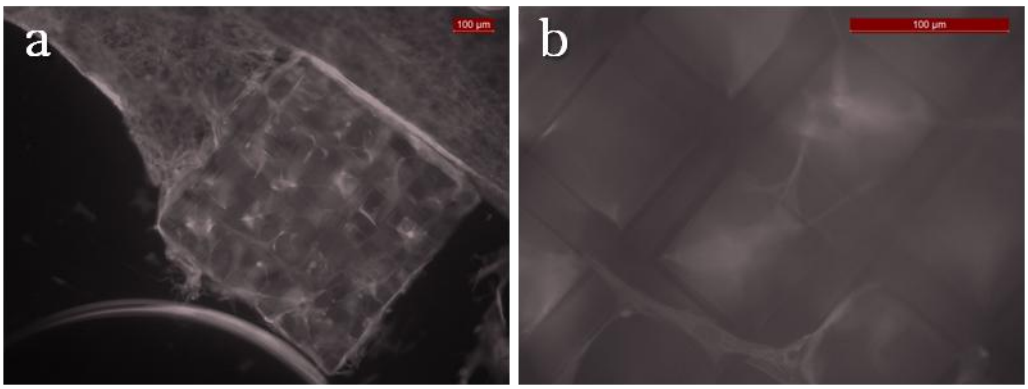

Figure 2. 8: (a) optical microscopy image of the 3D cell culture onto a rectangular matrix of square-shaped 3D pores scaffold and (b) high magnification image of the same culture.

4. Conclusions

3D structures based on GelMA were fabricated using a multi-photon, initiator-free, cross-linking process. The use of a green laser at 520 nm allowed the fabrication of precise and mechanically stable 3D structures, in the absence of a toxic PI via the formation of the triplet state of the methacrylamide vinyl bonds via multi-photon absorption. At the same time, the use of high writing velocities enabled the fabrication of 3D scaffolds in 5 to 20 mins. The elimination of the PI, and the highly diffusive free radicals derived from the initiator during the polymerization/cross-linking process, along with the use of a proteinaceous biopolymer hydrogel that mimics the ECM, render these scaffolds particularly attractive for cell adhesion and growth[23]. Future work will exploit the use of this approach for the *in-situ* fabrication of biocompatible 3D scaffolds in the presence of living cells for tissue engineering applications.

5. References

1. B. Klotz et. al., *Trends Biotechnol.*, **2013**, *34*, 394.
2. J. Torgersen et. al., *Adv. Funct. Mater.*, **2013**, 23, 4542.
3. B. Slaughter et. al., *Adv. Mater.* **2009**, 21, 32.
4. M. Tibbitt et. al., *Biotechnol. Bioeng.*, **2009**, 103, 655.
5. N. Peppas et. al., *Eur. J. Pharm. Biopharm.*, **2000**, 50, 27.
6. J. Rosiak et. al., *Nucl. Instrum. Methods Phys. Res. Sec. B*, **1999**, 151, 56.
7. M. Parente et. al., *Int. J. Cosmet. Sci.*, **2015**, 37, 511.

8. T. Hoare et. al., *Polymer*, **2008**, 49, 1993.
9. E. Sherbiny et. al., *IM. Glob. Cardiol. Sci. Pract*., **2013**, 3, 316.
10. B. Slaughter et. al., *Adv. Mater*., **2009**, 21, 32.
11. B. Van Den et. al., *Biomacromolecules*, **2000**, *1*, 31.
12. A. Ovsianikov et. al., *Materials*, **2011**, *4*, 288.
13. A. Ovsianikov et. al., *Biomacromolecules*, **2011**, *12*, 851.
14. J. Van Hoorick et. al., *Biomacromolecules*, **2017**, *18*, 3260.
15. A. Brigo et. al., *Acta Biomate.*, **2017**, *55*, 373.
16. H. Sun et. al., *Adv. Polym. Sci.*, **2004**, *170*, 169.
17. S. Bryant, et. al., *J. Biomater. Sci., Polym. Ed.*, **2000**, *11*, 439.
18. A. Ovsianikov et. al., *Langmuir*, **2014**, *30*, 3787.
19. M. Tromayer et. al., *Polym. Chem.*, **2018**, 9, 3108.
20. X. Li et. al., *Polymers*, **2016**, *8*, 269.
21. G. Brown et. al., *Macromol. Biosci.*, **2017**, *17*, 1700158
22. W. Knolle et. al., *Radiat. Phys. Chem.*, **2003**, *67*, 341
23. K. Parkatzidis et. al., *Mac. Biom. Eng.*, **2018**, 1800458.

Chapter 3

Near IR light photopolymerization of a hybrid GelMA-chitosan modified biomaterials: Towards a highly biocompatible bioink.

1. Introduction

The success of TERM is based on the choice of the 3D matrix to support the adhesion, proliferation and differentiation of cells.[1] The chemical composition, the physical and mechanical properties, the biodegradability, biocompatibility, and functionality of the 3D scaffolds are crucial characteristics in TERM applications. Chitosan, commonly found in the shells of marine crustaceans, the cell walls of fungi and in the arthropod exoskeleton,[2-4] is the deacetylated derivative of chitin, and compreses a linear polysaccharide consisting of N-acetyl D-glycosamine and D-glycosamine units[5] Chitosan's biocompatibility[6 biodegradability, antimicrobial properties[7], capacity to stimulate macrophages and induce bone formation[8] and its interactions with negatively charged molecules such as glycosaminoglycans (GAGs) and proteoglycans are the main reasons to account for its widespread use as a biomaterial scaffold. On the other hand, gelatin, is derived from collagen, and comprises another widely studied natural biomaterial that promotes cell adhesion, proliferation, migration, and differentiation[9]owing to the Arg-Gly-Asp (RGD) sequence derived from collagen[10]. Previous reports on the use of chitosan/gelatin blends as cell scaffolds indicate an enhancement of the biological response compared to pure chitosan[11] ,demonstrating positive results in TERM applications, such as skin, cartilage and bone regeneration, due to their biocompatibility, biodegradability, and low antigenicity. However, the mechanical instability of the chitosan/gelatin scaffold structures in aqueous solutions limits their applications for long term implantation in vivo. This limitation can be overcome by the modification of these biopolymers and their chemical crosslinking. Photo-crosslinking, a type of chemical crosslinking, is performed in the presence of ultraviolet (UV) light and a photoinitiator (PI). A variety of macromers, such as methacrylated derivatives of natural or synthetic polymers, have been used to form hydrogels by photo activation in the presence of photoinitiators[12].However, UV light is known to be hazardous to cells causing DNA damage and cancer[13]. Therefore, in the last years there has been a shift in the photopolymerization, towards the visible light and/or near IR, in order to avoid the harmful effects of UV irradiation. These studies have demonstrated that the combination of visible and/or near IR light and safer photoinitiators for the crosslinking reaction, can enhance the utility of photocrosslinkable hydrogels in TERM applications. Additionally, visible and/or near IR light has been shown to penetrate deeper into the tissues and has lower energy, compared to UV light[14]. Among the different photoinitiators eosin Y is Food and Drug Administration (FDA)-approved and is excited by visible light (450–550 nm). In MPP, there is great deal for water soluble, biocompatible, photoinitiators which can used at the wavelength of 800

nm. There are also a few studies which demonstrate the use of eosin-Y, riboflavin and rose bengal as water soluble type II photoinitiators[15] However, these studies used 520 nm or 1040 nm laser irradiation[16] . To the best of our knowledge, there is no study in the literature using eosin-Y as photoinitiator at 800 nm, which is the most extensively used wavelength in MPL setups.
In our study, we have modified both gelatin and chitosan to bear photopolymerizable vinyl bonds. These biomaterials were used in the formation a hybrid material which was photostructured by MPP. In addition, water soluble, FDA-approved eosin-Y was used as the photoinitiator, for MPP, producing biocompatible and well-defined 3D scaffolds with good mechanical properties. Biological studies were performed using Dental Palm Stem Cells, which showed excellent biocompatibility and 3D culture formation rendering the fabricated scaffolds attractive for dental TERM applications.

2. Experimental

2.1. Materials

Gelatin from bovine skin, gel strength ~225 g Bloom, type B, methacrylic anhydride (MAA) 94%, Maleic anhydride (MA) 98%, Glycidyl methacrylate (GMA) 97%, deuterium oxide (D_2O) 99.9 % atom D, Trifluoroacetic acid-d (TFA-d), 99.5 atom % D, phosphate buffered saline (PBS), 3-(trimethoxysilyl)propyl methacrylate, hexamethyldisilanaze (HMDS) 99% and all solvents were purchased from Sigma-Aldrich (Steinheim, Germany) and were used without further purification. Chitosan of 30.000 gr/mol molecular weight was obtained from Glentham life science. Cell culture medium, (alpha-MEM), fetal bovine serum (FBS), antibiotic/antimycotic, glutamine, as well as the PrestoBlue® reagent were purchased from Invitrogen (Karlsruhe, Germany). Ascorbic acid, Phalloidin-Atto 488 and 4′,6-diamidino-2-phenylindole (DAPI) were obtained from Sigma-Aldrich (Steinheim, Germany) and Triton X-100 from Merck (Darmstadt, Germany).

2.2 Determination of the degree of deacetylation of chitosan

Chitosan is typically obtained by partial deacetylation of chitin. The degree of deacetylation (DD) is an important parameter which determines its properties and was determined by ^{1}H NMR spectrometry.

2.3 Synthesis of Gelatin methacrylamide (GelMA)

GelMA was synthesized as described in the experimental section of Chapter 2.

2.4 Synthesis of water soluble Chitosan-MA (C-MA)

As naturally derived chitosan shows poor water-solubility, the first step of the synthesis was performed to obtain a water-soluble derivative of chitosan. For this, low molecular wight chitosan (MW = 30000 g/mol) was modified using MA. Briefly, 1 g of 88% deacetylated chitosan was dissolved in 50 mL DMSO and was intensively stirred for 1h. Next, 2.34gr MA were added into the solution and the mixture was stirred overnigh at 45^{o}C. The product was precipitated in acetonitrile and washed several times with dionized water. The modified chitosan was dissolved again indionized water at pH 10 (adjusted using 1 M NaOH solution). Finally, Chitosan-MA was dried under vacuum and was stored in the fridge until use.

2.5 Synthesis of photopolymerizable Chitosan-MA-GMA

The water-soluble chitosan-MA was converted into a photopolymerizable product by the incorporation of photosensitive methacrylate/methacrylamide groups to the chitosan backbone using GMA as a methacrylating agent. 1 gr of chitosa-MA, was dissolved in 50ml water and 2 ml of GMA was added in the solution. The reaction was stirred overnight, at 45^{o}C. Next, the solution was precipitated in acetonitrile and was washed several times with tetrahydrofuran. Finally, the product Chitosan-MA-GMA was dried under vacuum and stored in the fridge until use.

2.6 ^{1}H NMR spectroscopy

^{1}H NMR spectra were obtained on a Bruker AMX-500 spectrometer by dissolving Chitosan in D_2O:TFA-d (1% v/v) and all the other samples in D_2O.

2.7 FT-IR spectroscopy

Attenuated Total Reflection-Fourier transform infrared (ATR-FTIR). Spectra were recorded on a Nicolet 6700 spectrometer (ThermoFisher Scientific, Waltham, MA, USA).

2.8 X-ray diffraction (XRD)

XRD patterns were collected on a Panalytical Expert Pro X-ray diffractometer, using a Cu Kα radiation (45 kv and 40 mA), from 5-40^{o} at a scan step size of 0.02^{o} and a 0.7 sec time per step.

2.9 Thermogravimetric analysis (TGA)

The biopolymers were characterized by TGA using a Perkin Elmer Pyris Diamond TG/DTA instrument. In a typical measurement, ~ 5-10 mg of the sample were placed in a platinum holder and were heated under a constant nitrogen flow from room temperature up to 600 ^{o}C at a heating rate of 10 ^{o}C/min.

2.10 Film preparation

80 μl of a 5% wt photosensitive material solution(GelMA:chitosan-MA-GMA in mass ration 1:1) in water, containing 1mM eosin-Y, were spin-coated (500rpm for 120sec and then 4000 rpm for 5 s) on 100 μm thick cover glass slips with a 13 mm diameter. For the photopolymerization, was used a 200 W mercury lamp (Oriel 6283), mounted in an arc lamp housing and powered by an arc lamp power supply. The irradiation of the sample with visible light was achieved utilizing a 400 nm long pass filter (Oriel 59472).Finally, the films were developed for 1h in dionized water at 40 ^{o}C and were dried at RT overnight.

2.11 MPP

The samples, for MPP, were prepared by drop casting an aqueous solution of the photostructurable biopolymers, in a mass ration 1:1 GelMA: chitosan-MA-GMA, onto 100 μm thick glass substrates silanized with MAPTMS. The experimental setup used for the MPL fabrication of the 3D structures has been described in Chapter 1. A Ti: Sapphire femtosecond laser (Femtolasers Fusion, 800 nm, 75 MHz, 20 fs) beam was tightly focused into the volume of the photosensitive hybrid material using a 20x microscope objective lens with NA of 0.8 (Zeiss, Plan Apochromat). Sample movement in the XY plane was achieved using an x-y galvanometric mirror digital scanner (Scanlabs Hurry-Scan II), while for the z-axis linear stages (Physik Instrumente) were employed. The MPL procedure was controlled by a computer using the SAMlight software. The structures were fabricated in a layer-by-layer process with the last layer attached to the glass substrate.

2.12 Biological studies

Dental pulp stem cells were generously provided by Prof. Athina Bakopoulou, School of Dentistry, Aristotle University of Thessaloniki from informed consent healthy donors according an approved protocol by the Institutional Ethics Committee (322/15-04-2013). DPSCs cultures were developed from wisdom teeth of young healthy donors using an enzymatic dissociation method as previously described, and immunophenotypically characterized by flow cytometry.

2.13 Cell culture

Early passages 2–4 of human dental pulp stem cells (DPSC) were grown in cell culture flasks using alpha-MEM, supplemented with glutamine (2 mM), penicillin (50 IU/ml), streptomycin (50 g/ml), amphotericin B (0.25 mg/ml), 100 μM ascorbic acid and 10% FBS in a humidified atmosphere and 5% CO_2 at 37 °C in a cell culture incubator (Thermo Scientific). Confluent cells were detached and passaged after trypsination with 0.25% trypsin-EDTA, seeded at a 90% confluence and allowed to grow for 4–5 days before the next passage.

2.14 Cell viability and proliferation assay

A suspension of $3x10^4$ cells in alpha-MEM were seeded on the specimens with film coatings from the hybrid material in (GelMA:Chitosan-MA-GMA) a 1:1 mass ratio and were placed into the cell culture incubator at 37 °C. On days 2, 4, and 7 post seeding, the cell viability and proliferation assay was performed with the resazurin-based PrestoBlue® reagent according to the manufacturer's instructions. The reagent was incubated on the cells at 37 °C for 60 min. The absorbance was measured in a spectrophotometer (Synergy HTX Multi-Mode Microplate Reader, BioTek, Winooski, VT, USA) and cell number quantification was performed by means of a calibration curve. Error bars representing the average of triplicates ± standard deviation in two independent experiments were calculated (n=6).

2.15 Optical microscopy

A suspension of $2x10^4$ cells in alpha-MEM were seeded on glass substrates covered with the photopolymerized films, as well as 3D scaffolds, from the hybrid material and were placed in the cell culture incubator at 37 °C. Cells on the specimens were examined daily for 7 days and were visualized by optical microscopy by means of a Zeiss Axiovert 200 microscope. Images were taken by a ProgResVR CFscan Jenoptik camera (Jena, Germany) using the ProgResVR CapturePro 2.0 software and objective lenses for 10-fold magnification.

2.16 Preparation of biological samples for scanning electron microscopy

A suspension of $2x10^4$ cells in alpha-MEM were seeded on 3D scaffolds of the hybrid material and were placed in the cell culture incubator at 37 °C for up to 5 days. Specimens were then removed from the incubator were and rinsed three times with PBS, fixed with 4% paraformaldehyde for 30 min, and dehydrated in increasing concentrations (from 30 to 100%) of ethanol. Then the samples were dried via HMDS overnight, were sputter-coated with a 10 nm thick layer of gold and were observed under a scanning electron microscope at an accelerating voltage of 20 kV.

2.17 Laser scanning confocal microscopy

A suspension of $2x10^4$ cells in alpha-MEM were seeded on the 3D scaffolds consisting of the hybrid material and were placed into the cell culture incubator at 37 °C for up to 7 days. After the incubation time, the samples were rinsed with PBS, fixed with 4% paraformaldehyde for 15 min and permeabilized with 0.1% Triton X-100 in PBS for 5 min. The non-specific binding sites were blocked with a 2% BSA solution in PBS for 30 min. Actin cytoskeleton was stained by incubating the cells

on the samples in 20 μl diluted phalloidin-atto-488 in blocking solution for 1 h at 37 °C and subsequently staining them by simultaneous incubation with 4′,6-diamidino-2-phenylindole (DAPI) for 5 min. The samples were then washed with PBS, mounted with a mounting fluid and observed under a Leica laser scanning confocal microscope.

2.18 Statistical analysis

Statistical analysis was performed using the one-way ANOVA Dunnett's multiple comparisons test. To statistically evaluate the difference in cell proliferation after certain time points (2, 4, and 7 days), we compared the hybrid material films at each time point against the control tissue culture polystyrene (TCPS) surface.

3. Results and Discussion

3.1 Synthesis and characterization of the biomaterials

Determination of the DD

The degree of deacetylation is an important property of chitosan, which affects the physicochemical as well as the biological properties of the polysaccharide. In order to determine the DD, we used ^{1}H NMR spectroscopy (**figure 3.1**) reported by R. Czechowska-Biskup et. al., and applies the below equation[17] .

$$DD[\%]= \left[1 - \frac{\frac{1}{3} * I_{CH7}}{\frac{1}{6} * I_{(CH2-13)}}\right] * 100 \qquad (1)$$

Where I_{CH7} is the integral of the protons 7 and $I_{CH2\text{-}13}$ is the integral of the protons 2-13. According to 1 the DD of chitosan was found 91%. This DD is of paramount importance for the solubility of chitosan, because the higher the percentage the better the solubility. However, despite the 91% DD, chitosan was insoluble in water, while it dissolved in 0.5% aqueous acetic acid solution. Moreover, there are earlier studies which underline the superior biological properties of chitosan with increasing of DD.

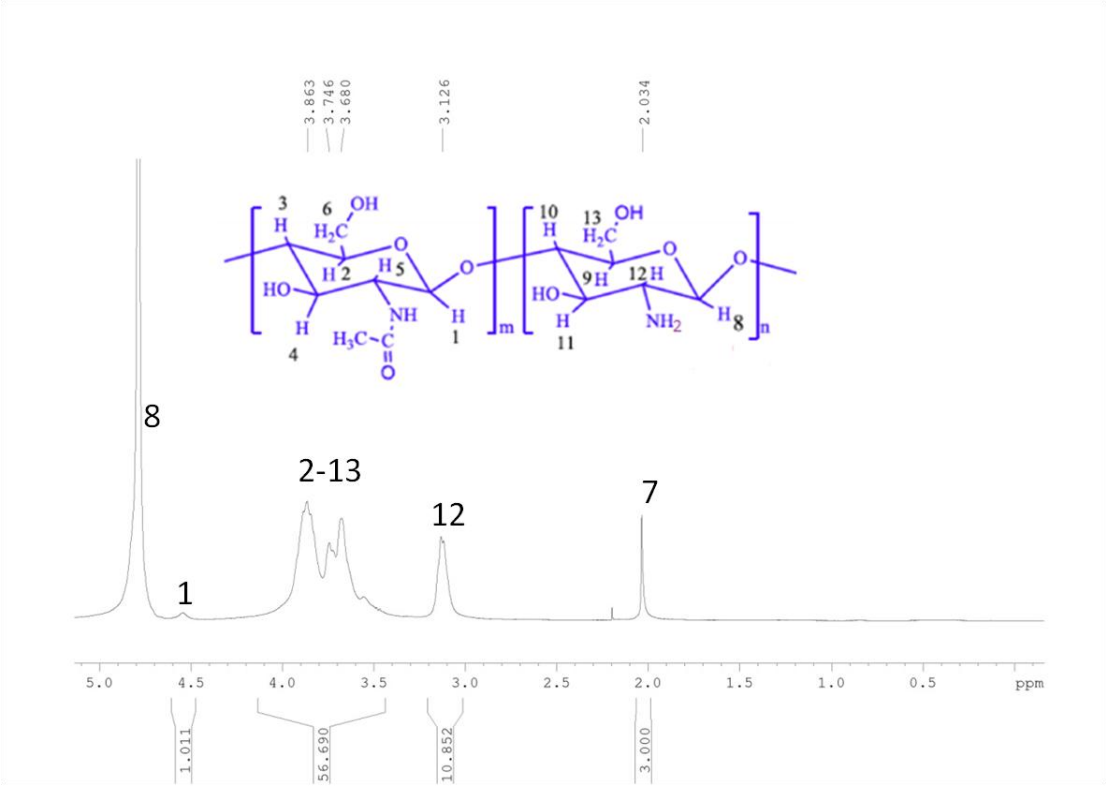

Figure 3.1: Chemical structure ^{1}H NMR spectrum (D2O:TFA-d) of chitosan.

Synthesis and ^{1}H NMR characterization of chitosan-MA

The low solubility of chitosan' in water, hinders its use in biomedical applications. In order to overcome this problem a plethora of chemical modification reactions have been proposed to improve its solubility in water[18]. We choose to modify chitosan with MA, which introduces carboxylic groups along the chitosan chains rendering it water soluble. The reaction is shown in **figure 3.2.a.** In this reaction both the amino and the hydroxyl groups can react with MA, to form amide and ester groups respectively. The ^{1}H NMR spectrum, after the modification reaction, showed several new peaks in the olefinic proton region (**figure 3.2.b.).** The peaks at 5.82 and 6.65 ppm were assigned to the olefinic protons next to the ester group while the peaks at 5.88 and 6.40 are due to the olefinic protons of the acrylamide group. The olefinic protons next to the ester are shifted in the spectrum to higher ppm compeared to the acrylamide olefinic protons, due to the higher electronic density of the former. In addition, one can observe that, the reaction of the amine groups with the anhydride is preferable, because of the higher nucleophilicity of the amine groups compared to the hydroxyl group. The ratio of acrylate to acrylamide groups after the modification reaction was found approximately 1:2.5. It was also noted that after modification with MA, chitosan became soluble in water.

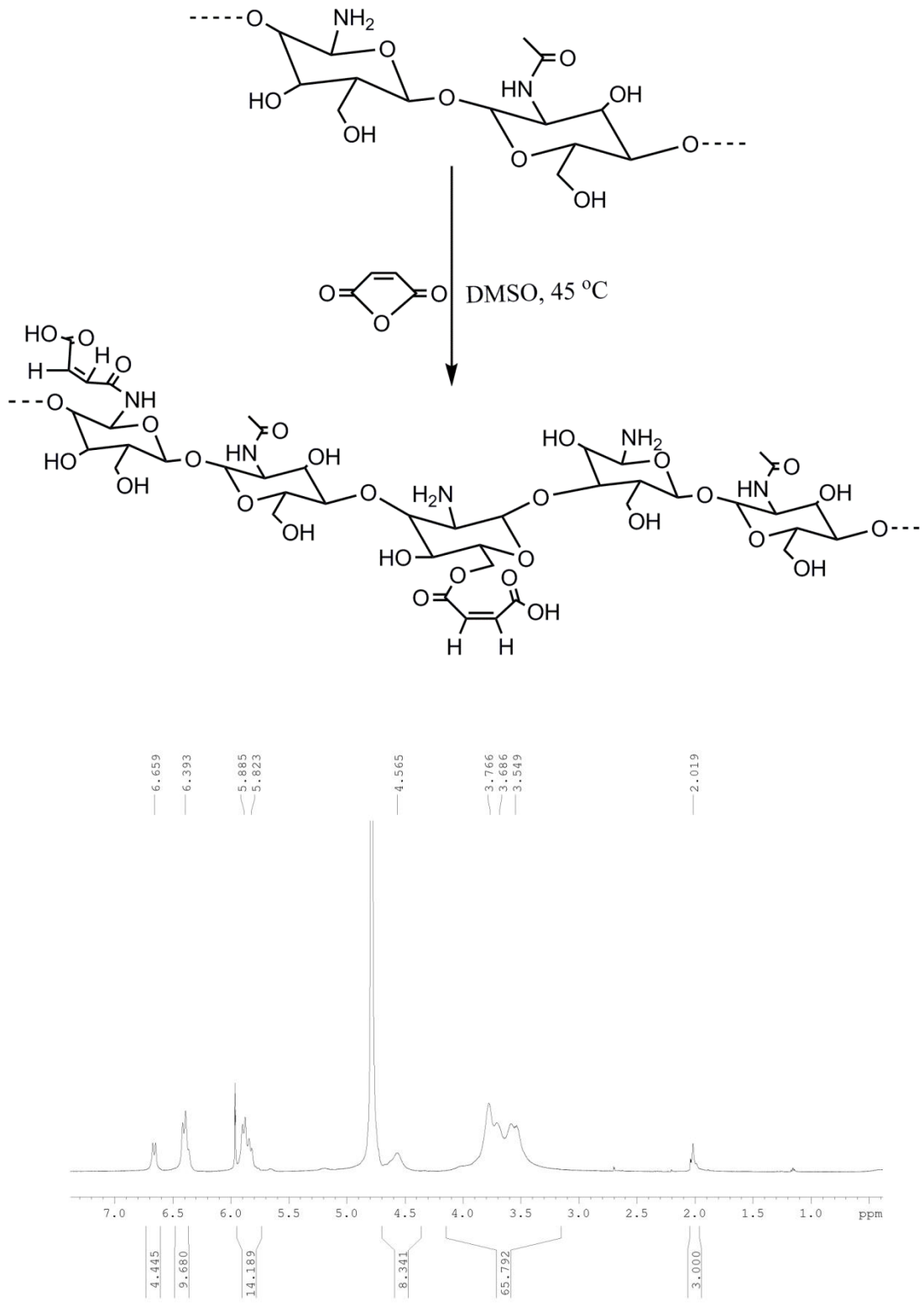

Figure 3.2: a) Schematic illustration of the reaction of chitosan with MA and b) ^{1}H NMR spectrum of chitosan-MA in D_2O

FT-IR spectroscopy

Chitosan-MA was also characterized by FT-IR spectroscopy. The FT-IR spectra of chitosan and chitosan-MA are shown in **figure 3.3.a.** The broad band at around 3260 cm^{-1}, in the spectrum of chitosan, was attribute to the N-H, O-H stretching vibrations and the peak at 2860 cm^{-1} was ascribed to the C-H stretching. The characteristic bands of C=O stretching and N-H bending vibration of amide I appeared at 1645 cm^{-1} and 1590 cm^{-1} respectively. The peakes at 1026 cm^{-1}, 1070 cm^{-1}, and 1150 cm^{-1} correspond to the saccharide group of chitosan. The FT-IR spectrum of chitosan-MA showed new bands at 1716 cm^{-1} assigned to the C=O stretching of the carboxylic acid, peaks at 1556 cm^{-1} and 1630 cm^{-1} attributed to the amine and C=C bond respectively, and the peak at 1633 cm^{-1} assigned to the C=O stretching of the ester group. The groups peak at 1350 cm^{-1} was attributed to the C-H bending vibration of $–C=CH_2$ and the peak at 1260 cm^{-1} to the secondary C-N group[19

X-ray diffraction (XRD)

The XRD diffraction patterns of chitosan and chitosan-MA are shown in **figure 3.3.b.** Chitosan exhibited two typical peaks at $2\theta = 10.5^{\circ}$ and 20°, attributed to the crystalline structure of chitosan, these results are in good agreement with the study by R. Samuels[20]. After modification, for chitosan-MA, the crystalline peak at 11^{o} disappeared and the peak at 20^{o} became broades. This suggested the loss of crystallinity which is attributed to the elimination of the interaction hydrogen bond formation, since both the amine and the hydroxyl groups, of chitosan, are reduced in chitosan-MA. Therefore, chitosan-MA is an amorphous polysaccharide.

TGA characterization

The TGA spectra for chitosan and chitosan-MA are shown in **figure 3.3.c.** As seen, the weight loss of chitosan occurs in two stages. In the first stage, a weight loss about 10% until $200^{o}C$ is observed and is attributed to the elimination of moisture. The second step from 200 to $600^{o}C$ is due to the degradation of the basic structural unit of chitosan. On the other hand, the weight loss of chitosan-MA has three stages. The slight difference between the chitosan and chitosan-MA degradation is due to the attached moieties in chitosan-MA, which degrade before the degradation of the basic structural units of chitosan occurs. However, due to the overlap of the different stages of weight loss it is not possible to calculate the % loss at each stage.

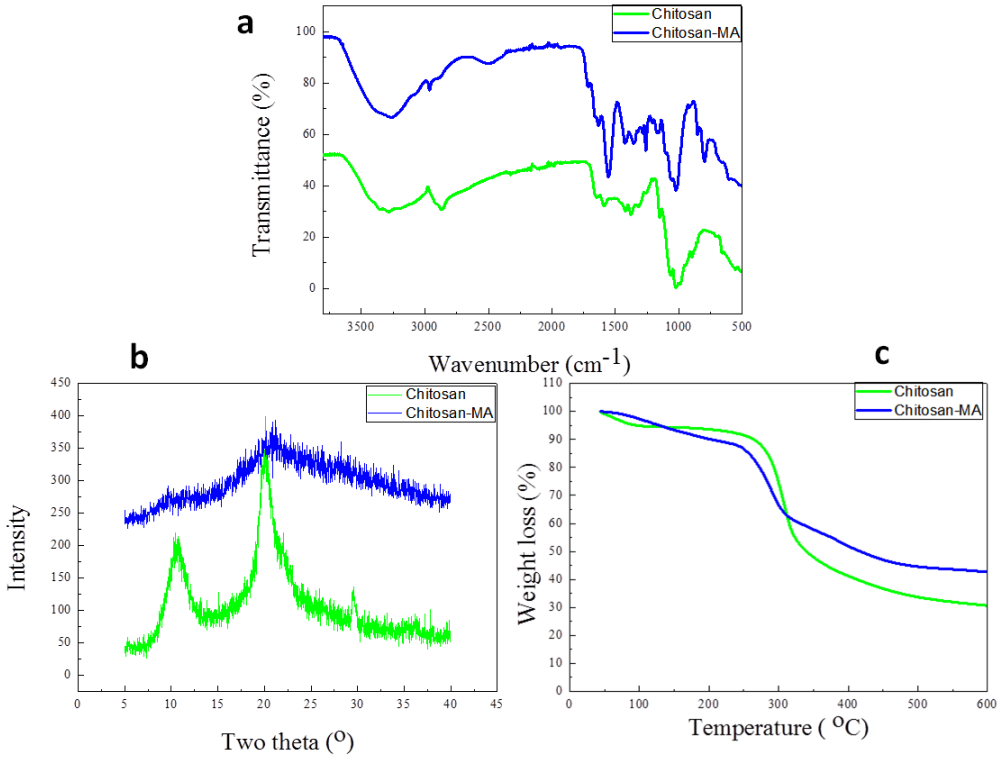

Figure 3.3: a) FT-IR spectra, b) XRD patterns and c) TGA curves of chitosan and chitosan-MA

Despite a report on the literature which shows the polymerization of chitosan-MA[21] in our study, we could not polymerize the polymer using neither a photoinitiator nor with a thermal initiator. To polymerize chitosan-MA by MPP, we made a second modification step, and introduced photopolymerizable met-acrylate groups along the chitosan-MA backbone (**figure3.4.a**). For this we used GMA, which reacts with the carboxylic acid, amine and hydroxyl groups of chitosan-MA. This reaction is hardly deepened on the PH of the reaction as well as on the steric interactions.[papaer gia to glycidil me ta diafora ph]. The reaction took place in dionized water at pH 6. The ^{1}H NMR spectrum clearly proved the non-selective reaction of GMA at this pH value, as 5 pairs of olefinic protons were observed which attributed to the olefinic protons of the ester and the amide groups, of chitosan-MA, which did not react, while two new peaks at 6.16 and 5.73 ppm were assigned to the protons of the double bond which is formed upon the reaction of the carboxylic acid group with GMA. It is noted that the integral of these peaks equals the decrease of the integral of the olefinic protons of chitosan-MA verifying the peak assignment. Moreover, peaks at 5.64 and 5.34 ppm are observed which are assigned to the olefinic protons which are introduced by the reaction of the amine groups of chitosan-MA with GMA producing methacrylamide groups. Finally, the hydroxyl groups of chitosan-MA can react with GMA to form ester groups. The olefinic protons of these ester groups were observed at 6.00 and 5.44 ppm.

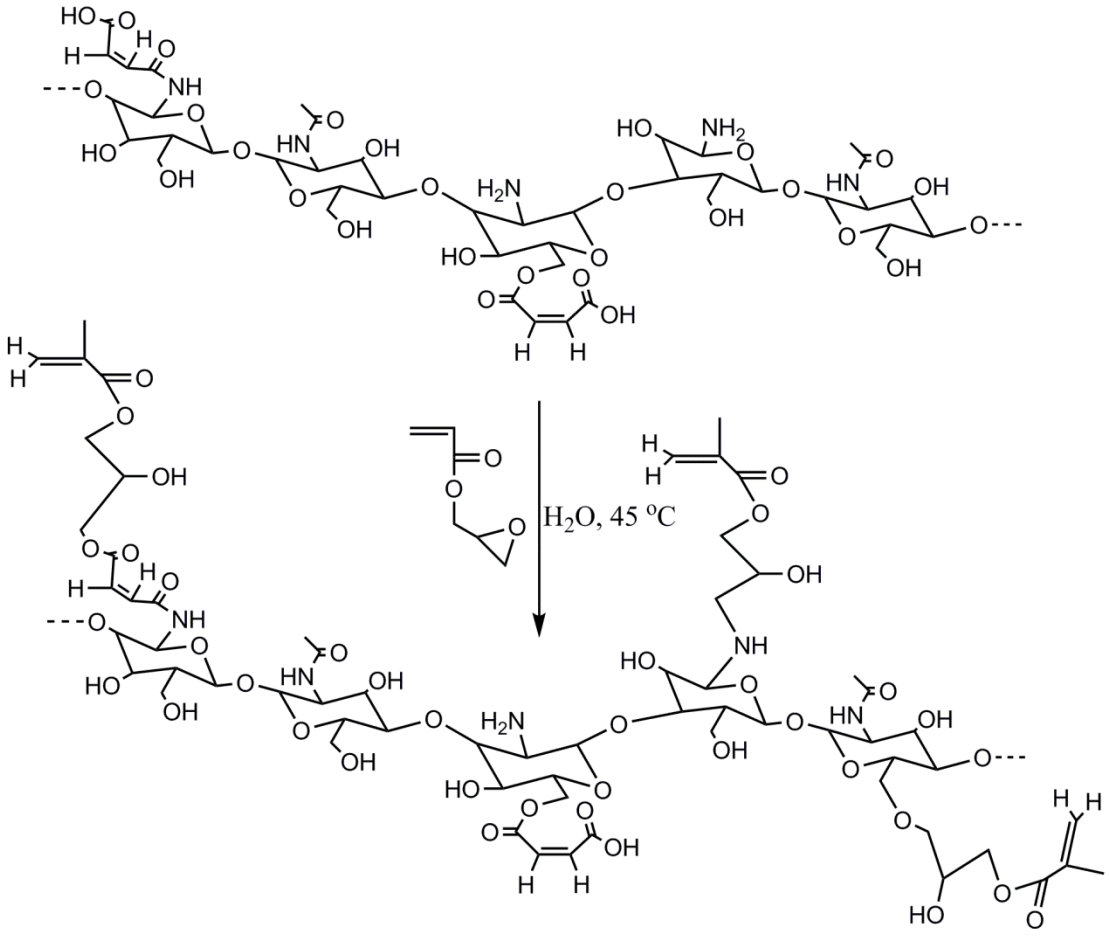
H2O, 45 °C

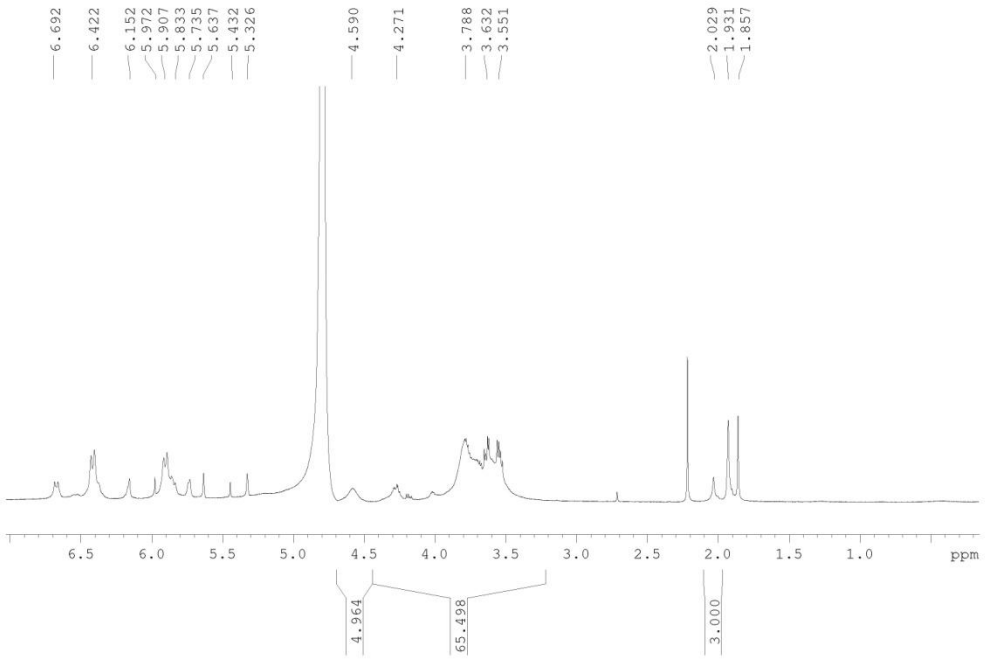
6.692
6.422
6.152
5.972
5.907
5.833
5.735
5.637
5.432
5.326
4.590
4.271
3.788
3.632
3.551
2.029
1.931
1.857
6.5
6.0
5.5
5.0
4.5
4.0
3.5
3.0
2.5
2.0
1.5
1.0
ppm
4.964
65.498
3.000

Figure 3.4: a) Schematic illustration of the reaction of chitosan-MA with GMA to produce the photopolymerizable chitosan-MA-GMA and b) ^{1}H NMR spectrum of chitosan-MA-GMA in D_2O

Chitosan-MA-GMA was further characterized by FT-IR spectroscopy and its spectrum was compeared to that of chitosan-MA (**figure 3.5.a**). The O-H, N-H band at around 3700-3200 cm^{-1} became more broad and overlapped with the C-H peak, at 2860 cm^{-1}. The broading of these peaks in this area is due to the hydroxyl groups which are introduced upon the modification with GMA. On the other hand, no significant differences were observed in the XRD spectra, but the peak at 10.5^{o} has completely disappeared (**figure 3.5.b**). Finally, the TGA curveof chitosan-MA-GMA shows multi-step degradation profile due to multiple side groups attached on the main chain of the polysaccharide (**figure 3.5.c**).

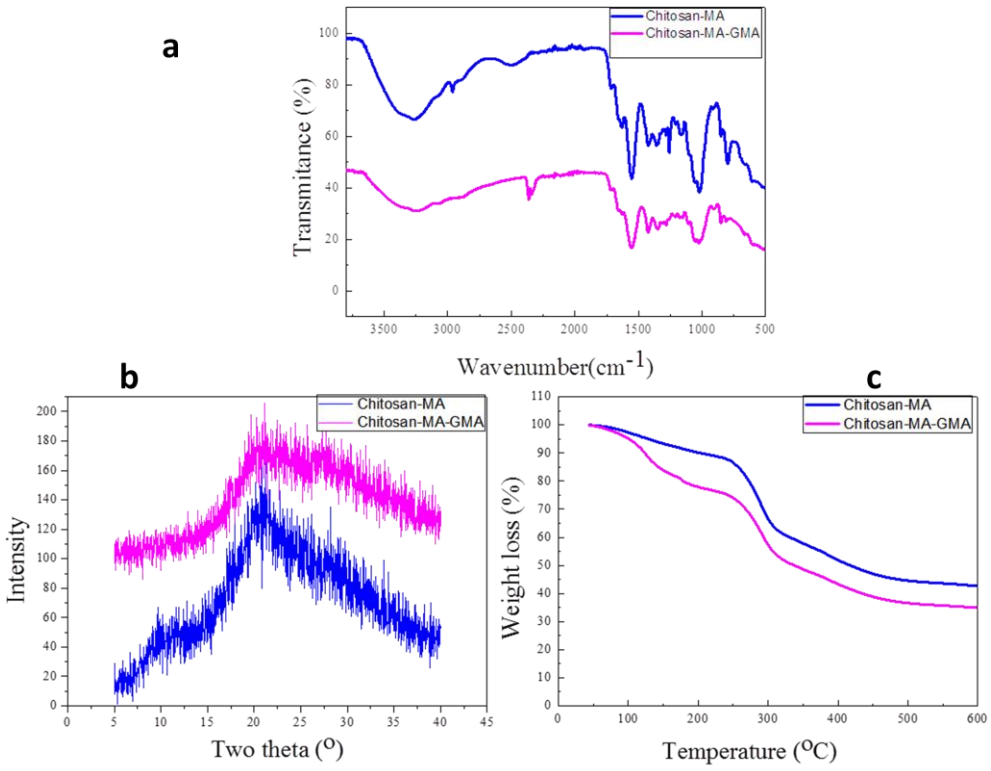

Figure 3.5: a) FT-IR spectra, b) XRD patterns and c) TGA curves of chitosan-MA and chitosan-MA-GMA

3.2 Polymerization of the modified biopolymers

Hybrid materials have attracted great attention, as they can combine by physicochemical as well as the biological properties of the individual components. Combination of chitosan with gelatin has been extensively studied, and it was shown that the mechanical as well as the biological activities of the hybrid materials can

improve. Besides, the photocrosslinking of hydrogels has attracted grat attention in bioprinting. Previous studies have utilized GelMA[22-25] with various photoinitiators as bioinks for bioprinting. In TERM, most of the widely used photoinitiators work in the UV range. Eosin-Y has attracted great attention the last years, as it can be used as a component in a potoinitiaton system, which combines triethanolamine (TEA) as a co-initiator and 1-vinyl-2 pyrrolidinone (NVP) as a co-monomer, and is activated via visible light irradiation in the range of 400-700nm. Considering the potential harmful effects of UV light, such as DNA damage to the cells[26], cancer[27], and the negative effects of near-UV blue light[28], the eosin-Y based visible light polymerization of a hydrogel has great advantages in maintaining cell function. Eosin-Y is a safe visible light photoinitiator that received Food and Drug Administration approval and has been also reported to be less toxic than Irgacure 2959[29]. Taking into account the above, an eosin-Y based photoinitiator is an excellent choice for bioprinting applications. Motivated by this, we investigated the feasibility of using a hybrid GelMA:chitosan-MA-GMA hydrogel with an eosin-Y based photoinitiator, in the absence of any co-initiator and co-monomer, as a convenient, biocompatible and safe strategy to fabricate visible light crosslinkable hydrogels.

For the biological assays, first 2D films of the hybrid biopolymers were prepared. 5% solution of the hybrid material, in a 1:1 weight ratio of the individual biopolymers, was mixed in dionized water with 0.1 mM Eosin Y. The samples were spin-coated and polymerized under visible light for 10 min. After polymerization the samples were developed in water at 40 ^{o}C for 1h to remove any non polymerized material and photoinitiator.

3D scaffolds were fabricated with the hybrid material, at a 1:1 weight ratio of the two biopolymers, at a 30% concentration in dionized water and 0.1 mM eosin-Y as photosensitizer. Samples were prepared via the drop casting method and were polymerized directly without drying. For MPP there are a few, commercial water soluble, photoinitiator systems, which contain water soluble salts as photosensytizers and co-initiators which contain hetero-atoms, such as amines, as the radical producers. However, there is no commercial water soluble photoinitiator for use at around 800 nm. Eosin-Y, was used as the only photoinitiator in the hybrid biopolymer system, which contain free amino groups, that act as co- initiator sites. Upon visible and/pr near IR exposure light, eosin-Y was excited to abstract a hydrogen from an amine of the GelMA thus forming amine radicals. These radicals propagate through the double bonds of GelMA and chitosan-MA-GMA macromers to induce their cross-linking.

In the present study, GelMA with different degree of modification were exam, and the medium-GelMA, with 50-60% of modification of the amine was used, as work better than GelMA with higher degree of modification. This supported our proposed mechanism, since free amines are required in the polymer chain to initiate the polymerization. This system allowed the highly accurate fabrication of 3D scaffolds. **Figures 3.6** shows SEM images of the hybrid material 3D scaffolds. Although some deformation of the scaffolds is observed this is attributed to the high vacuum used during the SEM observation and the organic nature of the biomaterial.

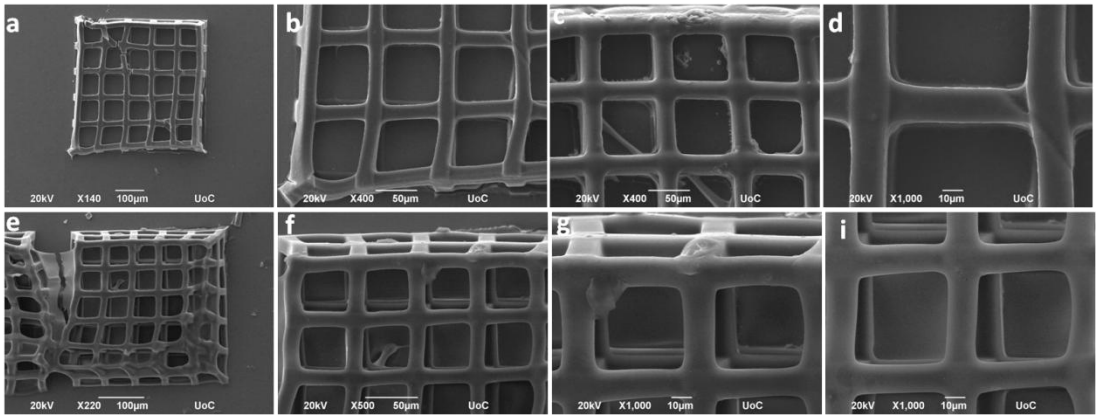

Figure 3.6: 3D grid-shaped scaffolds produced from the hybrid material by MPL, using a 20× plan achromat lens (N.A. = 0.8) at a 60 mW laser power and writing speed 100 μm s^{-1}. The upper panel show top view images while the bottom panel presents the same samples tilted by 45°. From the left to the right, images higher magnification.

3.3 Biological studies

Representative optical microscopy images (**figure 3.7**) show the morphology of DPSC cultured on the hybrid materials and on the polystyrene control surface for 2 and 7 days in culture. Cells seeded for 2 days in culture indicate a spindle-shaped morphology, which is similar to that on the polystyrene control surface (**figures 3.7 a and b)**. After 7 days in culture, a clear increase in proliferation was observed with a dense layer of well-spread flattened cells completely covering the material surface, as shown in **figures 3.7 c and d.** Although, DPSC have not been studied on this hybrid material before, our results are similar to those of M. Bousnaki et al, who study the DPSC behavior on gelatin/alginate scaffolds[30].

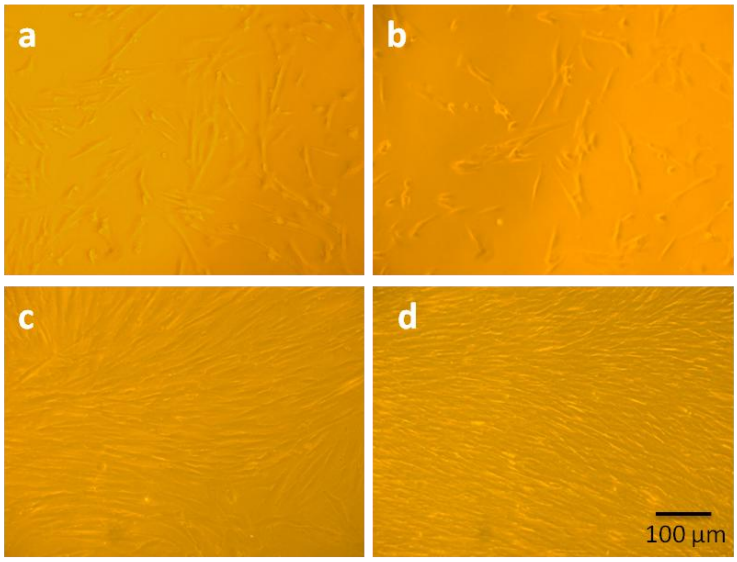

Figure 3.7: Optical microscopy images showing the adhesion of human dental pulp stem cells on hybrid (GelMA:Chitosan-MA-GMA) films (a, c) and tissue culture treated polystyrene (TCPS) control (b, d) after 2 days (a, b) (upper panel), and 7 days (c, d) (lower panel) in culture. Scale bar represents 100 µm and it is same in all images.

Figure 3.8 shows the results from the investigation the viability of the DPSC on the hybrid material films as well as on the GelMA films performed using the PrestoBlue assay after 2, 4, and 7 days in culture. We carried out the cytocompatibility investigations on geometrically well-defined films in order to quantify the cell proliferation results. For both materials we observed a strong initial cell adhesion and a subsequent cell proliferation increase after 3 and 7 days. The cell number on both films increased approximately by two times from day 2 to day 4 and approximately 4 times from day 2 to day 7. The results indicate the absence of any cytotoxic effects and suggest that the GelMA as well as the hybrid material is biocompatible, and therefore can be used for the fabrication of biomaterial scaffolds. In addition one can observe that the hybrid (GelMA:Chitosan-MA-GMA) materials shows better biocompatibility than the GelMA as well as better than the TCPS control.

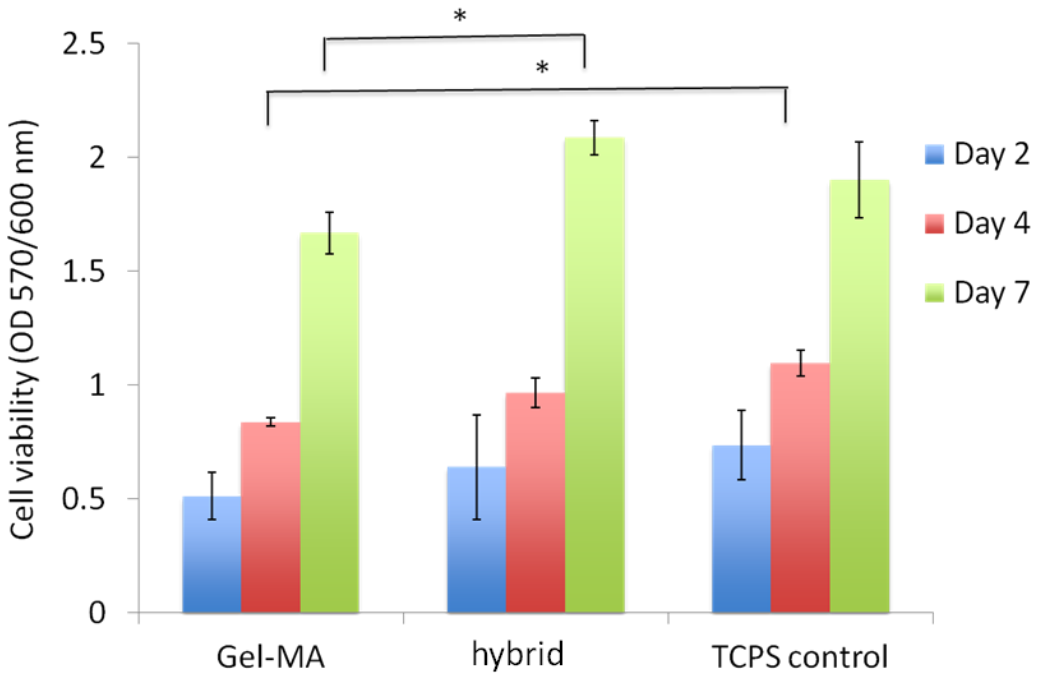

Figure 3.8: Cell viability of human dental pulp stem cells onto GelMA films, hybrid (GelMa:chitosan-MA-GMA) films, and tissue culture treated polystyrene (TCPS) control after 2, 4, and 7 days in culture as determined by the PrestoBlue® viability assay. Statistical analysis by means of GraphPad Prism 7.0 one-way ANOVA multi-comparison test indicates no significance in the differences between the three surfaces on day 2, significant differences for GelMA vs. control on day 4 ($p=0.0143$), and significant differences for GelMA vs. hybrid on day 7 ($p=0.0164$)

After examining the materials in 2D cell culture, in which they exhibit excellent cell viability and proliferation profile, the hybrid material porous 3D scaffolds were used to study the behavior of the cells in 3D culture. For this propose, $2x10^4$ cells were cultured on a glass substrate with dimensions 1x1 cm^2 which contained 9 scaffolds with dimensions 400x400x40 μm^3. The 3D cell culture was followed for 5 days. **Figure 3.9** shows the optical microscopy images, of the cell culture, on the 3D scaffolds at different time points. The upper panel shows the 3D cultures on the hybrid scaffolds after 2 days in cell culture and the lower panel shows the 3D cell culture at the 4^{th} day in culture. From these images one can clearly observe a good cell adhesion onto the 3D scaffolds. Both in the early time point (2 days) and after 4 days a large number of cells cover the scaffolds and proliferate within its pores. The full coverage of the scaffolds by the DPSC and a homogenous 3D cell culture are observed after 4 days. The quick cell attachment on the 3D scaffolds means that the present hybrid material is an excellent candidate for 3D cell culturing. Our results on the 3D cell culture are in good agreement with previous studies on mixed unmodified gelatin/chitosan hybrid material 3D scaffolds produced by freeze drying[31] or electospinning[32]. The similar behavior of the cells on the modified and

unmodified biopolymers, as well as the controlled 3D shape of the scaffolds, proved that the present modification not does only affect negatively the biocompatibility of the scaffolds but more importantly presents a unique opportunity to use MPP for 3D μ-bioprinting.

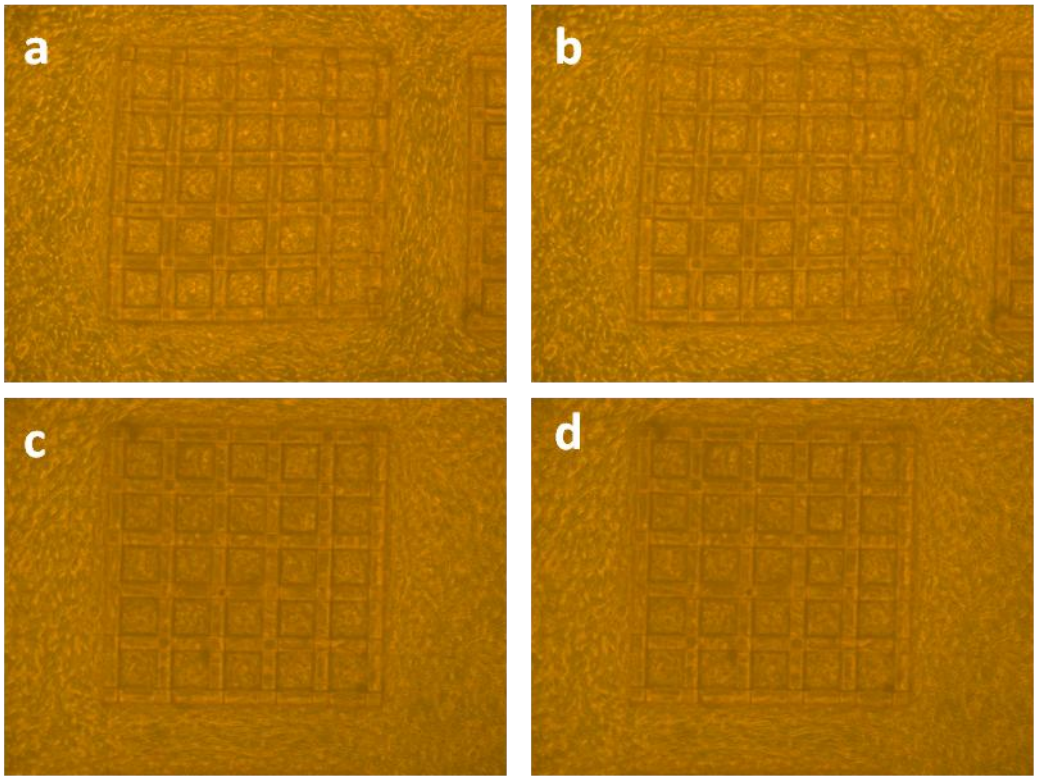

Figure 3.9 : Optical microscopy images showing the adhesion of human dental pulp stem cells on the hybrid (GelMA-Chitosan-MA-GMA) 3D scaffolds, fabricated via MPP after 2 days (a and b) (upper panel), and 3 days (c and d) (lower panel) in culture. Scale bar represents 100 μm and it is same in all images.

In order to visualize cell adhesion on the 3D scaffolds immunocytochemistry, the actin/DAPI assay was exployed. In this assay, the cell cytoskeleton is stained with green color while the nucleus with blue color. However, the high autofluorescence of the PI presents a great challenge for this assay since it overlaps with the fluoresence of the dyes. In **figure 3.10** laser scanning confocal microscopy images of the hybrid 3D scaffolds with DPSC after 5 days of culture are presented. There are few cells atatched on the 3D scaffolds having good cytoskeleton producrion. However due to the fluorescence of the structures the cytosceleton, which is stained in green, cannot be visualized clearly.

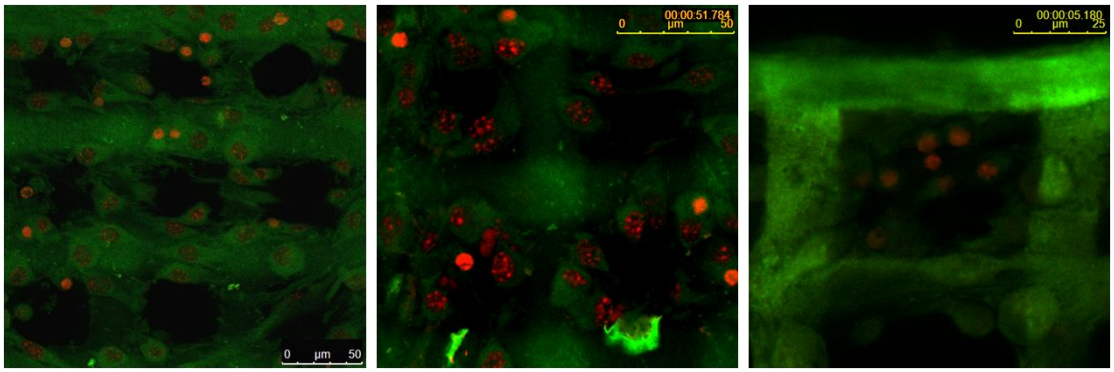

Figure 3.10: Laser scanning confocal microscopy images showing the adhesion of human dental pulp stem cells onto two-photon polymerized grid-shaped 3G hybrid scaffolds after 5 days in culture. The cells were stained with phalloidin (green: actin filaments) and DAPI (red: nucleus).

Next the 3D cultures were characterized by SEM. Different methods of sample drying were applied to avoid the use of critical point drying which deformed our scaffolds and cells. Instead we dried the samples using HMDS. **Figure 3.11** shows the 3D cultures of DPSC onto the 3D hybrid porous scaffold, after 5 days in culture. Both the mild drying method used and the improved mechanical properties of the hybrid 3D materials, enhanced the SEM characterization of the 3D cultures. Despite the single time point used, one can clearly observe the huge amount of cells that are attached on the 3D scaffolds and attain their characteristic spindle-shaped morphology.

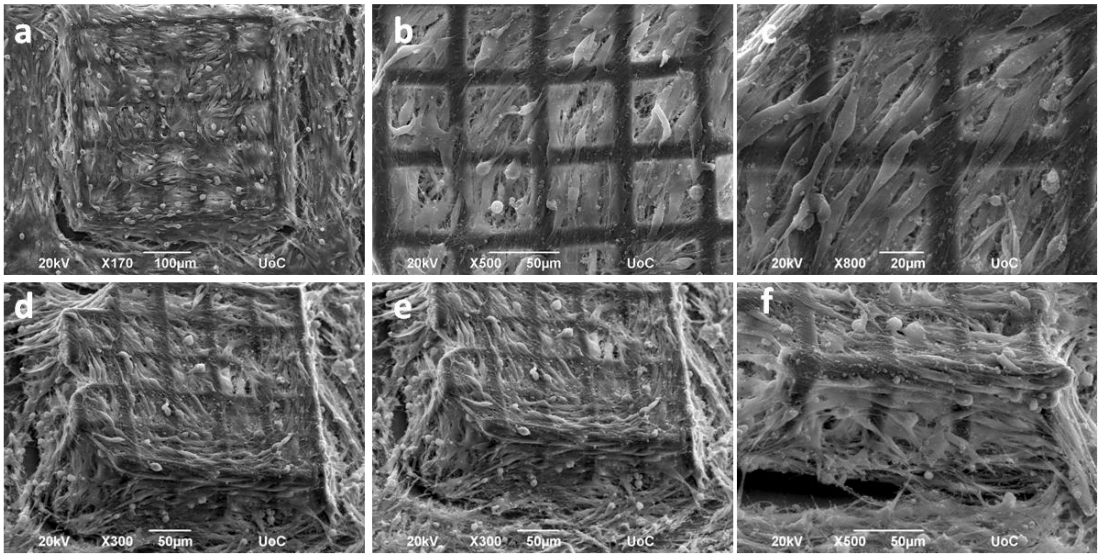

Figure 3.11: SEM images showing the adhesion of human dental pulp stem cells onto two-photon polymerized grid-shaped scaffolds after 5 days in culture. The upper panel images (a, b, c) represent the hybrid material culture and the lower panel (d, e, f) the same samples tilted by 45^{o}. From the left to the right higher magnification images.

4. Conclusios

In the present work GelMA and a water-soluble and photopolymerizable chitosan-derivative were synthesized. 3D hybrid, GelMA:Chitosan-MA-GMA, scaffolds were fabricated using MPP. The combination of two biopolymers gives excellent biomaterials for TERM applications, with enhanced mechanical properties, and better biocompatibility, compared to the GelMA 3D scaffolds and Chitosan alone. Moreover, eosin-Y was employed as an FDA-approved, biocompatible, water soluble photoinitiator. Primary mesenchimal dental pulm stem cells isolated from patients, were cultured on the scaffolds and proved the biocompatibility and good cell adhesion and proliferation behavior of the hybrid materials.

5. References

1. J. O'Brien et. al., *Mater. Today*., **2011**;14, 88.
2. W. Thein-Han et. al., *Acta Biomater*., **2009**, 5, 3453.
3. A. Di Martino et. al., *Biomaterials*, **2005**, 26, 5983.
4. C. Miranda et. al., *Arch Oral Biol.* **2011**, 56, 1.
5. W. Thein-Han et. al., *Acta Biomater.*, **2009**, 5, 3453.
6. A. Lahiji et. al., *J. Biomed. Mater. Res*., **2000**, 51, 586.
7. C. Miranda et. al., *Arch. Oral. Biol*., **2011**, 56, 1.
8. A. Muzzarelli et. al., *Biomaterials*, **1994**, 15, 1075.
9. M. Santoro et. al., *J. Control. Release.*, **2014**, 190, 210.
10. Y. Huang et. al., *Biomaterials*, **2005**, 26, 7616.
11. Y. Huang et. al., *Biomaterials*, **2005**, 26, 7616.
12. T. Rickett, *Biomacromolecules*, **2011**, 12, 57.
13. H. Shih et. al., *Macromol. Rapid. Commun*., **2013**, 34, 269.
14. W. Zongjie et. al., *Biofabrication*, **2015**,7, 045009.
15. J-P. Fouassier et. al., *Materials*, **2010**, 3, 5130.
16. M. Farsari et. al., *J. Photochm. Photobio. Chemistry*, **2006**, 181, 132.
17. R. Czechowska-Biskup et. al., *Chem. Appl. Chitin Its Deriv.*, **2012**, 17, 5.
18. S. Hitoshi et. al., *Biomacromolecules*, **2002**, 3, 1126.
19. C. Carvalho et. al., *Mater. Sci. Eng. C Mater. Biol. Appl.*, **2017**, 78, 690.
20. R. Samuels *J. Pol. Sci. Pol. Phy. Ed.*, **1981**, 191081.
21. E. Bertassoni et. al., *Lab. Chip.*, **2014**, 14, 2202.
22. P. Grogan et. al., *Acta Biomater.*, **2013**, 9, 7218.
23. R. Gauvin et. al., *Biomaterials*, **2012**, 33, 3824.
24. H. Lin et. al., *Biomaterials*, **2013**, 34, 331.
25. P. Sinha et. al., *Photochem. Photobiol. Sci.*, **2002**, 1, 225.
26. B. Armstrong et. al., *J. Photochem. Photobiol. B Biol*., **2001**, 63, 8.
27. S. Smith et. al., *IFMBE Proc.*, **2009**, 23, 1352.

28. S. Bahney et. al., *Eur. Cells Mater.*, **2011**, 22, 43.
29. M. Bousnaki et. al., J. *Mater. Sci.: Mater. Med.*, **2018**, 29, 97.
30. Y. Huang et. al., *Biomaterials*, **2005**, 26, 7616.
31. J. Jafari et. al., *Biomed. Mater. Eng.*, **2005**, 21, 99.

Chapter 4

Bioinspired, thymol functionalized, 3D scaffolds with simultaneussly biocompatibility and antimicrobial activity

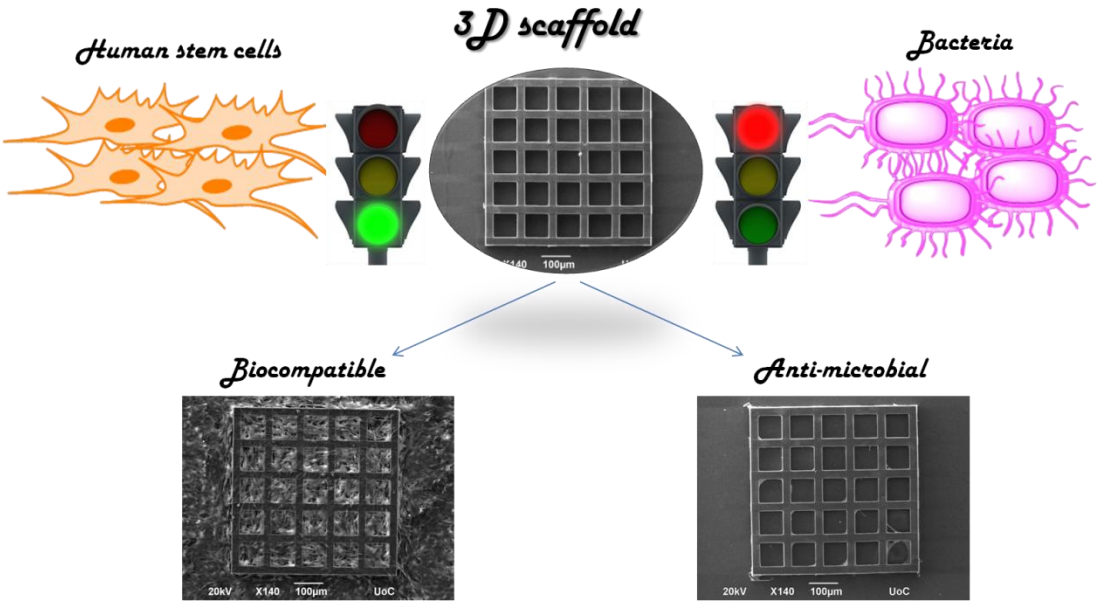

1. Introduction

Tissue loss due to trauma, disease or congenital abnormalities is a major healthcare problem worldwide. If that takes place in the craniofacial region, it induces serious physiological and psychological consequences for the patients. Chronic diseases in the craniofacial area could have a dramatic effect on human health. Among most common diseases in this area are dental diseases or dental loss. In recent years, there has been a clear shift in RM from using medical devices and whole tissue grafts, to a more sophisticated approach that utilizes specific bioactive, biodegradable synthetic or natural scaffolds combined with cells and/or biological molecules, to create a functional tissue replacement in the diseased or damaged site.[1] In craniofacial and dental TERM the use of dental stem cells is the most common approach.[2] The discovery of stem cells and recent advances in cellular and molecular biology has led to the development of novel therapeutic strategies that aim at the regeneration of injured or diseased tissues. Generally, stem cells have two major properties: they are capable of self-renewal and, upon division, they can give rise to cells that have the potential to differentiate.[3]

The first stem cells isolated from adult human dental pulp were the so called dental pulp stem cells (DPSC). They were isolated from permanent third molars and exhibited high proliferation and high frequency of colony formation that produced calcified nodules[4]. DPSC cultures from impacted third molars at the stage of root development were able to differentiate into odontoblast-like cells with a very active migratory and mineralization potential, leading to organized three-dimensional dentin-like structures *in vitro*.[5] In terms of their functionality, dental pulp cells can regenerate dentin and supply to it oxygen, nutrition, and innervation, whereas the hard dentin can protect soft dental pulp tissue. Together, they maintain the integrity of tooth shape and function. Several studies have shown that DPSC plays a vital role in the dentin-pulp tissue regeneration. Materials, in dental TERM, as in all TERM applications, play a vital role. Since the interactions of the cells with the biomaterial is a vital element in the evaluation of a scaffold, great research effort has focusesed on designing biomaterial structures that facilitate favorable interactions and enhance tissue regeneration. Inspired by nature, researchers have developed organic/inorganic hybrid materials with a clear structure-performance relationship. Almost everything in nature, including pearls, shells, corals, bones, and teeth, is composed of organic and inorganic components[6] At the same time, the structure of each component determines the final performance of the composites, and the organic/inorganic interfacial interactions play a pivotal role on their properties. However, the failure upon implantation is in most cases due to inflammation that happens during the implantation[7] In order for the researchers to overcome this problem, they are focusing on creating multifunctional materials which exhibit simultaneously antimicrobial and biocompatible activity.[8-12] The preparation of antibacterial restorative dental materials has attracted great attention in order to prevent secondary caries[13]. Since the discovery of penicillin in 1928, antibiotics have played an

important role in fighting bacterial infections by inhibiting the growth or killing the bacteria. However, the overuse of antibiotics has led to a worldwide rise in bacterial resistance, a new challenge in infectious disease treatment today. Antibacterial activity in dental restorative materials can be provided by the incorporation of biocides like silver[14] and zinc[15] metals as well as organic compounds such as chlorhexidine,[16], quaternary ammonium salts[17] etc. The gradual release of these antibacterial compounds results in short lasting antibacterial activity, reduction in the mechanical properties of the dental composites and toxic side effects on the surrounding soft tissues. Polymers with quaternary ammonium groups are probably the most widely explored type of polymeric biocides, and they kill the bacteria via a membrane disruption mechanism. Although these cationic polymers shown high antibacterial efficiency and ease of preparation, their high cytotoxic and hemolytic effects on human cells have limited their widespread applications. Another very important class of anti-microbial agents are the natural products. "Natural product" is the general term for molecules derived from natural organisms including plants, fungi, and animals. Natural products usually show remarkable biological properties through their high activity and selectivity[18]. The other outstanding characteristic of natural products is that they are easily degraded in the natural environment because of their eco-friendly structure, derived from biosynthesis processes[19]. Recently, many biological and engineering studies have suggested the use of natural products as novel compounds for the control of biological events and disease.[20,21] Other studies are focused on the release of these products from the polymeric matrixes[22-25]. The released molecules have shown great anti-microbial activity, however, but one main disadvantage is their cell toxicity.

Therefore, the development of materials with immobilized anti-microbial moieties have currently attracted great attention for overcoming the deficiencies of systems based on released bactericides. While these materials inhibit the activity of contacted bacteria, the active agents are chemically bound to the matrix and cannot leach out.
Thymol (2-isopropyl-5-methylphenol), an essential oil found in thyme and extracted from Thymus vulgaris, is used in dentistry, mainly for trating oral infections. Thymol has a strong bacteriostatic and bactericidal activity against a wide range of bacteria.[26] Very few studies have reported the use of thymol for the preparation of polymeric materials. In 1994, Moszner et al. described the preparation of methacrylic and p-styrene sulfonic acid esters of thymol and studied their free-radical polymerization. They showed an antibacterial activity for the methacrylic polymer in water suspension against Streptococcus mutans probably caused by the enzymatic release of thymol. To the best of our knowledge, no further insights into those type of polymers have been reported [27]. More recently, Bedel et. al., have shown the synthesis and antimicrobial activity of poly(ethylene terephthalate)-co-Thymol methacrylate brush polymers. Antimicrobial tests showed that PET-poly(MT) is highly effective against bio-adhesion of P. aeruginosa, L. monocytogenes, and S. aureus. Moreover, results on biofilm proved a strong resistance to biofilm formation against S. aureus[28]. However, no biological studies have been performed on these polymers so far.

In the current study, we gave synthesized a hybrid organic/inorganic material, which was functionalized with TM. The material was suitable for MPP and allowed the fabrication of highly accurate 3D porous scaffolds. Moreover, we studied the biocompatibility of the synthesized material using prior MDPSCs. The hybrid material showed great biocompatibility and promoted cell adhesion and proliferation. At the same time, anti-microbial activity of 3D porous scaffolds, fabricated via MPP using the thymol-functionalized material, was examined with promising results.

2. Experimental

1.1 Materials

All solvents, dichloromethane, diethyl ether, petroleum ether, ethyl acetate, 4-methyl-2-pentanone, deuterium diclromethane were purchased from Sigma-Aldrich (Steinheim, Germany) and were used without further purification. Thymol 98.5%, methacrylic anhydride 94%, Methacryloxypropyl trimethoxysilane 97% (MAPTMS), 2-(methylamino) ethyl methacrylate 98% (DMAEMA), Zirconium n-propoxide (ZPO, 70% in propanol), 4,4-bis(diethylamino) benzophenone (BIS), triethylamine 99%) were purchased from Sigma-Aldrich (Steinheim, Germany). Magnesium sulfide anhydrous >98% and HCl 1 M solution were obtained from Fluka. Silica gel was purchased from Alfa Aesar. Cell culture medium, (alpha-MEM), fetal bovine serum (FBS), antibiotic/antimycotic, glutamine, as well as the PrestoBlue® reagent were purchased from Invitrogen (Karlsruhe, Germany). Ascorbic acid, Phalloidin-Atto 488 and 4′,6-diamidino-2-phenylindole (DAPI) were obtained from Sigma-Aldrich (Steinheim, Germany) and Triton X-100 from Merck (Darmstadt, Germany).

1.2 Thymol methacrylate (TM) Monomer synthesis

Thymol (3.5 g, 23.3 mmol), dichloromethane (10 mL) and triethylamine (6.49 mL, 46.6 mmol) were introduced in a dried round bottom flask. Then methacrylic anhydride (3.82 mL, 25.6 mmol) was added and the reaction mixture was stirred at 40℃ overnight. The next day, triethylammonium salts were removed by filtration and washed with diethyl ether. The filtrate was extracted with a concentrated aqueous solution of $NaHCO_3$. The organic phase was dried with anhydrous magnesium sulfide, was filtered and the solvent was evaporated in a rotary to give a yellow viscous liquid. The product was purified by column chromatography using petroleum ether/ethyl acetate (98/2 v/v %) as the mobile phase. The fractions were firally evaporated to remove the solvent and afford the product as a clear syrup (3.56g, 70% yield).

1.3 TM functionalized hybrid material synthesis

MAPTMS (1ml, 4.2mmol) was hydrolyzed using 0.01M HCl (1:0.1 v/v MAPTMS:HCl). In a separate flask DMAEMA (0.47ml, 2.8mmol) was mixed with ZPO (0.87ml, 2.8mmol). After 15 min of stirring the solution of DMAEMA/ZPO was added dropwise into the solution of hydrolyzed MAPTMS and the mixture was stirred for another 15 minutes. TM (0.6gr, 2.8mmol) was added and the mixture was left under stirring overnight. Finally, BIS 1 wt% to the monomers (0.02gr, $6.2*10^{-5}$mol) was added, and the solution was stirred for another 15 min. The mixture was filtered with a 0.45 μm hydrophobic filter to remove any non dissolved photoinitiator.

As a control, a similar hybrid material in the absence of TM was also prepared using the procedure described above.

1.4 Hybrid thin film preparation

40 μl of the above-mentioned photosensitive hybrid materials were spin-coated (4000 rpm for 60 s) on 100 m thick cover glass slips with a 13 mm diameter. For the photopolymerization, a UV lamp at 365 nm was used resulting in the covalent linkage of the organic vinyl of the material to form a hybrid double network. Finally, the films were developed for 1h in 4-methyl-2-pentanone and dried at 100 °C for 30 min.

1.5 Fabrication of 3D scaffolds by MPP

The samples were prepared by drop casting the hybrid materials onto 100 μm thick glass substrates silanized with MAPTMS. The experimental setup used for the fabrication of the 3D structures has been described in Chapter 1. A Ti:Sapphire femtosecond laser (Femtolasers Fusion, 800 nm, 75 MHz, 20 fs) beam was tightly focused into the volume of the photosensitive hybrid material using a 20x microscope objective lens with NA of 0.8 (Zeiss, Plan Apochromat). Sample movement in the XY plane was achieved using an x-y galvanometric mirror digital scanner (Scanlabs Hurry-Scan II), while for the z-axis linear stages (Physik Instrumente) were employed. The MPL procedure was controlled by a computer using the SAMlight software. The structures were fabricated in a layer-by-layer process with the last layer attached to the glass substrate.

1.6 ^{1}H /^{13}C NMR spectroscopy

^{1}H/^{13}C NMR spectra were obtained on a Bruker AMX-500 spectrometer (Billerica, MA, USA) by dissolving the TM in deuturated dicloromethane.

1.7FT-IR spectroscopy

Attenuated Total Reflection-Fourier transform infrared (ATR-FTIR) spectroscopy was used to characterize the samples. The ATR-FTIR spectra were recorded on a Nicolet 6700 spectrometer (ThermoFisher Scientific, Waltham, MA, USA).

1.8 Biological studies

DPSC were generously provided by Prof. Athina Bakopoulou, School of Dentistry, Aristotle University of Thessaloniki from informed consent healthy donors according to an approved protocol by the Institutional Ethics Committee (322/15-04-2013). DPSCs cultures were developed from wisdom teeth of young healthy donors using an enzymatic dissociation method as previously described, and immunophenotypically characterized by flow cytometry.

1.9 Cell culture

Early passages 2–4 of human DPSC were grown in cell culture flasks using alpha-MEM, supplemented with glutamine (2 mM), penicillin (50 IU/ml), streptomycin (50 g/ml), amphotericin B (0.25 mg/ml), 100 μM ascorbic acid and 10% FBS in a humidified atmosphere and 5% CO_2 at 37 °C in a cell culture incubator (Thermo Scientific). Confluent cells were detached and passaged after trypsination with 0.25% trypsin-EDTA, seeded at a 90% confluence and allowed to grow for 4–5 days before the next passage.

1.10 Cell viability and proliferation assay

A suspension of $3x10^4$ cells in alpha-MEM were seeded on the film specimens of the materials hybrid and thymol-functionalized hybrid materials and were placed into the cell culture incubator at 37 °C. On days 2, 4, and 7 post seeding, the cell viability and proliferation assay was performed with the resazurin-based PrestoBlue® reagent according to the manufacturer's instructions. The reagent was incubated on the cells at 37 °C for 60 min. The absorbance was measured in a spectrophotometer (Synergy HTX Multi-Mode Microplate Reader, BioTek, Winooski, VT, USA) and cell number quantification was performed by means of a calibration curve. Error bars representing the average of triplicates ± standard deviation in two independent experiments were calculated (n=6). (ns) symbol denotes not significant differences according to statistical analysis by one-way analysis of variance (ANOVA) Dunnett's multiple comparisons test.

1.11 Optical microscopy

A suspension of $2x10^4$ cells in alpha-MEM were seeded on glass substrates covered by spin-coating, as well as 3D scaffolds, with the hybrid and thymol-functionalized hybrid materials films and were placed in the cell culture incubator at 37 °C. Cells on the specimens were examined daily for 7 days and were visualized by optical microscopy by means of a Zeiss Axiovert 200 microscope. Images were taken by a ProgResVR CFscan Jenoptik camera (Jena, Germany) using the ProgResVR CapturePro 2.0 software and objective lenses for 10-fold magnification.

1.12 Preparation of biological samples for scanning electron microscopy

A suspension of $2x10^4$ cells in alpha-MEM were seeded on glass substrates covered by spin-coating with the hybrid and thymol-functionalized hybrid materials films and were placed in the cell culture incubator at 37 °C for up to 7 d. Specimens were then removed from the incubator and rinsed three times with PBS, fixed with 4% paraformaldehyde for 30 min, and dehydrated in increasing concentrations (from 30 to 100%) of ethanol. The specimens were then dried in a critical point drier (Baltec CPD 030), sputter-coated with a 10 nm thick layer of gold and observed under a scanning electron microscope at an accelerating voltage of 20 kV.

1.13 Laser scanning confocal microscopy

A suspension of $2x10^4$ cells in alpha-MEM were seeded on glass substrates with 3D scaffolds consisting of the hybrid and thymol-functionalized hybrid materials and were placed into the cell culture incubator at 37 °C for up to 7 days. After the incubation time, the samples were rinsed with PBS, fixed with 4% paraformaldehyde for 15 min and permeabilized with 0.1% Triton X-100 in PBS for 5 min. The non-specific binding sites were blocked with a 2% BSA solution in PBS for 30 min. Actin cytoskeleton was stained by incubating the cells on the samples in 20 μl diluted phalloidin-atto-488 in blocking solution for 1 h at 37 °C and subsequently staining them by simultaneous incubation with 4′,6-diamidino-2-phenylindole (DAPI) for 5 min. The samples were washed with PBS, mounted with a mounting fluid and observed under a Leica laser scanning confocal microscope.

1.14 Statistical analysis

Statistical analysis was performed using the one-way ANOVA Dunnett's multiple comparisons test. To statistically evaluate the difference in cell proliferation after certain time points (2, 4, and 7 days), we compared the hybrid films, the thymol-functionalized hybrid films at each time point against the control tissue culture polystyrene (TCPS) surface.

1.15 Anti-microbial studies

1.15.1 Bacteria Culture

A suspension of 1 x 10^8 CFU/mL *E. coli* in LB medium were seeded on glass substrates with 3D scaffolds consisting of hybrid and thymol-functionalized hybrid and incubated at 37 °C for 1, 2, 3 and 4 days.

1.15.2 Preparation of samples for SEM observation

After the incubation time, the samples were rinsed with PBS twice, washed with cacodylat 0.1 M buffer solution for 10 min twice, fixed with 2.5% paraformaldehyde overnight, washed with cacodylate 0.1 M buffer for 10 min twice and then dehydrated in increasing concentrations (from 30 to 100%) of ethanol, 10 min for each consentration. The specimens were then dried in a critical point dryer, sputter-coated with a 10 nm thick layer of gold and observed under a scanning electron microscope at an accelerating voltage of 20 kV.

3. Results and discussion

3.1 Materials synthesis and characterization

The synthesis of the TM monomer was carried out by the nuchleophilic substitution of the hydroxyl group of thymol, with methacrylic anhydride (**figure 4. 1**.). After the reaction took place, the monomer was purified by column chromatography as was obtained pure in 70% yield, and was characterized via $^1H/^{13}C$ NMR spectroscopy (**figures 4.1 b and c**) as well as FT-IRspectroscopy.

In the ^1H NMR spectrum of the product the appearance of new peaks attributed to the olefinic protons at δ 6.3522- 6.3504 and δ 5.7823- 5.7763 and the methyl protons at δ 2.34 of the methacrylate group, confirms the successful synthesis of the product.

At the spectrum of ^{13}C NMR four new peaks were observed. O-C=O at δ 165.82, $C=CH_2$ at δ 135.85 and 122.56 and the $C-CH_3$ at δ 19.97.

NMR analysis:

^1H NMR (500MHz, CD_2Cl_2): δ 7.24-7.23 (d, J = 8 Hz, 1H), δ 7.08-7.06 (m, 1H), δ 6,86 (s, 1H), δ 6.3522- 6.3504 (m, 1H), δ 5.7823- 5.7763 (m, 1H), δ 3.03- 2.94 (hept, J=6.9 1H), δ 2.34 (s, 3H), δ 2.0868- 2.0839 (m, 3H), δ 1.2 (s, 3H), δ 1.19 (s, 3H).

^{13}C NMR (500 MHz, CD_2Cl_2): δ 165.82, 148.05, 136.99, 136.46, 135.85, 126.68, 126.49, 126.12, 122.56 26.97, 22.49, 20.28, 17.97.

In the FT-IR spectra **figure 4.1.d** of thymol (black line) and TM (red line) the characteristic peaks are obsearved. The broad band at around 3150 cm^{-1}, which is attributed to the O-H stretching vibration, of thymol has completely disappeared in the spectrum of TM, while new peaks at 1733 cm^{-1} and 1673 cm^{-1} which correspond to the C=O and C=C to the stretching vibrations of the methacrylate group of TM have appeared. The intense peak in the spectrum of TM at 1126 cm^{-1} is attributed to the C-O-C stretching vibration verifying the successful synthesis of the ester product.

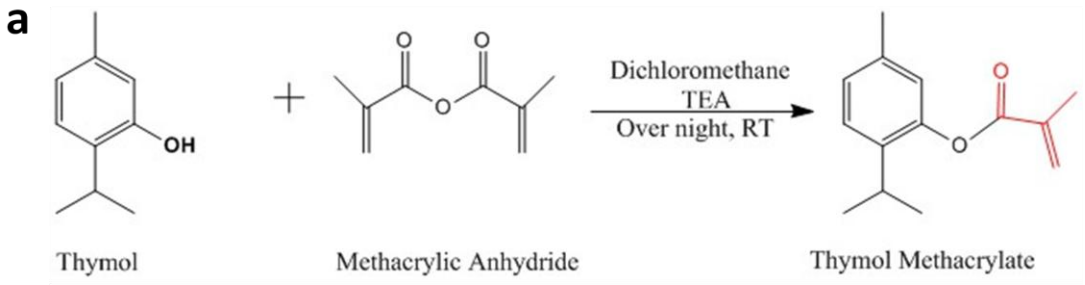

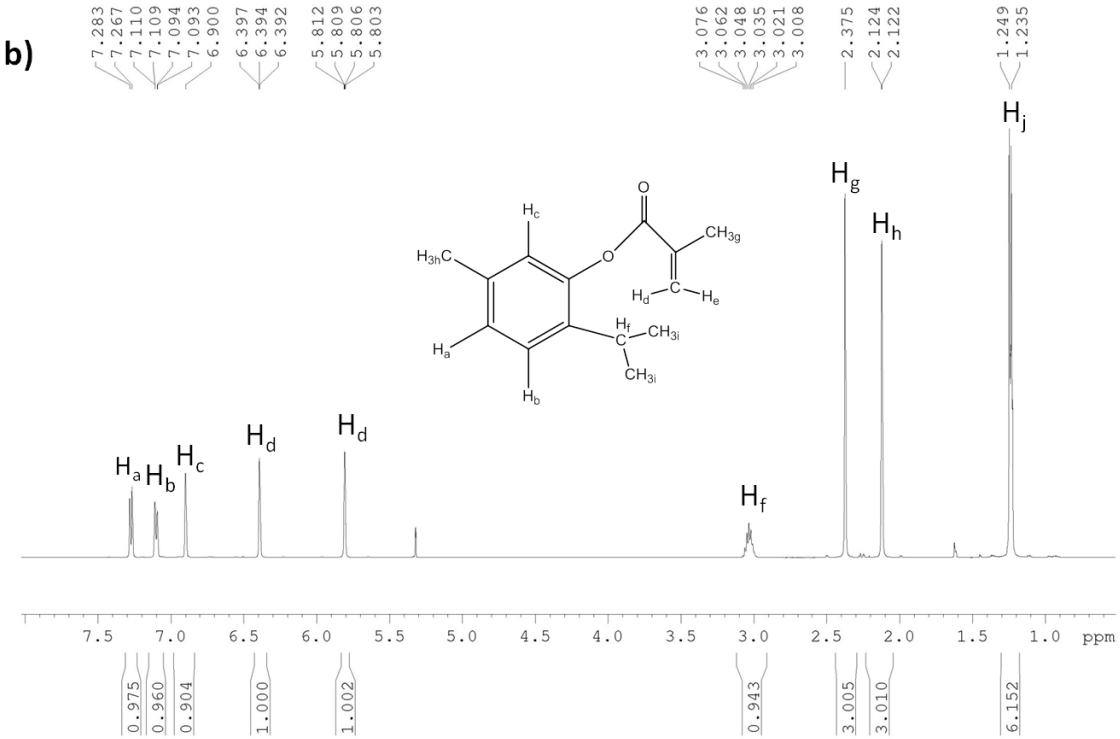

c)

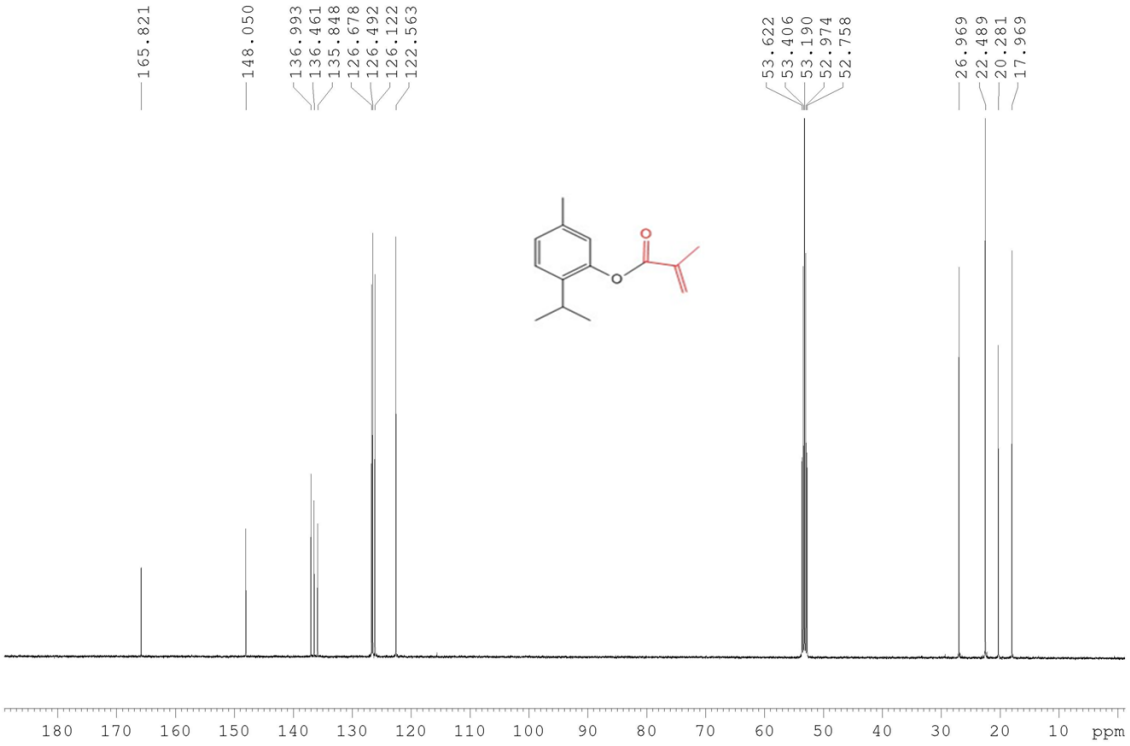
165.821
148.050
136.993
136.461
135.848
126.678
126.492
126.122
122.563
53.622
53.406
53.190
52.974
52.758
26.969
22.489
20.281
17.969
180 170 160 150 140 130 120 110 100 90 80 70 60 50 40 30 20 10 ppm

d

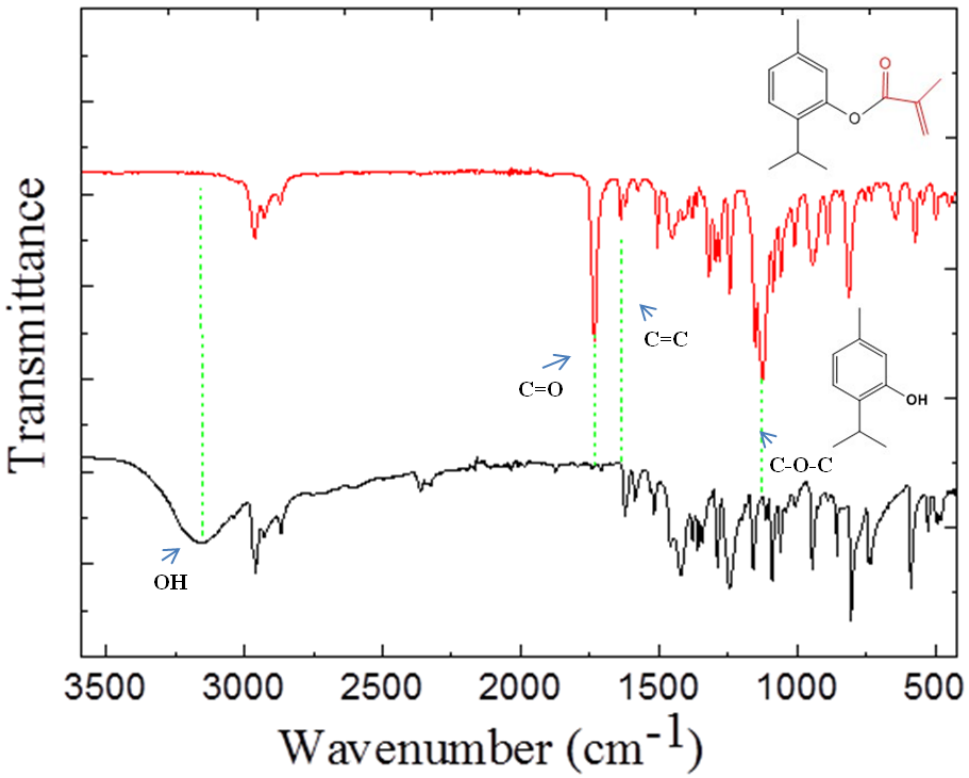
Transmittance
C=C
C=O
OH
C-O-C
OH
3500 3000 2500 2000 1500 1000 500
Wavenumber (cm-1)

Figure 4. 1: a) Schematic representation of the synthetic procedure followed for the synthesis of TM, b) ^{1}H NMR spectrum of TM in CD_2Cl_2, c) ^{13}C NMR spectrum of TM in CD_2Cl_2 and d) FT-IR spectra of thymol (red line, upperbspectrum) and TM (black line, lower spectrum)

The hybrid material was synthesized using a sol-gel reaction (**figure 4. 2)**. In the first step MAPTMS was hydrolyzed by HCl. In this step the methoxy groups of MAPTMS react with HCl and become hydrolyzed, to yield hydroxyl groups while the by-product of the reaction is methanol **(figure 4.2.a)**. In the second step a mixture of DMAEMA/ZPO is added in the solution of hydrolyzed MAPTMS and condensation takes place between the hydrolyzed MAPTMS and ZPO (**figure 4. 2.b)**. In this step the inorganic matrix is formed. Next, TM was added and BIS to serve as the photoinitiator which will absorb two photons of 800 nm wavelength and produce radical species, that will initiate the polymerization process (**figure 4.2.c)**. The above procedure produce a viscous liquid mixture, which was drop casted onto glass slide. The samples of the photocurable material were allowed to dry for 3-5 days in a vacuum oven in order for methanol and propanol which are produced by the hydrolysis reactions as well as the isopropanol of the ZPO solution, to eavaporate. After drying and condensation was complete, the drops were transformed into a gel which was polymerized.

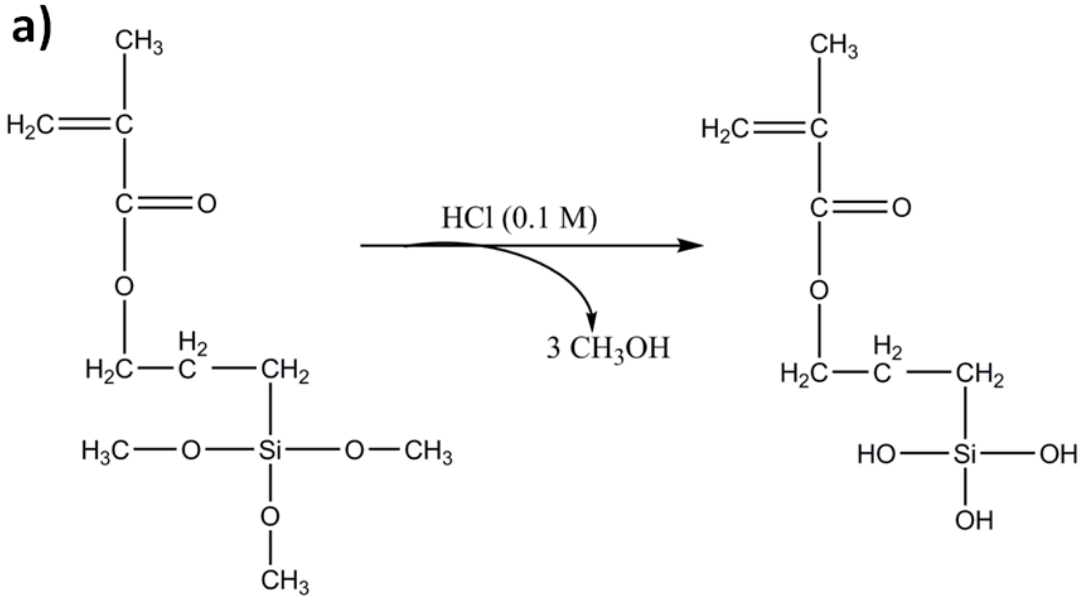

b)

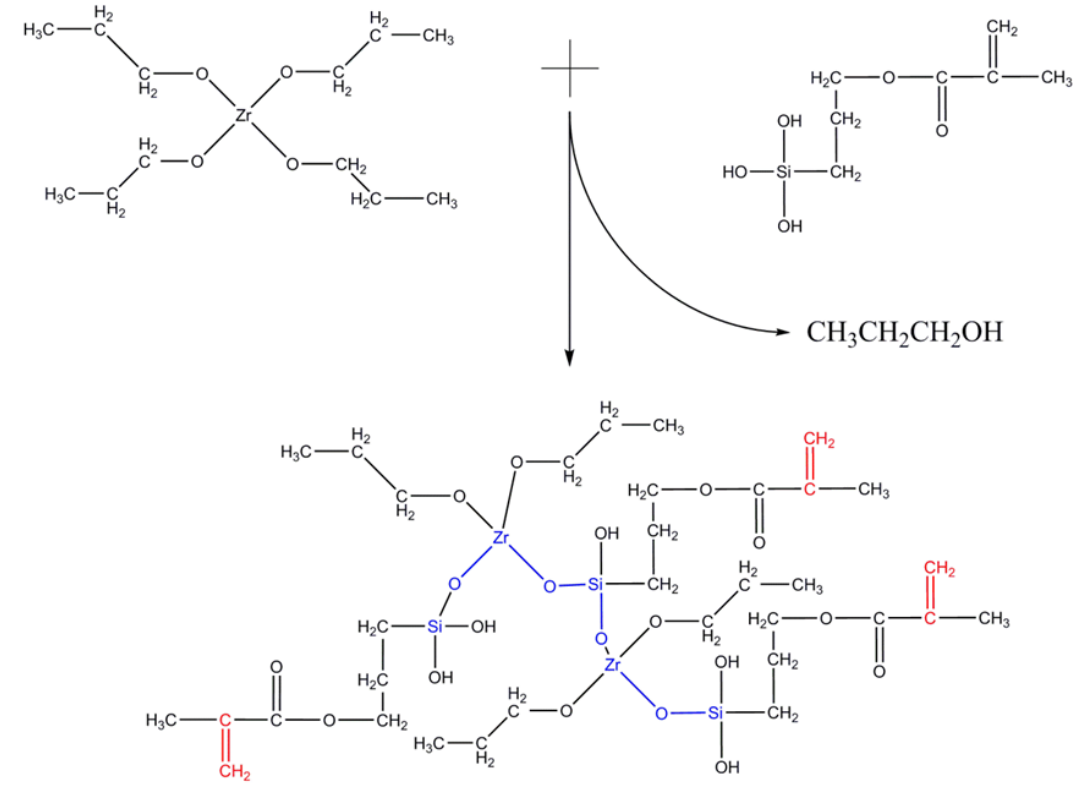

c)

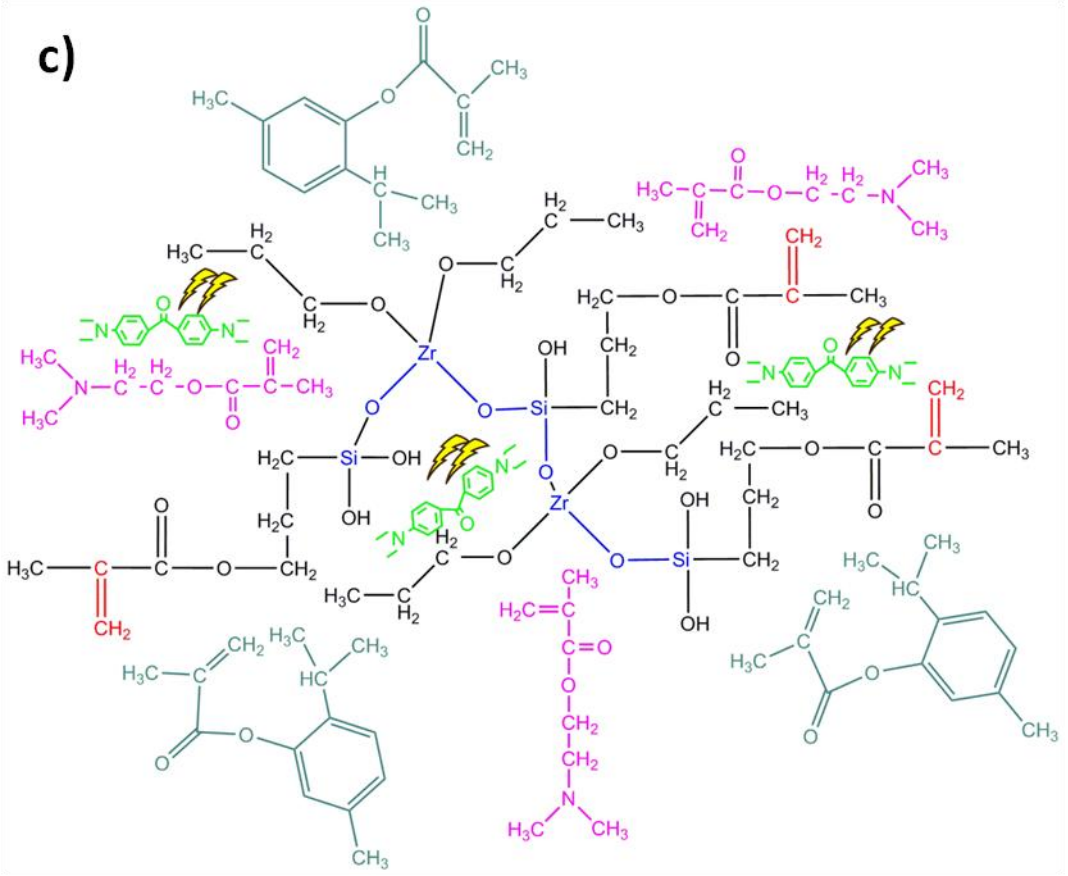

Figure 4. 2: a) Hydrolysis of MAPTMS, b) Condensation reaction and inorganic network formation and c) final photoprecursor containing the inorganic mnetwork, DMAEMA (pink) as a co-monomer and radical quencher, thymol methacrylate (blue) as a co-monomer and BIS (green) as the photoinitiator.

3D structures were fabricated by the MPP process. A grid-shape porous scaffolds with pores size of 80 μm and dimensions of 555x555x50 μm^3 was chosen. A velocity-energy scanning was perform to find the best fabrication parameters which were 60mW laser power and 1000 μm s^{-1}writing speed. This combination of velocity-energy allowed to fabricate highly accurate structures in 10 min each. **Figure 4.3** shows the SEM images of the fabricated 3D scaffolds. Top view **figures 4.3 a and b** as well as 45^o tilted **figures 4.3 c and d** and side view **figures 4.3 e and f** images, show highly accurate 3D porous scaffolds. Slight deformation in **figures 3 a,b** could be observed, a fact that was attributed to the development and sputtering processes. The produced 3D scaffolds confirm that the synthesized TM functionalized hybrid organic-inorganic material is suitable for MPP and can be used for the fabrication of highly accurate 3D structures.[29-30]

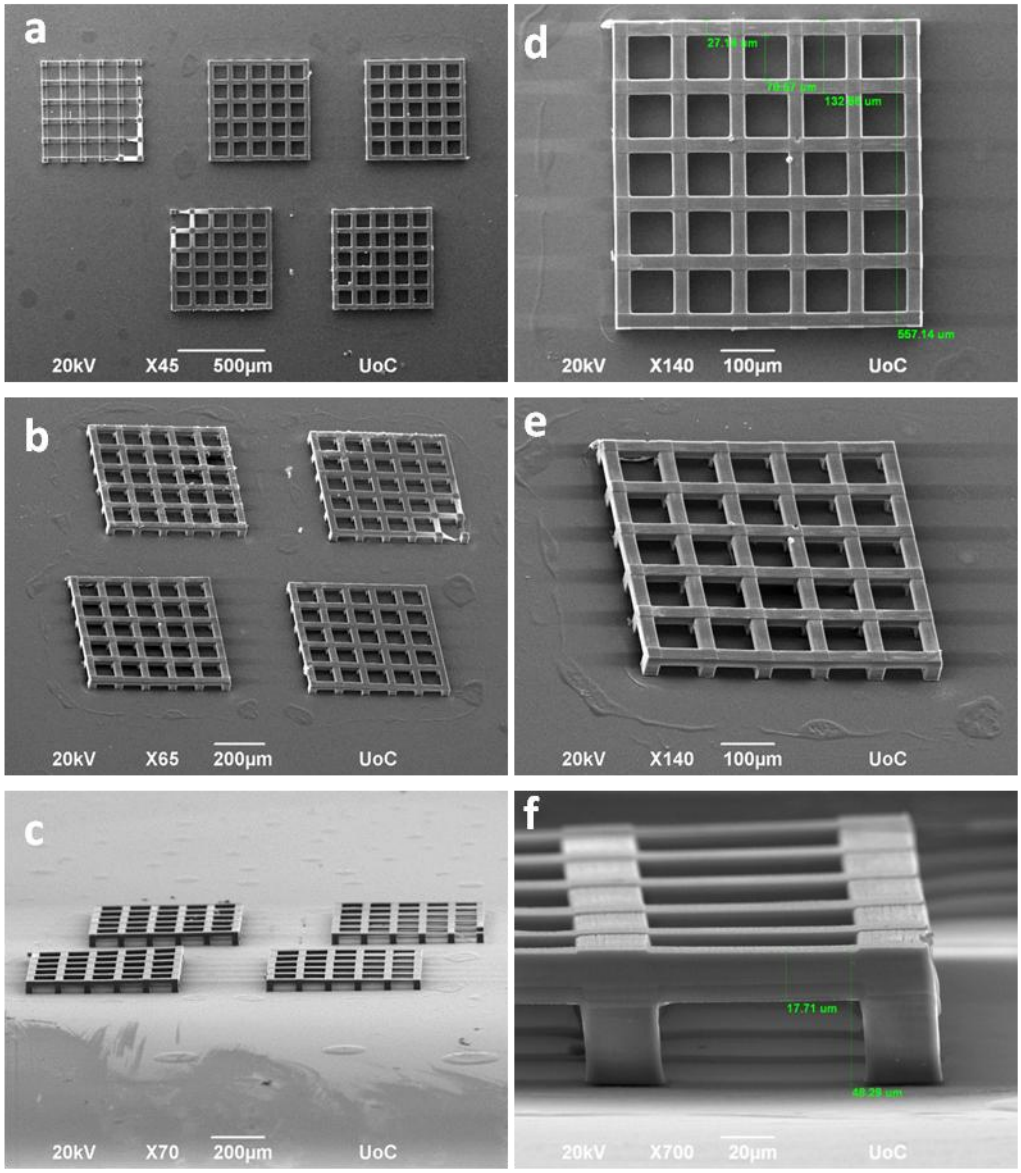

Figure 4. 3: The 3D grid-shaped scaffolds produced from the thymol-functionalized hybrid material, fabricated by MPL, using a 20× plan achromat lens (N.A. = 0.8) at a 60 mW laser power and writing speed 1000 μm s^{-1}: a) top view, b) tilted 45^{o}, c) side view and d-f) higher magnification imagies.

3.2 Biological studies

Representative optical microscopy images (**figure 4.4**) show the morphology of the DPSC cultured on the hybrid and thymol-functioalized hybrid materials and on the polystyrene control surface for 2 and 7 days in culture. Cells seeded for 2 days in culture indicate a similar spindle-shaped morphology on the different film surfaces the hybrid and thymol-functionalized hybrid material, which is similar to that on the polystyrene control surface (**figure 4.4, top panel**). After 7 days in culture, a clear increase in proliferation was observed with a dense layer of well-spread flattened cells completely covering all material surfaces, as shown in the bottom panel of **figure 4.4**.

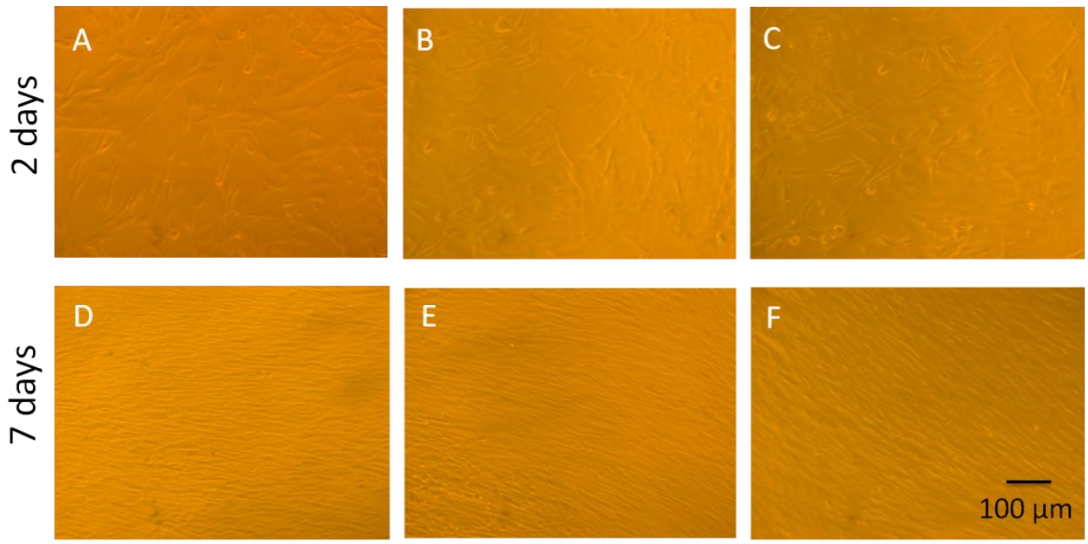

Figure 4. 4: Optical microscopy images showing the adhesion of human dental pulp stem cells on the hybrid material films (A, D), thymol-functionalized hybrid material films (B, E), and tissue culture treated polystyrene (TCPS) control (C, F) after 2 days (A, B, C upper panel), and 7 days (D, E, F lower panel) in culture. Scale bar represents 100 µm and is same in all images.

Figures 4.5 and 4.6 show the results from the investigation the viability of the DPSC on the hybrid and thymol-functionalized hybrid materials films performed using the PrestoBlue assay after 2, 4, and 7 days in culture. We carried out the cytocompatibility investigations on geometrically well-defined films in order to quantify the cell proliferation results. For both materials we observed a strong initial cell adhesion and a subsequent cell proliferation increase after 3 and 7 days. The cell number on both films increased approximately by two times from day 2 to day 4 and approximately 4 times from day 2 to day 7. The cell viability (**figure 4.6**) was around 100% compared to the tissue culture treated polystyrene surface for both materials at the three investigated time points. The results indicate the absence of any cytotoxic effects and suggest that the thymol–functionalized material is biocompatible, and therefore can be used for the fabrication of biomaterial scaffolds.

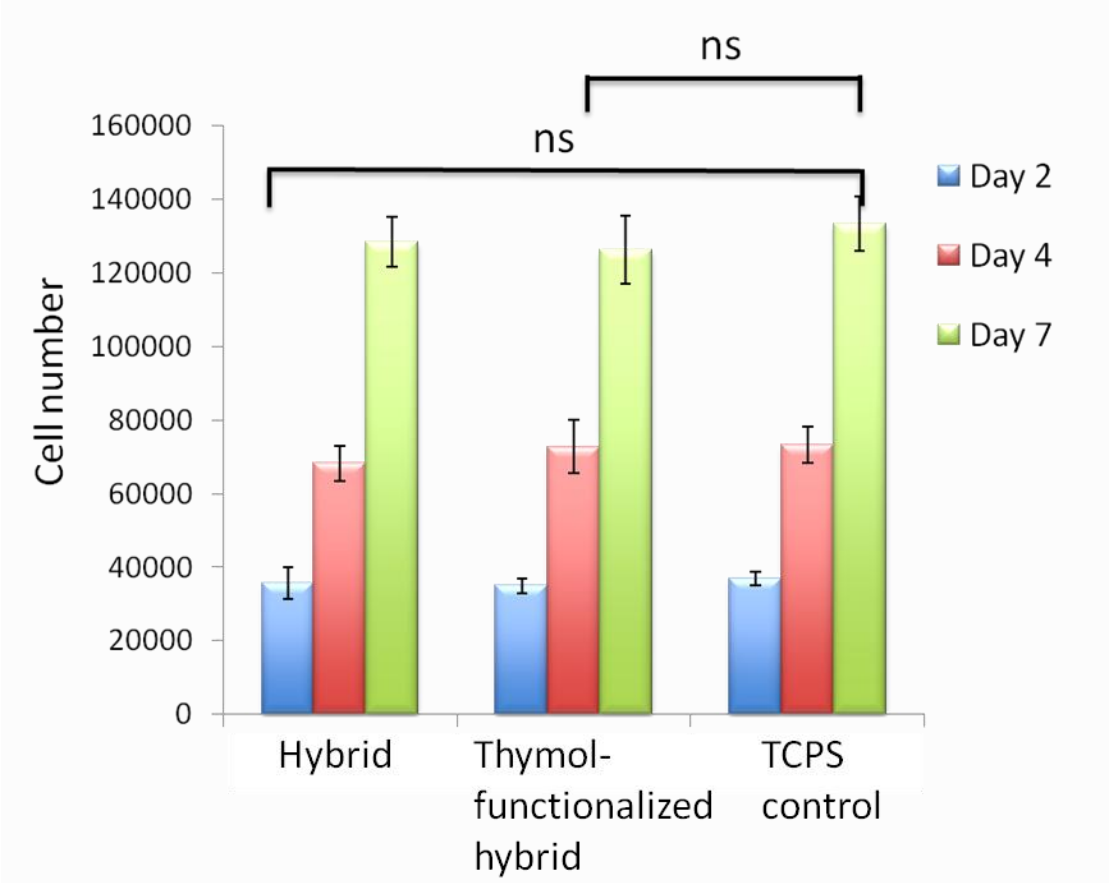

Figure 4.5. Cell proliferation showing the number of human dental pulp stem cells onto the hybrid material films, the thymol-functionalized hybrid material films, and the tissue culture treated polystyrene (TCPS) control after 2, 4, and 7 days in culture. The cell number was determined by the PrestoBlue® viability assay, by means of a calibration curve correlating the absorbance (OD) values to cell number. The initial number of cells was $3x10^4$. Statistical analysis by means of GraphPad Prism 7.0 one-way ANOVA indicates no significant (ns) differences between the two hybrid materials vs. the control TCPS at each time point ($p=0.25$)

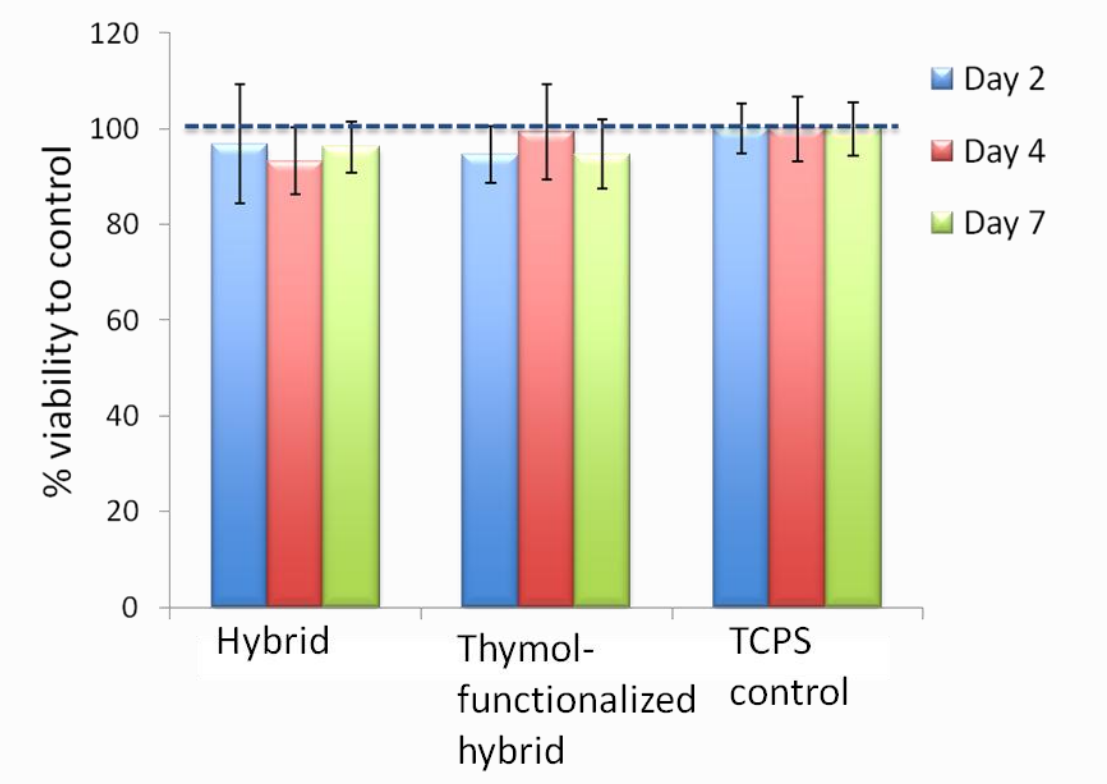

Figure 4. 6 % viability of the human dental pulp stem cells onto the hybrid films, the thymol-functionalized hybrid films, and the tissue culture treated polystyrene (TCPS) control after 2, 4, and 7 days in culture as determined by the PrestoBlue® cell viability assay

After examining the materials in 2D cell culture, in which they exhibit an excellent cell viability and proliferation profile, the hybrid and thymol-functionalized hybrid material 3D porous scaffolds were used to study the behavior of the cells in 3D culture. For that propose, $2x10^4$ cells were cultured on a glass substrate with dimensions 1x1 cm^2 which contained 9 scaffolds with dimensions 550x550x50 μm^3. The 3D cell culture was followed for 7 days. **Figure 4.7** shows the optical microscopy images, of the cell culture, on the 3D scaffolds at different time points. The upper panel shows the 3D cultures on the hybrid material, which was used as a control material due to it's biocompatibility. From these images one can clearly observe a good cell adhesion onto the 3D scaffolds. In the early time point of 2 days, a few cells have managed to hang on the scaffolds while after 4 days a large number of cells cover the scaffolds and proliferate within the scaffolds. Finally, at the late time point of 7 days, one can clearly observe the full coverage of the scaffolds by the DPSC and a homogenous 3D cell culture. In the bottom panel, the thymol-functionalized hybrid material 3D cultures are shown. A similar adhesion and proliferation behivor of the cells was observed in the thymol-functionalized hybrid material, structure which confirms the biocompatibility of the thymol-based material.

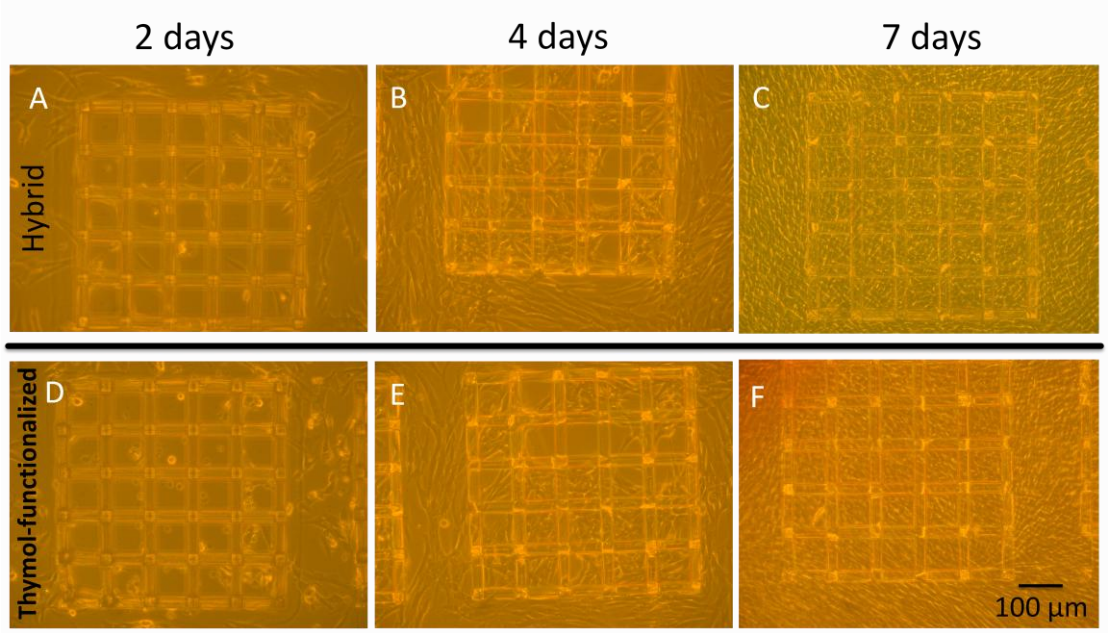

Figure 4. 7 Optical microscopy images showing the adhesion of human dental pulp stem cells onto two-photon polymerized grid-shaped scaffolds after 2 days (A, D), 4 days (B, E) and 7 days (C, F) in culture. The upper panel images (A, B, C) represent the hybrid material cultures and the lower panel (D, E, F) the thymol-functionalized hybrid material cultures. Scale bar represents 100 µm and was the same in all images.

In order to visualize cell adhesion on the 3D scaffolds immunocytochemistry, the actin/DAPI assay was exployed. In this assay, the cell cytoskeleton is stained with green color while the nucleus with blue color. However, the high autofluorescence of the PI presents a great challenge for this assay since it overlaps with the fluoresence of the dyes. In **figure 4.8** laser scanning confocal microscopy images of the hybrid and the thymol-functionalized hybrid 3D scaffolds with DPSC after 7 days of culture are presented. In both materials, good cytoskeleton production observed. However it was not possible to scan the whole structure due to the fluorescence of the structures and therefore the cells which attached on the top of the scaffolds could not be visualized. In fact, **Figure 4.8.** shows that there are cells on top of the 3D scaffolds but they cannot be visualized. SEM microscopy was also used to visualized the cells on the 3D scaffolds after 4 days of culture.

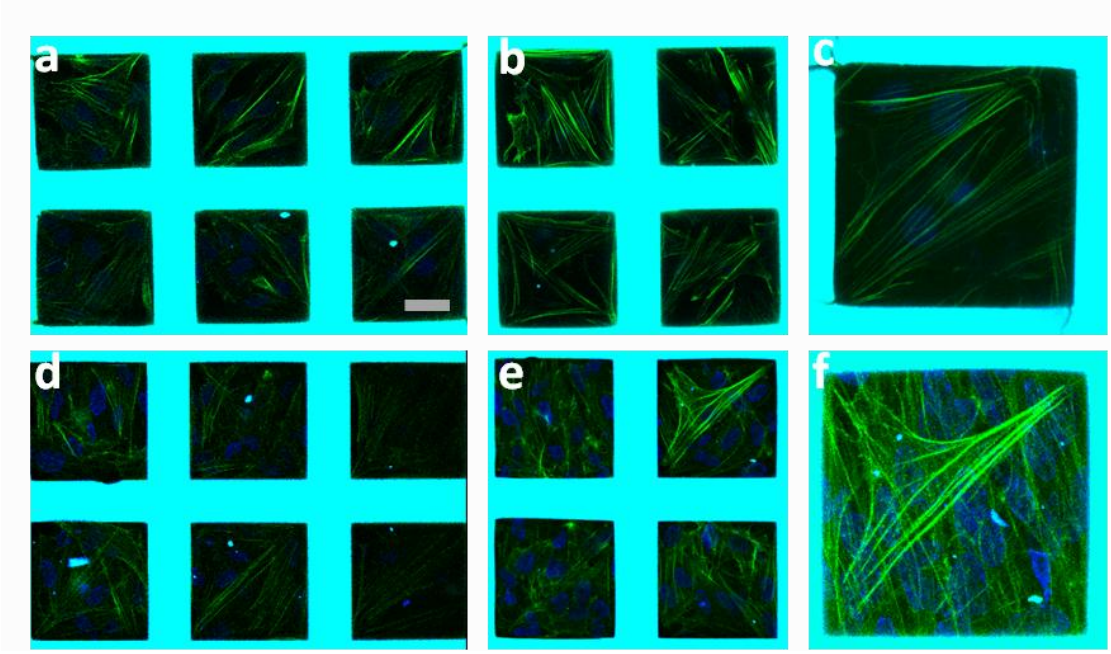

Figure 4.8. Laser scanning confocal microscopy images showing the adhesion of human dental pulp stem cells onto two-photon polymerized grid-shaped scaffolds after 7 days in culture. The upper panel images (A, B, C) represent the hybrid material culture and the lower panel (D, E, F) the thymol-functionalized hybrid material cultures. The cells were stained with phalloidin (green: actin filaments) and DAPI (blue: nucleus). Scale bar represents 25 μm and is simmilar in all images.

Next the 3D cultures were characterized by SEM. **Figure 4.9** shows the 3D cultures of DPSC onto the 3D hybrid and thymol-functionalized hybrid material porous scaffold, after 4 days in culture. The great cell attachment and proliferation within the 3D porous scaffold of both materials can clearly observed. Despite the single time point used, one can observe the huge amount of cells that are attached on the 3D scaffolds and attain their characteristic spindle-shaped morphology. The cell morphology on our hybrid scaffolds are in good agreement with the previous results by the group of prof. Chatzinikolaidou[31-34].

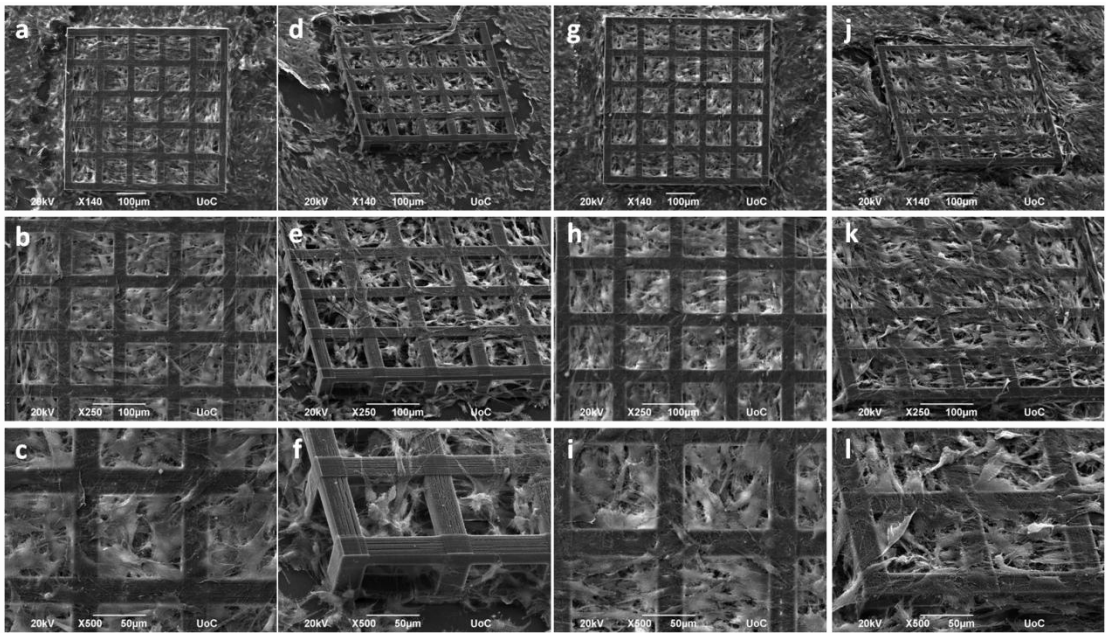

Figure 4. 9: SEM images showing the adhesion of human dental pulp stem cells onto two-photon polymerized grid-shaped scaffolds after 5 days in culture. Images (a-c) represent the top view images of the hybrid material culture and (d-f) show the same samples tilted by 45^{o}. Respectively, (g-i) represent the top view images of the thymol-functionalized hybrid material culture and (j-l) tilted by 45^{o} of the same samples.

Antimicrobial studies

Following the biocompatibility of the TM-functionalized hybrid material, we examined how bacteria behave on the 3D scaffolds. *E-coli* were cultured on the 3D scaffolds for 1,2,3 and 4 days. After 1day in culture the 3D scaffolds were observed in SEM. **Figures 4.10 a and b** show the bacteria on the hybrid material while **figures 4.10 c and d** show the thymol-functionalized scaffolds with the bacteria. At the first time point of day 1, bacteria are mainly growing on the glass substrate whereas a few bacteria are observed on the hybrid 3D scaffolds. Moreover, no bacteria attach and grow on the thymol-functionalized hybrid material scaffolds. In the final time period of 4 days, the difference in the two materials is obvious. **Figures 4.10 e and d** show the *e-coli* on the hybrid 3D scaffolds after 4 days in culture. In these scaffolds, a very large number of bacteria are attached and grow onto the structures, signifying the lack of any anti-microbial action of the hybrid material. On the other hand, **figure 4.10** shows the thymol-functionalized hybrid material scaffolds after 4 days in culture. A dramatic reduction of bacteria on the scaffolds is observed with only very few attached bacteria, a fact that underlines the potency of TM to act as an anti-microbial agent.

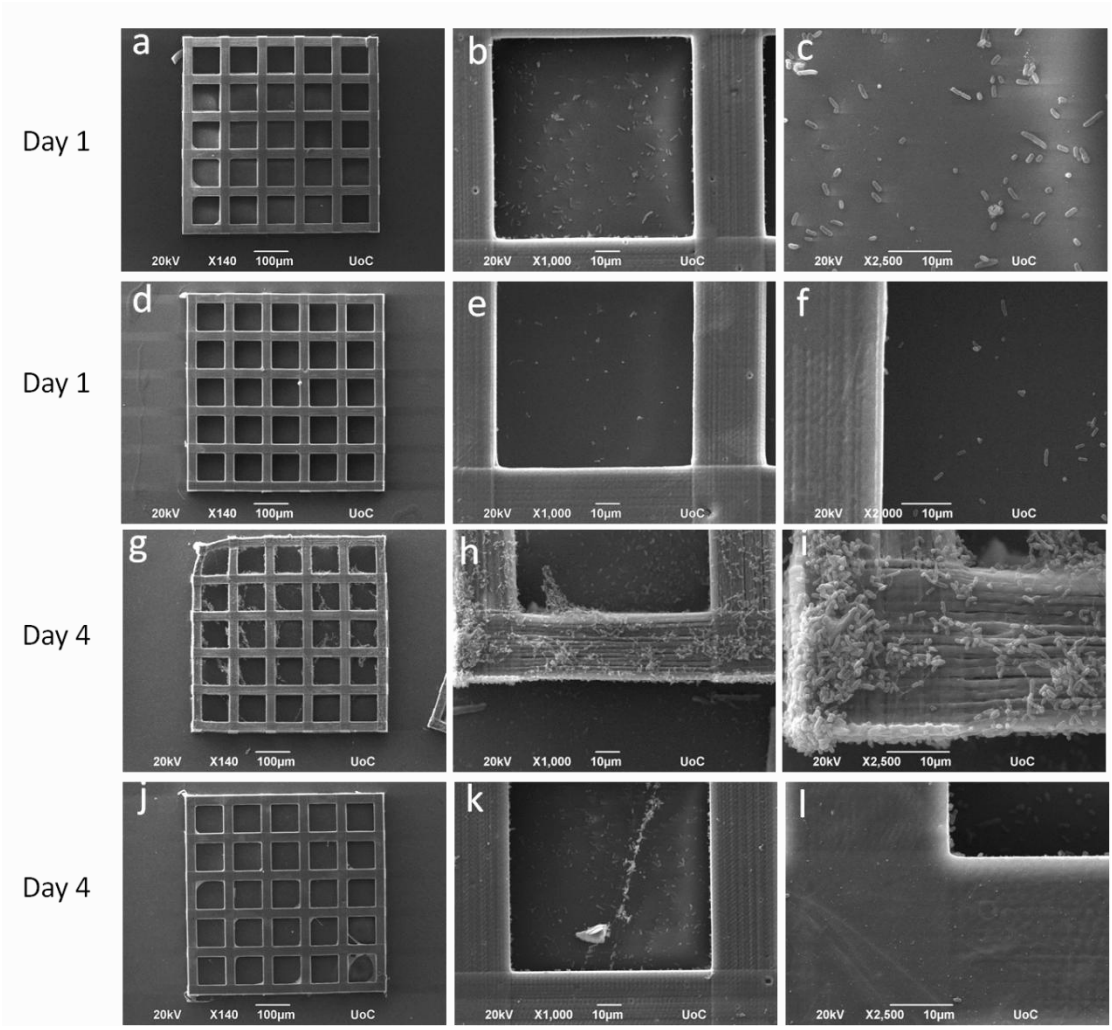

Figure 4.10: SEM images of the *e-coli* culture on the 3D scaffolds at different time points, a-c) 3D scaffolds of the hybrid material after 1 day in culture, d-f) 3D scaffolds of the thymol-functionalized hybrid material after 1 day in culture, g-i) 3D scaffolds of the hybrid material after 4 days in culture and j-l) 3D scaffolds of the thymol-functionalized hybrid material after 4 days in culture. Higher magnification from the left to the right.

4. Conclusions

3D scaffolds for dental tissue engineering were fabricated using MPP. The fabricated scaffolds are dual-functional, exhibiting simultaneously biocompatibility and antimicrobial activity. The biocompatibility is based on the hybrid organic/inorganic nature of the material, while the antimicrobial activity is due to the use of an essential oil natural product, thymol, which was appropriately modified and covalently bound onto the hybrid material. Primary mesenchimal dental pulm stem cells isolated from patients, were cultured on the scaffolds and proved the biocompatibility and good cell

adhesion and proliferation on the hybrid materials, whereas e-coli verified the antimicrobial action of the 3D scaffolds.

5. References

1. E. Alsberg et. al., *Crit. Rev. Oral. Biol. Med*., **2001**, 12, 64.
2. J. Mao et. al., *J. Dent. Res.*, **2006**, 85, 966.
3. D. Howard et. al. .*J Anat*., **2008**, 213, 66.
4. S. Gronthos et. al., *Proc Natl Acad Sci USA,* **2000**, 97, 13625.
5. A. Bakopoulou et. al., *Arch. Oral. Biol.*, **2011**, 56, 709.
6. S. Liao et. al., *J. Biomed. Mater. Res. B,* **2004**, *69*, 158.
7. L. Tang et. al., *Am. J. Clin. Pathol.*,**1995**, 103, 466.
8. R. Gharibi et. al., *J. Mater. Sci.*, **2018**, 53, 1581.
9. A. Nasajpour *et. al., Adv. Funct. Mater.,* **2017**, 1703437.
10. H. Xu *et. al., Adv. Mater.,* **2018**, 1801100.
11. R. Song et. al., *ACS Appl. Bio Mater.*, **2018**, 1, 1056.
12. R. Qi et. al., *ACS Appl. Bio Mater,z.,* **2018**, 1, 21.
13. S. Imazato et. al., *J. Dent.* **1998**, 26, 267.
14. N. Capanema et. al., Inc. J. Appl. Polym. Sci., **2017**, 134, 45812.
15. Y. Xieet. al., *Appl. Environ. Microbiol.*, 2011, 77, 2325.
16. R. Shi et. al., J. Colloid. Interface. Sci., **2018**, 1, 275.
17. T. Manouras et. al., *Soft Matter*, **2017,** 24, 3777.
18. M. Wang et. al., *Philos. Trans. R. Soc. Lond. B Biol. Sci*., **2007**, 362, 1093.
19. K. Nicolaou et. al., *Angew. Chem. Int. Ed. Engl.*, **2005**, 44, 1012.
20. A. Bauer et. al., *Nat. Prod. Rep.*, **2014**, 3, 35.
21. F. Koehn et. al., *Nat. Rev. Drug. Discov.*, **2005**, 4, 206.
22. Z. Zamani et. al., *Iran. J. Pharm. Res.*, **2015**, 14, 1031.
23. M. Del Nobile et. al., *J. Food Eng.*, **2008**, 89, 57.
24. I. Martins et. al., *Chem. Eng. J.*, **2012**, 245, 191.
25. M. Ramos et. al., *J. Food Eng.*, **2012**, 109, 513.
26. M. Stefanakis et. al., *Food Control*, **2013**, 34, 539.
27. N. Moszner et. al., *Polymer Bulletin*, **1994**, 33, 7.
28. S. Bedel et. al., J. *Polym. Sci., Part A: Polym. Chem.*, **2015**, 53, 1975.
29. I. Sakellari et. al., *ACS Nano*, **2012**, 6, 2302.
30. A. Ovsianikov et. al., *ACS Nano*, **2008**, 2, 225.
31. M. Chatzinikolaidou et. al., *Mater. Sci. Eng. C*, **2015**, 48, 301.
32. M. Chatzinikolaidou et. al., *Colloids Surf. B Biointerfaces*, **2016**, 149, 233.
33. K. Terzaki et. al., *Biofabrication*, **2013**, 5, 045002
34. K. Terzaki et. al., *J. Biomed. Mater. Res. Part A*, **2013**, 101, 2283.